FORCE BASED DESIGN GUIDELINE FOR TIMBER-STEEL HYBRID STRUCTURE: STEEL MOMENT RESISTING FRAMES WITH CLT INFILL WALLS

Prepared for
Forestry Innovation Investment Ltd.
#1200 - 1130 West Pender Street, Vancouver, BC Canada V6E 4A4

By
The University of British Columbia
3333 University Way, Kelowna, BC Canada V1V 1W7

April 2015

Principal investigators

Dr. Solomon Tesfamariam (Associate Professor, UBC Okanagan)

Dr. Siegfried F. Stiemer (Professor, UBC Vancouver)

Students

Caleb Goertz (MASc Student, UBC Okanagan)

Matiyas Bezabeh (PhD Student, UBC Okanagan)

Industry collaborator

Dr. Marjan Popovski (Principal Scientist, FP Innovation)

Academic collaborator

Dr. Katsuichiro Goda (Senior Lecturer, Bristol University)

Disclaimers

???

Executive Summary

In order to satisfy the urban housing demand in western Canadian cities, recently, the 2009 BC building code has increased the wood buildings height limits from 4 to 6 storeys. In this study, feasibility studies of timber-based hybrid building is carried at The University of British Columbia (UBC). In this project, funded through Forestry Innovation Investment's (FII) Wood First Program, it is envisioned to develop a design guideline for the steel–timber hybrid structure. The objective of this research proposal is to develop the design guideline for the next generation "steel-timber hybrid structures" that is limited in scope to 20 storey office or residential buildings.

The steel-timber hybrid structure incorporates Cross Laminated Timber (CLT) infill walls in the steel moment resisting frames. This structure is aimed to couple the ductile and strong steel moment frames with lighter and stiff CLT infill walls. L-shaped steel bracket connectors were proposed to connect the steel frames to the CLT panels. Thorough experimental studies have been carried out on the seismic behaviour of the bracket connections at UBC for the past four years. These connection brackets are bolted to the steel frame and nailed to the CLT infill walls. Moreover, the provided brackets ensure full confinement between the structural elements and energy dissipation under intense seismic shaking.

The National Building Code of Canada (NBCC) recommends an equivalent static force design (ESFD) method with appropriate overstrength and ductility factors for the seismic design of structures. However, NBCC (NRC 2010) does not have the appropriate overstrength and ductility factors to design the proposed hybrid structure. Thus, in this preliminary report, overstrength and ductility factors are quantified analytically. A robust finite element model of the hybrid structure that accounts for the CLT panel and frame interactions was used for the analytical investigation. For the investigation, 36 different hybrid buildings were modeled and subjected to monotonic static pushover loading by varying the following modeling variables: building height {1, 3, 6, 9, 12, 15 and 20 storey},

CLT infill configuration {one-bay infilled and two-bay infilled}, connection bracket spacing {800 mm}, and ductility class {D and LD}. A nonlinear static pushover analysis has been performed to quantify the overstrength and ductility factors of the modelled hybrid buildings. Analysis was done using a high performance computation method with 200 clusters of computers at The University of British Columbia research computing service centre (UBCIT). A bilinear approximation method has been adopted to obtain the system yielding point. The results show that the presence of CLT infill walls significantly affects the systems overstrength value, by sacrificing ductility. From this preliminary study, it can be concluded that an overstrength factor of 1.2 and ductility factor of 3 will yield a safe and conservative design of the proposed hybrid structure.

Acknowledgements

Enter acknowledgements here.

Table of Contents

List of Figures

List of Tables

Insert List of Tables here.

Chapter 1
Background

1.1 Motivation

The timber industry, on a Canada wide scale, has initiated a major push for use of timber products in building construction. In the Province of British Columbia this goes so far that the government has issued a "Wood First Initiate" in order to create a "Culture of Wood." The current timber building height, however, is limited to six storey. There is a unique opportunity for designers to take advantage of innovative design (e.g. hybrid structures) to overcome the height restriction required by the building code. In the current proposal, the building height limits constraint can be met with the use of hybrid structures. Over the last five year, through NSERC network funded project (NewBuilds) researchers at The University of British Columbia (UBC) and FPInnovations have developed timber-steel hybrid building that can potentially meet the current performance requirement to exceed the current height limit. Thus, this application is to develop a design guideline for a novel timber-steel hybrid structures, up to 20 storey height. With this type of structures, the volume of wood used is increased substantially.

Through this proposed research, is in line with the Forestry Innovation Investment's (FII) Wood First Program, the following objective are met:

1) Maximize the appropriate use of wood in public and private projects: increase the volume of wood used through hybrid taller structures.
2) Strengthen BC's capacity to produce competitive wood-based products and building systems that create and respond to market demand: the proposed hybrid structures (that utilizes steel moment resisting frames and cross-laminated timber (CLT) as infill and floor material)

3) Accelerate adoption of existing and emerging wood-based products and building systems: the proposed method will extend the work done by the applicant and develop the required design parameters (e.g. overstrength and ductility factors) needed in the building code. This will indeed motivate the engineers to adopt the proposed method and utilize it widely.

4) Position BC as a world leader in sustainable and innovative wood-based products, and building systems in design, production, and application: this proposed hybrid

structure is novel and the knowledge and experience can be exported globally.

Figure 1: CLT-steel hybrid building

1.2 Timber-Steel Hybrid systems

Infill walls in hybrid structures have often being considered in the design as non-structural components. However, the work undertaken by the co-applicants have highlighted that CLT does indeed significantly contribute to lateral load resistance capacity of a building (Dickof *et al*. 2012; Dickof 2013; Tesfamariam *et al*. 2014). Where different seismic force–resisting systems are combined, conservative seismic forces resisting limitation is contained in the code. Without explicit consideration of the CLT, the structures will be over designed. Currently, CLT is not used as a structural infill in a hybrid system.

The proposed system allows the cross laminated timber and connections to dissipate energy and sustain the damage rather than the steel frame. Adding the infill to the steel moment frame indeed reduces the ductility of the system however allows the users to occupy the space after an extreme event with the damage being sustained by the infill panels. After the extreme event the infill panels will be crushed and need replacing, which will be a minor cost in comparison to repairing gravity load components of a structure. The new infill CLT panels can be replaced with new connections in a timely manner.

This hybrid structure's benefit will be obvious with understanding the contribution of CLT to the seismic resistance. As well, recognizing the benefit of using CLT more, the overall steel used is reduced, and cost of the building can potentially be reduced. This will encourage the designer/owners select this type of material. There are no current design guidelines for hybrid structures, and this proposal will indeed fill this gap.

The objective of this research proposal is to develop the design guideline for the next generation "wood-steel hybrid structures" that is limited in scope to 20-storey office or residential buildings. The structure selected will not have any plan irregularity, as such the design will be considered as a two dimensional frame. For different building height and infill configuration, archetypical building will be developed. Archetype is a prototypical

representation of a seismic-force-resisting system. Given the limited information and guidelines, for the proposed wood-steel hybrid buildings, in this proposal, the following objectives are achieved:

- over-strength reduction factor R_o and ductility reduction factor R_d in congruence with the NBCC 2010 for hybrid structures,
- empirical equation to quantify fundamental period of the hybrid structures for code implementation, and
- force based design guideline following the capacity based design principles. Thus in this design guideline, the complex interaction of steel frame, CLT infill, connection, and its impact on the overall seismic performance of the structure will be considered.

With the knowledge gained from this project, more hybrid structures that uses CLT can potentially increase. The National Building Code of Canada (NBCC) (NRC, 2010) recommends an equivalent static force design (ESFD) method with appropriate overstrength and ductility factors for the seismic design of structures. However, the NBCC (NRC, 2010) does not have the appropriate overstrength and ductility factors to design the proposed hybrid structure. To increase the applicability of the proposed system, in this research, overstrength and ductility factors are quantified analytically following FEMA P695. Furthermore, a fundamental period empirical formula is developed for the proposed steel-timber hybrid structure.

1.3 Research approach

The current preliminary work considered only 3-bays, with two CLT infill patterns (one interior bay and two exterior bays). The performance of the CLT-steel hybrid system is affected by CLT thickness, steel section used, connection type, distribution of connection, etc. Thus, the design consideration and building type should take this into consideration. The structure selected will not have any plan irregularity, as such the design will be considered as

a two dimensional frame. For different building height and infill configuration, archetypical building will be developed. Archetype is a prototypical representation of a seismic-force-resisting system. The archetypical buildings considered are:

- Building height
- CLT-steel connections and infill pattern
- Steel moment resisting frame design level.

The archetype buildings are selected based on the building type considered by the co-applicants and FEMA's P695 guidelines (FEMA P695). As such, these archetype buildings are not intended to simulate a specific complex building to be used; rather this study is to develop the required engineering design parameters needed for design. Once the overstrength factor, ductility factor and fundamental period of the hybrid building is developed in congruence with national building code, designers will use this factors to select the appropriate seismic load (for example) and proportion the loads on each floor following the standard design guideline.

1.4 Developing codified overstrength, ductility factor and fundamental period

The overstrength and ductility factors will be developed following the guidelines of FEMA P695 for overall system. This process accounts for potential uncertainties in ground motions, component design parameters, structural configuration, and behavioral characteristics of structural elements based on available laboratory test data.

FEMA's P695 (Quantification of Building Seismic Performance Factors FEMA P695 / June 2009) and FEMA's 795 (Quantification of Building Seismic Performance Factors: Component Equivalency Methodology FEMA P-795 / June 2011) methodology will be followed for evaluating the seismic performance equivalency of components, which are structural elements, connections, or subassemblies experiencing inelastic response that

controls the collapse performance of a seismic-force-resisting system. The recommended Component Equivalency Methodology described in FEMA P-795 report balances the competing objectives of: (1) maintaining consistency with the probabilistic, analytical, system-based collapse assessment concepts of the FEMA P-695 Methodology; and (2) providing simple procedures for comparing the tested performance of different components.

The overall steps to be followed are (FEMA P-695):

- Develop system concept (the process of quantifying overstrength and ductility starts with the development of a well-defined concept for the seismic-force-resisting system, including type of construction materials, system configuration, inelastic dissipation mechanisms, and intended range of application. Part of this already achieved through the NSERC Network research grant).
- Obtain required information (required information includes detailed design requirements and results from material, component, and system testing. This step is already achieved through the NSERC Network research grant).
- Characterize behaviour (system behavior is characterized through the use of structural system archetypes).
- Develop suitable models (development of structural models for collapse assessment).
- Analyze models (collapse assessment is performed using both nonlinear static (pushover) and nonlinear dynamic (response history) analysis procedures. The collapse for the response history will be achieved using incremental dynamic analysis).
- Evaluate performance (this step entails utilizing results from nonlinear static analyses to determine an appropriate value of the system overstrength factor, and results from nonlinear dynamic analyses to evaluate the acceptability of a trial value of ductility factor. As well, using modal analysis, the fundamental period will be computed, and the code equations will be calibrated to develop empirical equations).
- Document results (the results of system development efforts must be thoroughly documented for review and approval by an independent peer review panel, review and approval by an authority having jurisdiction, and eventual use in design and construction).

Chapter 2
Steel-Timber Hybrid System: Component Experimental Tests

The steel-timber hybrid structure incorporates Cross Laminated Timber (CLT) infill walls within the steel moment resisting frames. This structure is aimed to couple the ductile and strong steel moment frames with lighter and stiff CLT infill walls.

2.1 Conceptual design of Steel Moment Resisting Frames with CLT Infill Walls

The composite action, for the proposed hybrid system, is achieved through discrete connectors along the interface of the steel frames and infill walls (Figure 2). The connections are required to ensure CLT fixed with the steel frame and for energy dissipation under seismic shaking. A small gap is provided at the interface between the CLT wall and steel frame to allow the brackets to deform and dissipate energy under lateral loading. In this research, the CLT wall to steel frame connection is achieved by angular L-shaped steel brackets. These connection brackets are bolted to the steel frames and nailed to the CLT infill walls. Recently extensive experimental tests were carried out on the seismic behaviour of bracket connectors for various nailing types and configurations at FPInnovations and UBC (Schneider *et al*. 2014 and Popovski and Karacabeyli 2010).

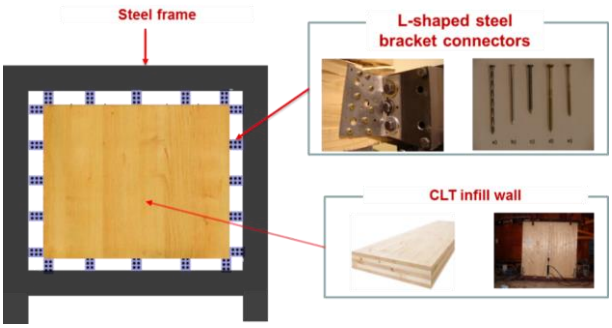

Figure 2: Conceptual representation of proposed hybrid system

2.1.1 Steel moment resisting frames (SMRFs)

Steel moment resisting frames (SMRFs) are structural systems comprised of steel beams and columns. These beams and columns are rigidly connected to allow for frame-action response under lateral loading. The frame elements and beam-column connections should be appropriately designed and detailed to resist the shear, flexural and axial load demand from earthquake and wind loads. Special detailing requirements of SMRFs are needed to ensure they have satisfactory performance under intense seismic shaking (Hamburger *et al*. 2009). SMRFs resist the lateral load demand without requiring steel bracing or shear walls. This necessitates the selection of bigger section sizes and labour intensive connections, requiring higher construction cost. In order to minimize this problem, the proposed CLT infill wall is aimed to share the lateral load demand with the SMRF which leads to economical steel sections.

2.1.2 CLT infill walls

Cross Laminated Timber (CLT) is a glued and laminated wood product consisting of flat dimensioned lumber layered in alternating directions and glued together. In Canada, CLT is typically made from Spruce/Pine/Fir (SPF) material and often used in stick framing construction. Alternating the direction of the grain in each layer creates a more isotropic panel. Furthermore, wood grain runs in two perpendicular directions in the plane of the panel resulting in a decrease of splitting and shrinkage. Typical CLT construction uses the panels as both the floor and wall systems, connected primarily with long screws and/or nailed L-shaped brackets. CLT walls are typically fastened to concrete foundations with L-shaped brackets and floor panels sit on the walls connected using either long European screws or nailed L-shaped brackets. Subsequent storeys are constructed in a similar manner with the walls on top of the floor panels and typically connected with similar L-shaped brackets.

2.1.3 Infill walls to frame connections

For the past four years, extensive experimental tests have been carried out on the seismic behaviour of angular L-shaped steel brackets (Schneider *et al*. 2014). The experimental tests considered 98 steel bracket connectors under parallel and perpendicular to the grain loading directions. Damage indices have been quantified from semi-static cyclic loading tests. From the perpendicular to the grain direction tests, the observed dominant type of failure was pull-out of nails. However, wood crushing failure mode was also observed on a few samples for tests parallel to the grain direction. In this research project, the CLT wall is connected to the steel frame using the studied angular L-shaped steel brackets.

2.2 Experimental tests

The following section presents a summary of the experimental tests carried out on the L-shaped steel brackets and CLT walls. The considered wall is a 3-ply CLT with an overall thickness of 94 mm. The layout of steel brackets and a sample test setup for the CLT wall is depicted in Figure 3a. During the tests, rigid body motion with negligible shear deformation was observed in the CLT walls. Moreover, for static and cyclic tests large deformations were observed in the brackets and fasteners. For details of the tested wall configurations and results see Popovski and Karacabeyli (2010). Schneider *et al*. (2014) performed experimental tests by considering one type of L-shaped steel bracket: the SIMPSON Strong Tie bracket 90*48*3.0*16 (Figure 3b). This bracket was implemented with different nail types including: spiral nail 16d*3 ½, screw 5*90, and screw 4*70, defined as Connection A, Connection B, and Connection C, respectively.

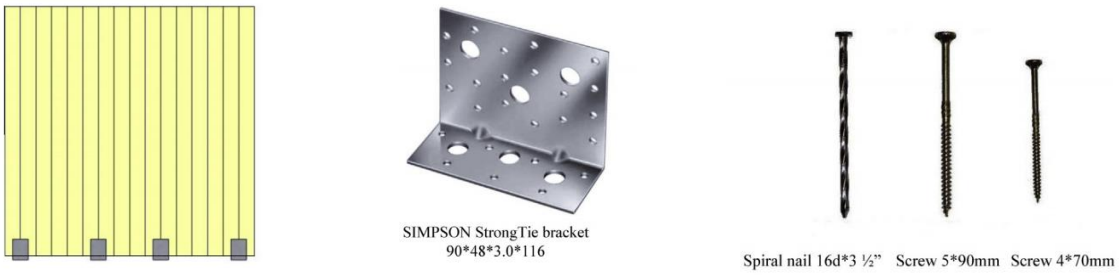

a) b) c)

Figure 3: Wall configuration and L-shaped steel bracket details (Shen *et al*. 2013)

The experimental test set-ups for the parallel and perpendicular to the grain loadings are shown in Figure 4 and Figure 5, respectively.

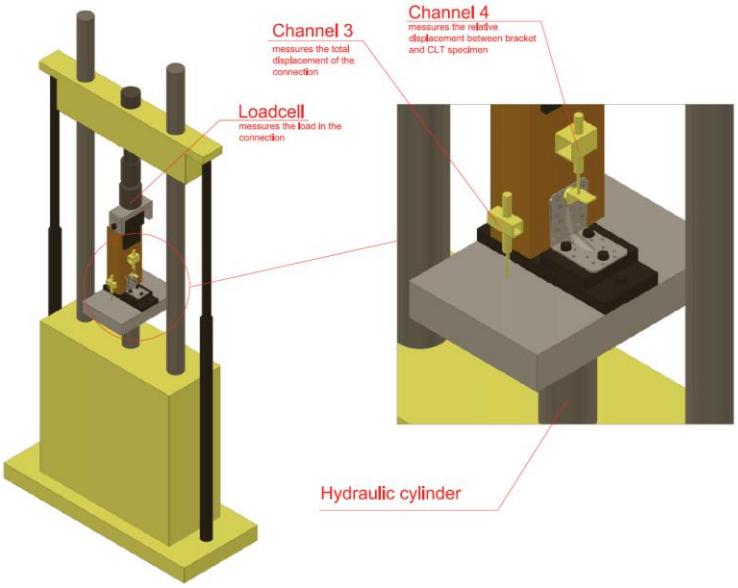

Figure 4: Bracket connection set-up for test along parallel to the grain direction (fully adopted from Schneider *et al*. 2014)

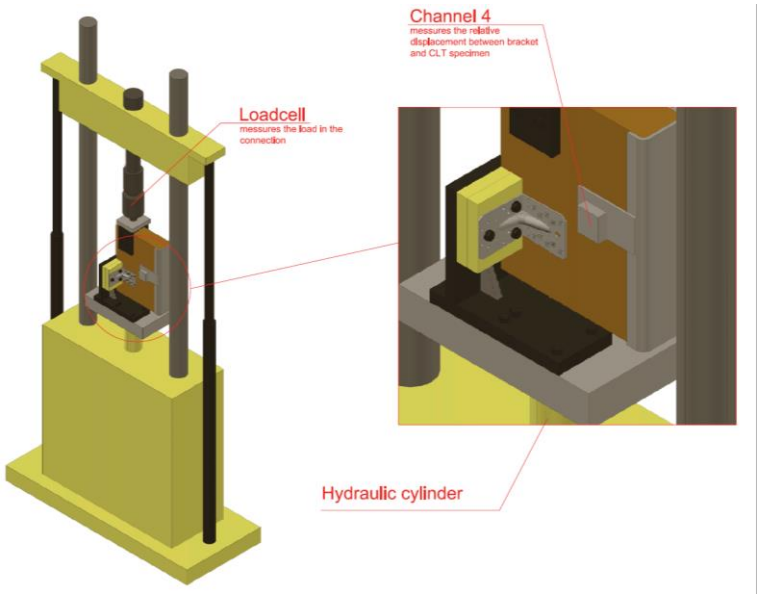

Figure 5: Bracket connection set-up for test along perpendicular to the grain direction (fully adopted from Schneider *et al*. 2014)

a) b)

Figure 6: Bracket connection testing; a) Parallel to the grain and b) Perpendicular to the grain (© 2014 Johannes Schneider, by permission)

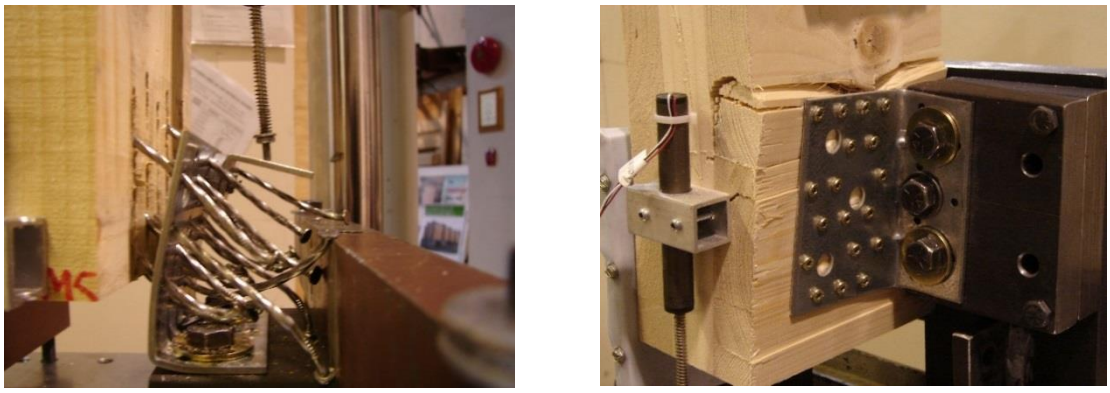

a) b)

Figure 7: Typical failure mode in Connection A; a) Parallel to the grain test and b) Perpendicular to the grain (© 2014 Johannes Schneider, by permission)

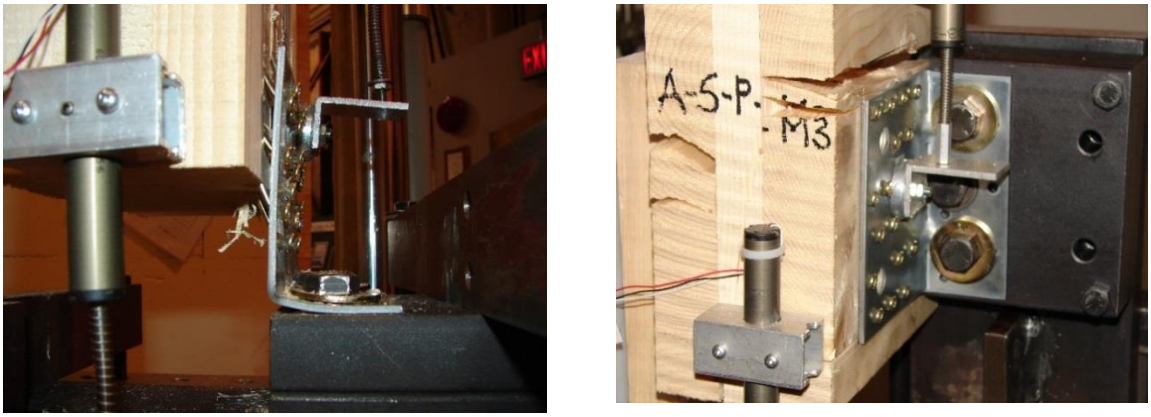

a) b)

Figure 8: Typical failure mode in Connection C; a) Parallel to the grain test and b) Perpendicular to the grain (© 2014 Johannes Schneider, by permission)

The test set up and common failure modes for the CLT walls tested are depicted in Figures 9-11.

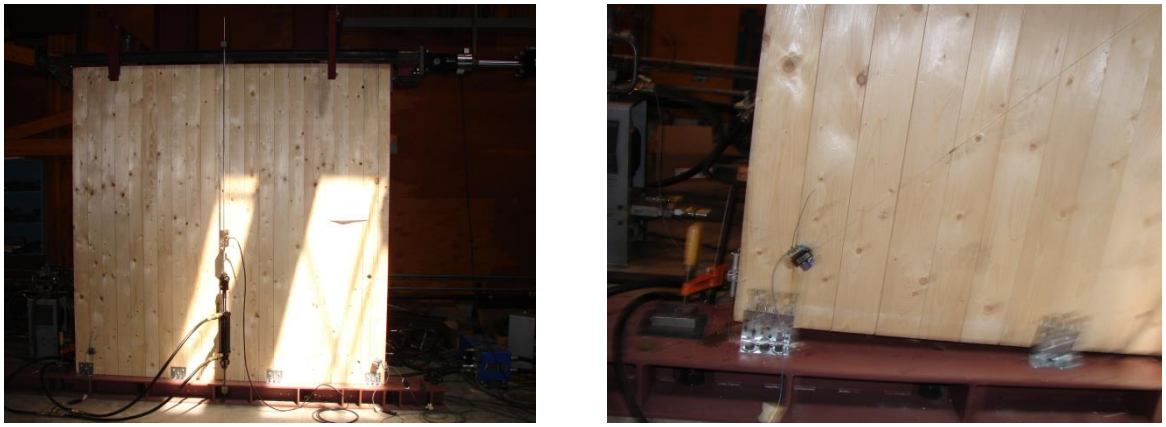

a) b)

Figure 9: CLT wall testing; a) test set up b) rocking of wall and failure of connectors (© 2014 Marjan Popovski, by permission)

a) b)

Figure 10: Failure of connectors during the test; a) low amplitude load b) high amplitude loads connectors (© 2014 Marjan Popovski, by permission)

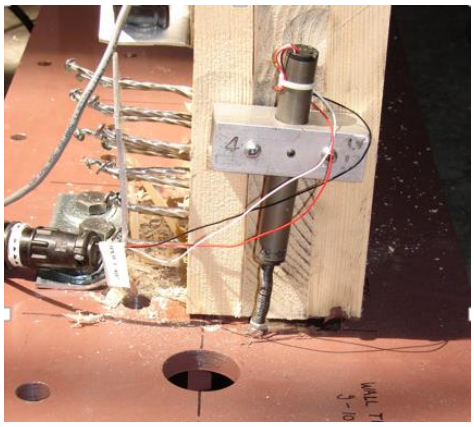

a)

b)

Figure 11: Failure of connectors during the test a) full pullout failure b) crushing of wood connectors (© 2014 Marjan Popovski, by permission)

Chapter 3

Steel-Timber Hybrid System: Numerical models

Numerical modeling was carried out using the Open System for Open System for Earthquake Engineering Simulation (OpeenSees) (Mazzoni *et al*. 2006) finite element program (OpenSees, 2010). For this research, a multi-scale modeling approach was adopted (Figure 12). The procedure outlined in Figure 12 entails:

- Carry out experimental tests for the different components and system (this is provided in Chapter 2).
- The spring element of the connection is calibrated for the pinching4 material model in OpenSees.
- The numerical model for the CLT system is determined.
- The components are assembled to form the hybrid system.

In this approach, component level modeling and calibrations are performed first for each element, i.e., steel brackets and CLT walls. Subsequently, these components are assembled in combinatorial form to achieve the desired system level property (CLT infilled SMRFs). The following subsections will illustrate both the component and system level modeling and calibration approaches.

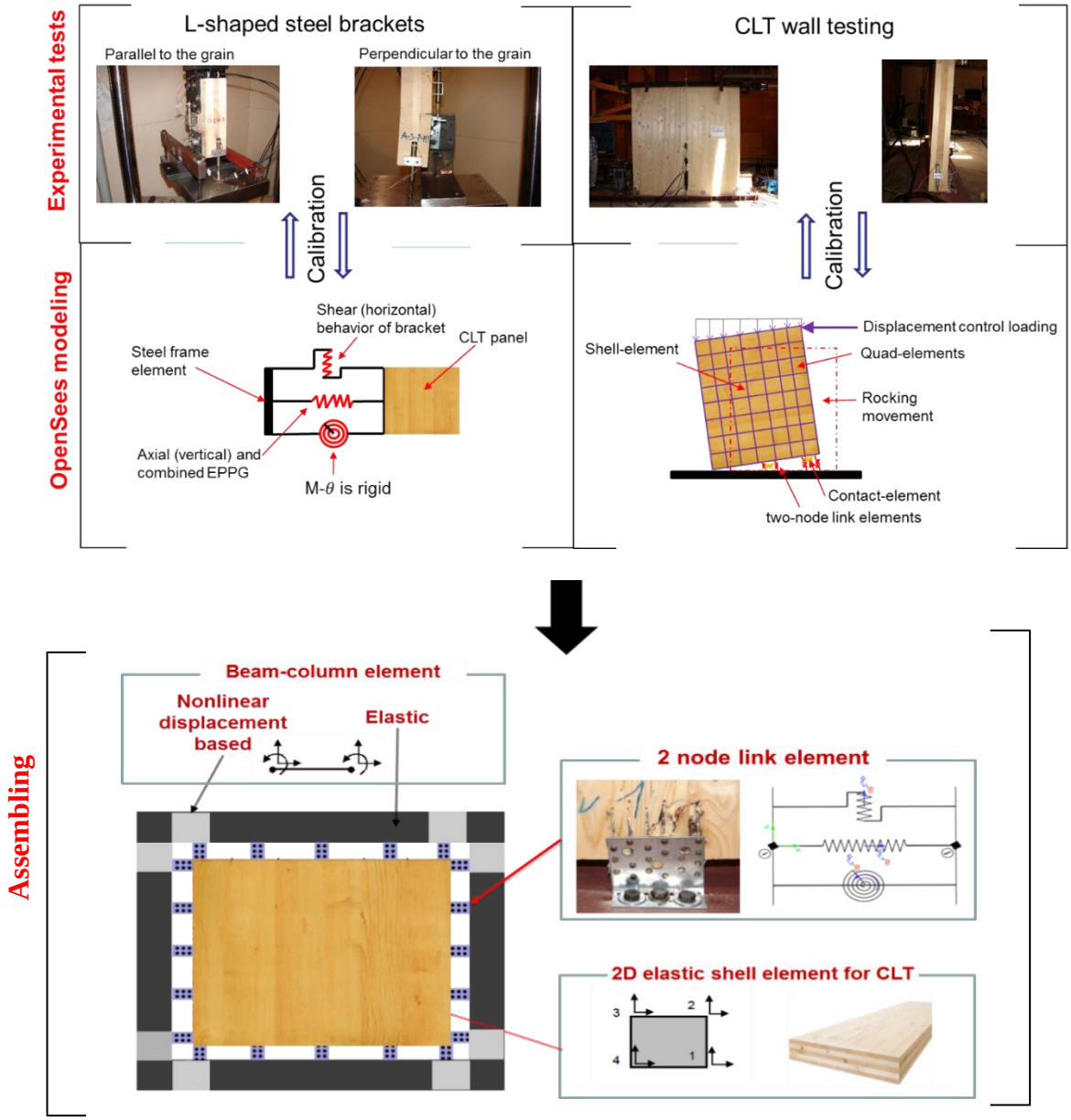

Figure 12: Component level modeling, calibration, and assembling process flowchart

3.1 Component level modeling

The following subsections provide the details of component model for the steel-timber hybrid structure.

3.1.1 Modeling of steel frame members

The steel frame members are modelled with nonlinear displacement-based beam-column elements at the end of the member (to represent the spreading plastic hinge zone) as displayed in Figure 12, and linear elastic beam-column elements for the middle portion of each member following Bezabeh (2014); Dickof (2013); Dickof *et al*. (2014). The nonlinear steel elements use the modified Ibarra-Krawinkler Deterioration model (Lignos and Krawinkler 2011) with parameters based on the moment-curvature relationship given in ASCE 41 (2006) to account for both stiffness and strength degradation during loading. Figure 13 (a and b) show the modified Ibarra-Krawinkler Deterioration model for monotonic loading and cyclic loading, respectively.

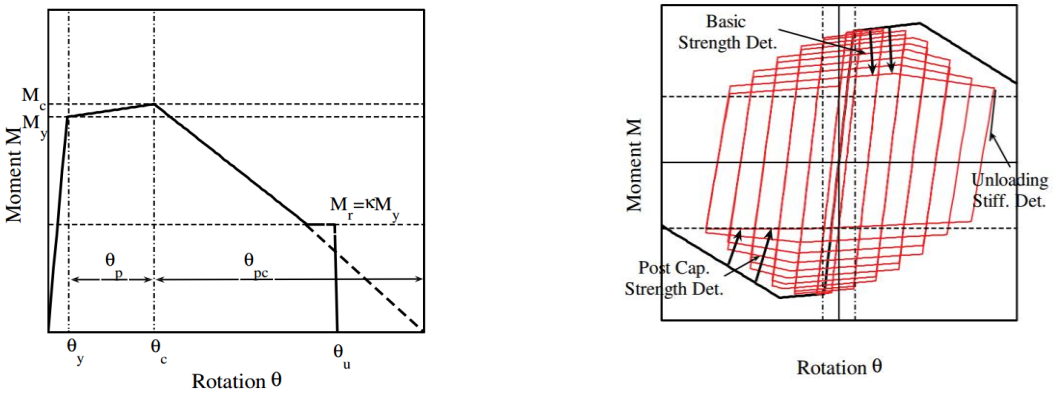

Figure 13: Modified Ibarra Krawinkler Deterioration model; a) Monotonic loading curve; b) basic modes of cyclic deterioration and associated definitions (fully adopted from Lignos and Krawinkler 2011)

The ASCE 41 (2006) recommendation to calculate the parameters (moment and rotation) of the model are illustrated in Figure 14 (a and b). In Figure 14, Q and Q_y are the generalized

component load and strength values, respectively. For frame members the rotation (θ) is calculated from the slope of the deflection curve of a beam member of length (L) as shown in Figure 13b. The plastic rotations (a and b) of Figure 13a are calculated based on the class of section. The detailed calculations of the parameters to define the specific deterioration model can be found elsewhere (ASCE 41, 2006 and Dickof, 2013).

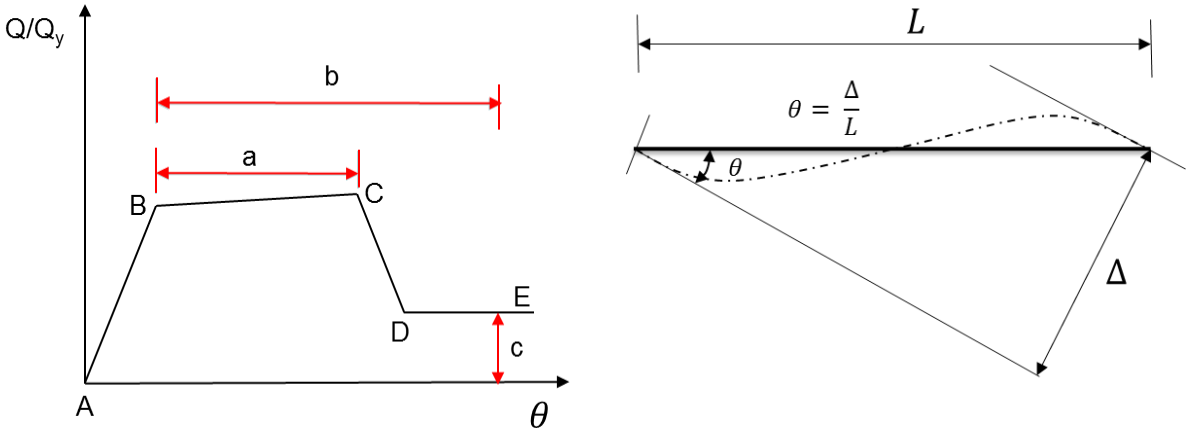

a) b)

Figure 14: Moment-curvature (rotation) relationship; a) Generalized force deformation for steel elements; b) definition of chord rotation
(fully adopted and reproduced from ASCE 41 2006)

3.1.2 Modeling of cross laminated timber (CLT)

Dickof *et al*. (2014) and Bezabeh (2014) have shown that varying the thickness of the panels has little effect on the global system behaviour during earthquake excitation. Therefore, the considered infill walls are 3-ply panels with outer lams of 32 mm and an inner lam of 35 mm, providing the overall thickness of 99 mm. The panels are modelled using Quad (quadrilateral) shell elements in OpenSees following work by Shen *et al*. (2013) and Dickof *et al*. (2014) as shown in Figure 15.

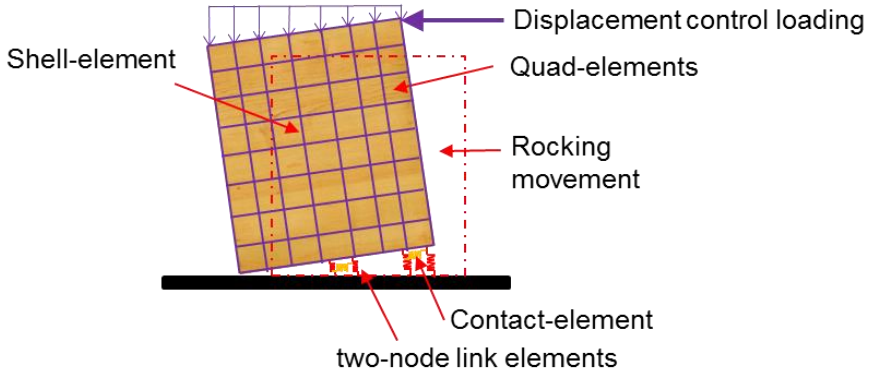

Figure 15: CLT wall model

In the finite element model, CLT panels were simplified to a single 99 mm panel element with homogeneous, isotropic, fully elastic properties using the OpenSees ndMaterial. ElasticIsotropic material with properties shown in Table 1 were assigned to model the ndMaterial. This simplification of the CLT panel behaviour is similar to simplifications made in other CLT panel behaviour studies (Ceccotti 2008; Fragiacomo *et al*. 2011; Shen *et al*. 2013).

Table 1: CLT material properties

Material Properties	Design Values
Elastic Modulus Ec	9500 MPa
Shear Strength (Fv,c)	1.5 MPa
Compression Strength (Fc,c)	30.0 MPa
Compression Strength Perp-to-Grain (Fcb,c)	5.0 MPa
Poisson's Ratio	0.46

The OpenSees command to model the Quad elements according to Mazzoni *et al*. (2007) takes the following form:

element quad $eleTag $iNode $jNode $kNode $lNode $thick $type $matTag <$pressure $rho $b1 $b2>,

where

$eleTag =	unique element object tag
$iNode $jNode $kNode $lNode =	four nodes defining element boundaries input in counter-clockwise order around the element.
$thick =	element thickness
$type =	string representing material behaviour. The type parameter can be either "PlaneStrain" or "PlaneStress."
$matTag =	tag of nDMaterial
$pressure =	surface pressure (optional, default = 0.0)
$rho =	element mass density (per unit volume) from which a lumped element mass matrix is computed (optional, default=0.0)
$b1 $b2 =	constant body forces defined in the isoparametric domain (optional, default=0.0)

3.1.3 Connections

The L-shaped steel brackets were modelled in OpenSees as two node link elements between the steel frame and CLT panel. The axial, shear, and rotational behaviour of these elements are defined by specific material models. Since the confinement between the frame and wall is provided with a small gap to allow for bracket deformation, the two node link elements are modelled as non-zero length elements. In this case, the rotational and transverse degree of freedoms are coupled as recommended by Mazzoni *et al*. (2007). However, to simplify the computational demand, P-Δ effects along the local axis are neglected. Moreover, it is assumed that these elements do not contribute to the Rayleigh damping during the nonlinear stage of loading. The two node link elements are modelled using the calibrated Pinching4 material model of OpenSees consistent with the approach of Dickof *et al*. (2014) and Bezabeh (2014). Moreover, in this approach the rotational component of the link is considered to be rigid and the axial component represents the vertical property of the bracket as shown in Figure 16.

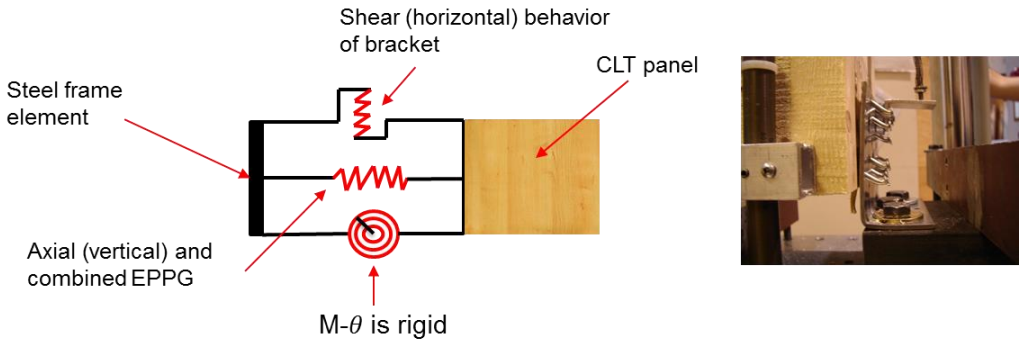

a) b)

Figure 16: a) Connection modeling using two node link element and b) typical frame to CLT panel connection failure

The details of the *Pinching4 material model* calibration, based on experimental data produced by Schneider *et al*. (2014), will be discussed in subsequent sections. For this specific research project, the nonlinear behaviour of the connections is modelled in both shear and axial directions. The OpenSees command to model the two node link element model according to Mazzoni *et al*. (2007) takes the following form:

element twoNodeLink $eleTag $iNode $jNode -mat $matTags -dir $dirs <-orient <$x1 $x2 $x3> $y1 $y2 $y3> <-pDelta (4 $Mratio)> <-shearDist (2 $sDratios)> <-doRayleigh> <-mass $m>

where

$eleTag =	unique element object tag
$iNode and $jNode =	end nodes
$matTags =	tags associated with previously-defined UniaxialMaterial objects
$dirs =	material directions: 2D-case: 1,2 - translations along local x, y axes; 3 - rotation about local z axis
$x1 $x2 $x3 =	vector components in global coordinates defining local x-axis (optional)
$y1 $y2 $y3 =	vector components in global coordinates defining local y-axis (optional)
$Mratios =	P-Delta moment contribution ratios, size of ratio vector is 2 for 2D-case and 4 for 3D-case
$sDratios =	shear distances from iNode as a fraction of the element length, size of ratio vector is 1 for 2D-case and 2 for 3D-case
-doRayleigh =	to include Rayleigh damping from the element (optional, default = no Rayleigh damping contribution)
$m =	element mass (optional, default = 0.0)

3.2 System level modeling

Following the component level experimental tests and numerical modeling, a typical CLT infilled SMRFs system is developed (Figure 19). This hybrid system combines ductile steel frames with CLT walls through angular L-shaped steel bracket connections. At the interface of the wall and frame a gap is provided in order to allow the brackets to deform and dissipate energy during the seismic shaking. The behaviour of the bracket and the confinement due to axial contact between the frame and panel were combined to form the axial component of the two node link element. The confinement behaviour to account for the space between the frame and panel was modelled using the elastic perfectly plastic gap uniaxial material (EPPG). EPPG is a trilinear hysteretic uniaxial material model which consists of a physical gap with zero stiffness and strength, linear elastic region, and post-yielding plastic region. Figure 17 (a and b) show the compression-only and tension-only gap hysteretic properties, respectively.

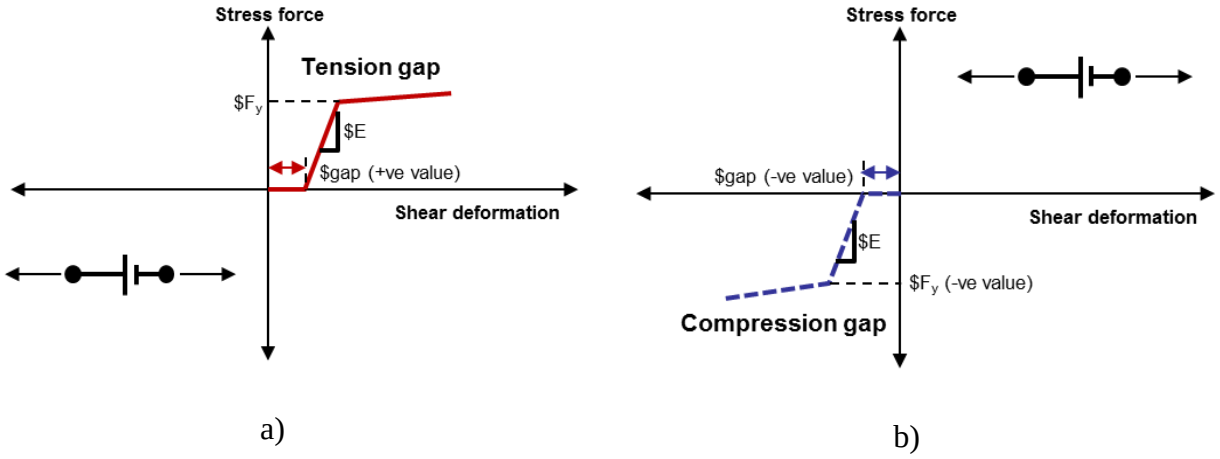

Figure 17: Elastic perfectly plastic gap (EPPG); a) Tension-only gap and b) Compression-only gap (Mazzoni *et al*. 2007)

The OpenSees command to model the EPPG uniaxial material model according to Mazzoni *et al*. (2007) takes the following form:

uniaxialMaterial ElasticPPGap $matTag $E $Fy $gap <$eta> <damage>

where

$matTag =	integer tag identifying material
$E =	tangent stiffness
$Fy =	stress or force at which material reaches plastic state
$gap =	initial gap
$eta =	hardening ratio
damage =	switch to accumulate damage in the material. If damage is omitted, default value, the gap material "re-centres" on load reversal.

For this research, accounting for the behaviour of wood under load, the compression only gap model that was depicted in Figure 17b was used to model the confinement property of the system. Since wood crushing is a local phenomenon around the steel brackets, the stress at which the material reaches a plastic state is calculated by considering the wood strength in parallel and perpendicular direction over a 200mm contact length. Reid and Peng (1997)

showed the dependence of the post crushing stiffness of wood over its density, and more specifically, they showed the increase in post crushing stiffness due to the densification of wood. For this reason, the post-yield stiffness of the panel was assigned to be 1% of elastic panel stiffness for this research. Following the approach of Dickof *et al*. (2014), this stiffness was quantified over the 200mm length and full thickness of the CLT panel.

The EPPG gap material and the two node link elements of bracket connections were combined using the parallel material combination approach as shown in Figure 18. In this approach, strains are kept equal while the stresses are added up to form a single material model (Dickof *et al*. 2014).

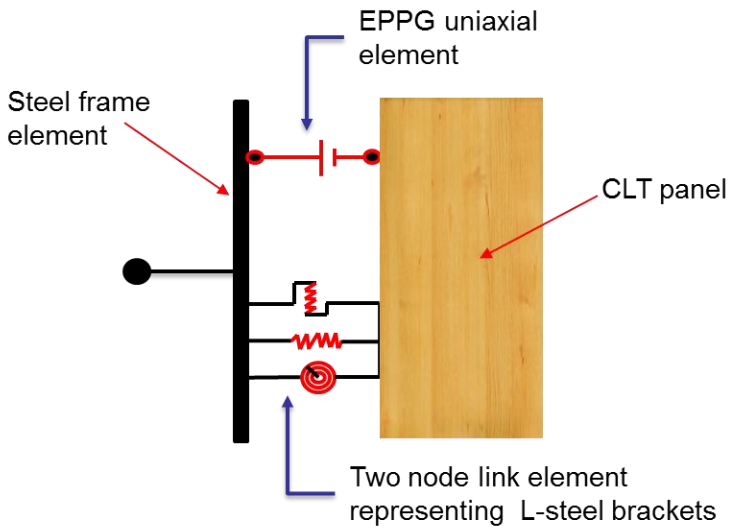

Figure 18: Parallel formulation of *EPPG* gap element and *two node link element*

The OpenSees command to model the parallel material combination according to Mazzoni *et al*. (2007) takes the following form:

UniaxialMaterial Parallel $matTag $tag1 $tag2...

where

$matTag = unique material object integer tag
$tag1 $tag2 = identification of materials making up the material model (two node link element of brackets and EPPG)

Following the parallel material model formulation, all components are assembled to give the final CLT infilled SMRFs as shown in Figure 19. The next sections will focus on the calibration of the component models and behaviour of the proposed hybrid system.

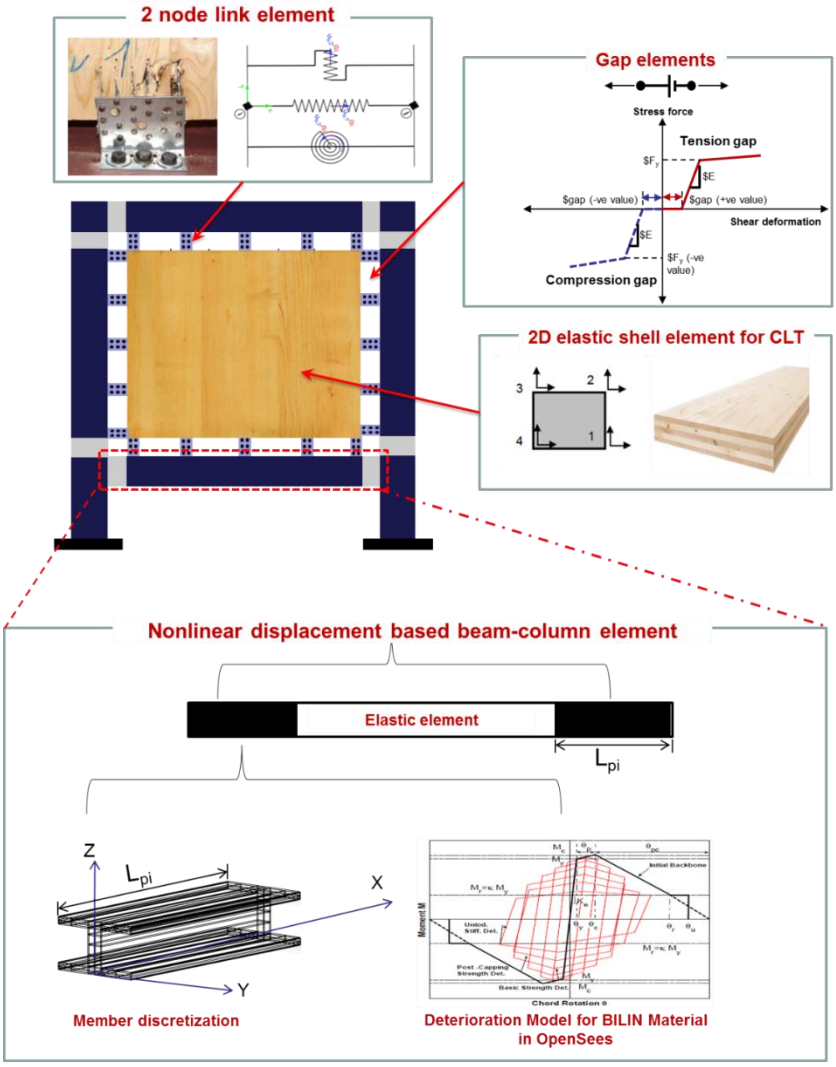

Figure 19: System level modeling of CLT infilled SMRFs (Bezabeh *et al*. 2014b)

3.3 Calibration of OpenSees models

This section presents the hysteretic model calibration of a Pinching4 material model of OpenSees. Following the experimental tests of Schneider *et al*. (2014), Shen *et al*. (2013), the researchers calibrated the connections with Saw and Pinching4 hysteretic models of OpenSees and suggested the latter one is a better representative of the seismic behaviour of connectors. In this section, calibration of the Pinching4 material model is carried out in detail considering three bracket connection types. This model comprises of piecewise linear curves to model the pinched force-deformation responses that accounts for stiffness and strength degradation when the bracket is subjected to cyclic loading (Shen *et al*. 2013; Mazzoni *et al*. 2007). This material model consists of 16 parameters, i.e., ePd1, ePf_1, ePd_2, ePf_2, ePd_3, ePf_3, ePd_4, ePf_4, eNd_1, eNf_1, eNd_2, eNf_2, eNd_3, eNf_3, eNd_4, and eNf_4 as shown in Figure 20.

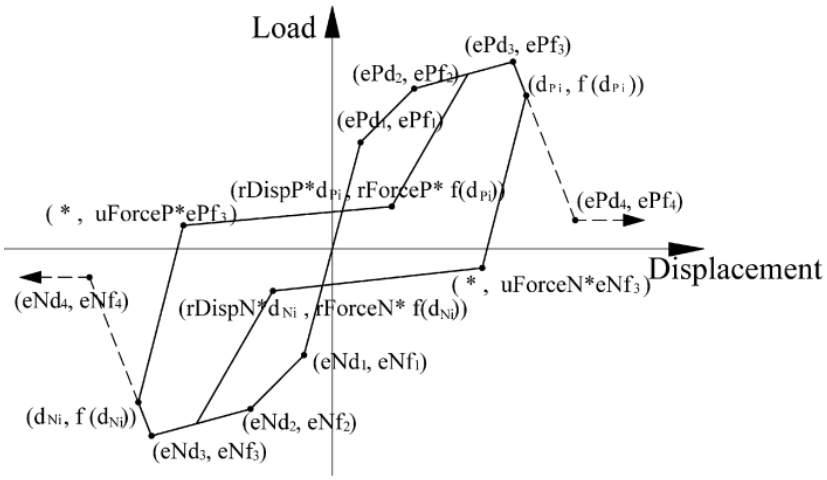

Figure 20: Hysteretic envelope for the Pinching4 model
(fully adopted from Shen *et al*., 2013)

The main goal of this section is to calculate these parameters by tuning the values manually until the experimental and finite element results are similar. The definitions and

procedures of calculations for the *Pinching4 hysteretic model* can be found elsewhere (Shen *et al*. 2013 and Mazzoni *et al*. 2007). In the Pinching4 material model the deterioration in stiffness is calculated using Equation 1 where; k_i is the unloading stiffness at time t_i, k_0 is the initial unloading stiffness, and δk_i is the value of the stiffness damage index at time t_i.

$$k_i = k_o(1-\delta k_i) \quad [1]$$

According to Mazzoni *et al*. (2007), the stiffness damage index at time t_i (δk_i) is calculated as follows:

$$\delta k_i = \left(gK1(d_{\max})^{gK3} + gK2\left(\frac{E_i}{E_{monotonic}}\right)^{gK3} \right) \leq gKLim \quad [2]$$

where dmax = the deformation demand (computed using Equation 3), gK1, gK2, and gK3 are floating point values to control the strength degradation, E is the hysteretic energy of the current displacement increment, Emonotonic is the energy required to define failure under monotonic load, and defmax and defmin are, respectively, positive and negative deformations to define failure (Mazzoni *et al*. 2007).

$$d_{\max} = \max\left[\frac{d_{\max i}}{def_{\max}}, \frac{d_{\min i}}{def_{\min}}\right] \quad [3]$$

Moreover, according to Lowes *et al*. (2003), the deformation that defines the reloading cycle ($d_{max\ i}$) is formulated as a function of maximum historic demand ($d_{max\ o}$) as:

$$d_{\max i} = d_{\max o}(1+\delta k_i) \quad [4]$$

For the purpose of calibration, the finite element model that was created in an earlier section is used as shown in Figure 19. The cyclic loading analyses were conducted by using CUREE loading protocols that consist of primary and trailing cycles which are functions of the ultimate displacement of monotonic loading analysis (Schneider *et al*. 2014). It is important to note that the loading protocol of the experimental tests of Schneider *et al*. (2014)

and finite element analyses are almost identical. Figure 21 and Figure 22 show the loading schedules for parallel to the grain and perpendicular to the grain loading directions, respectively.

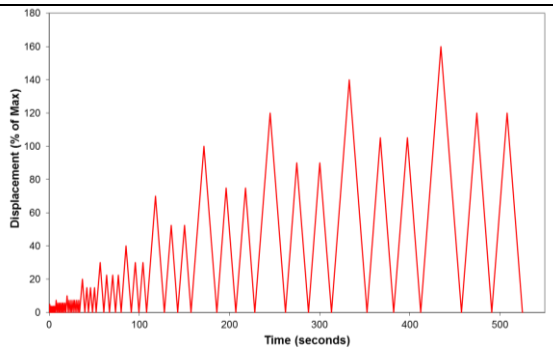

Figure 21: Cyclic displacement schedule CUREE Test protocol for parallel to the grain test (© 2014 Johannes Schneider, by permission)

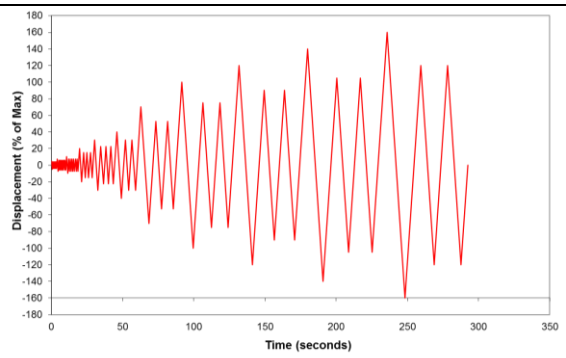

Figure 22: Cyclic displacement schedule CUREE test protocol for perpendicular to the grain test (© 2014 Johannes Schneider, by permission)

Cyclic loading analyses were carried out using OpenSees along both parallel and perpendicular to the outer layer grain direction for all three Connections: A, B, and C.

3.3.1 Hysteretic model calibration of connection A

As defined in an earlier section, Connection A consisted of a SIMPSON Strong Tie bracket (90*48*3.0*16) with 18 Spiral nails (16d*3 ½). Shen *et al*. (2013) reported the loss of contact between the brackets and CLT element as deformation accumulates. The obtained OpenSees results and experimental data compared in Figure 22 and Figure 23 for tests along parallel and perpendicular loading directions, respectively.

Figure 23 shows a good agreement between the experimental and OpenSees analysis result. In general, the hysteretic envelope from OpenSees analysis is slightly larger than the experimental results. Moreover, better agreement is observed in the reloading stiffness at the initial loading stages. Figure 24 shows the comparison of responses for tests along perpendicular to the grain direction. As can be seen in Figure 24 there is better agreement in

negative backbone region than the positive loading region. For both test directions, Figure 23 and Figure 23 revealed that the OpenSees Pinching4 material model predicts the pinching part very well.

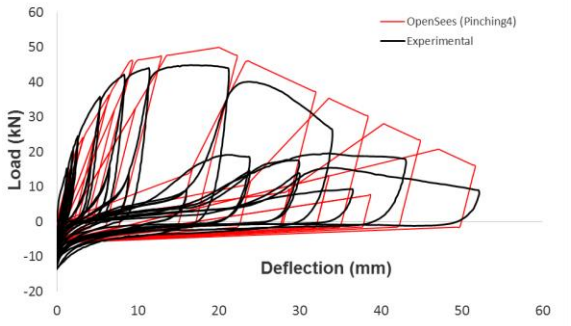

Figure 23: Comparison of experimental and OpenSees pinching4 material model for Connection A in parallel to the grain direction

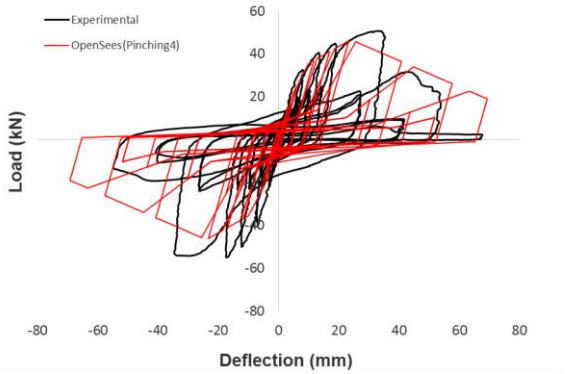

Figure 24: Comparison of experimental and OpenSees pinching4 material model for Connection A in perpendicular to the grain direction

3.3.2 Hysteretic model calibration of connection B

Connection B consists of a SIMPSON Strong Tie bracket (90*48*3.0*16) with 18 Screws (5*90). The obtained OpenSees results and experimental data are compared in Figure 25 and Figure 26 for tests along parallel and perpendicular loading directions, respectively. Figure 25 shows better agreement in the initial loading stiffness is obtained. However, the failure displacement of the experiment was shown to be larger than the Pinching4 model prediction.

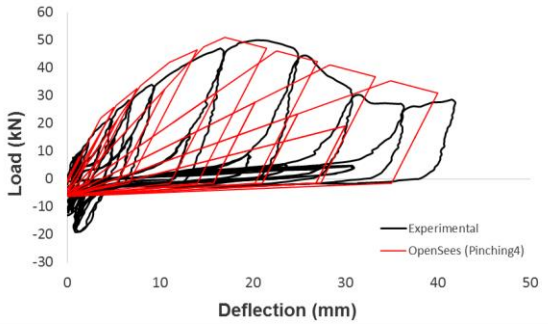

Figure 25: Comparison of experimental and OpenSees pinching4 material model for Connection B in parallel to the grain direction

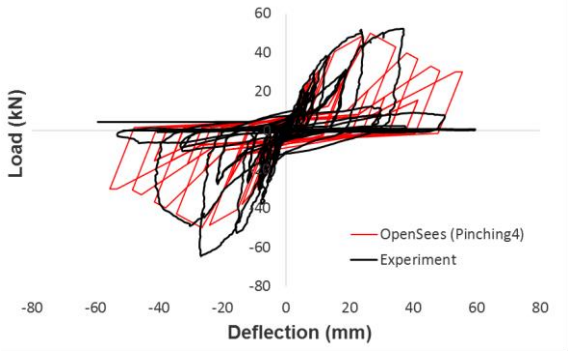

Figure 26: Comparison of experimental and OpenSees pinching4 material model for Connection B in perpendicular to the grain direction

3.3.3 Hysteretic model calibration of connection C

Connection C was comprised of a SIMPSON Strong Tie bracket (90*48*3.0*16) with 9 Screws (4*70). The obtained OpenSees results and experimental data are compared in Figures 27 and 28 for tests along parallel and perpendicular loading directions, respectively. As can be seen in Figure 27, better agreement in the initial loading stiffness is obtained. However, the failure displacement for the analysis proved to be larger than the experiment.

Figure 27 shows better agreement in the negative backbone region than the positive loading region. Furthermore, for both test directions, Figure 27 and Figure 28 revealed that the OpenSees Pinching4 material model predicts the pinching part very well.

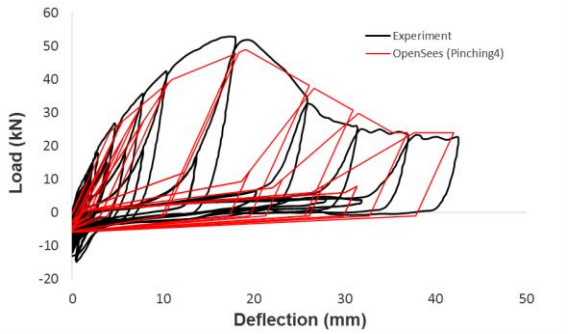

Figure 27: Comparison of experimental and OpenSees pinching4 material model for Connection C (parallel to the grain direction)

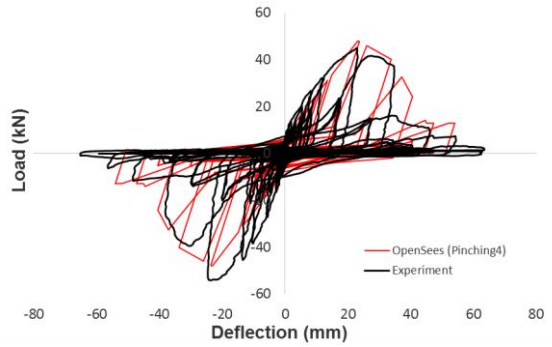

Figure 28: Comparison of experimental and OpenSees pinching4 material model for Connection C (perpendicular to the grain direction)

The final calibrated hysteretic curve parameters for all connection types are summarized in Table 2. At this point it is important to note that these parameters of the Pinching4 material model are used to model the nonlinearity and cyclic behaviour of connection brackets that are used to perform seismic and collapse simulations of the CLT infilled SMRFs.

Table 2: Calibrated Pinching4 model parameters

Connection type		**Connection-A**		**Connection-B**		**Connection-C**	
Direction	**Parameters**	**Parallel to grain**	**Perpendicular to grain**	**Parallel to grain**	**Perpendicular to grain**	**Parallel to grain**	**Perpendicular to grain**
Positive backbone	ePf_1 [kN]	20	18.68	21	20.5	24	13
	ePf_2 [kN]	46	35.6	42	40.2	40	48.1
	ePf_3 [kN]	50	48	51	50.4	49	39.8
	ePf_4 [kN]	7	17.1	18.7	30.6	24	12.91
	ePd_1 [mm]	2.15	4	3.23	4.9	4	3.1
	ePd_2 [mm]	9	9.8	11	15	11	23.2
	ePd_3 [mm]	20	24	17	26	19.1	34.3
	ePd_4 [mm]	60	70	54	49	35	45.1
Negative backbone	eNf_1 [kN]	-20	-18.68	-21	-20.5	-24	-13
	eNf_2 [kN]	-46	-35.6	-42	-40.2	-40	-48.1
	eNf_3 [kN]	-50	-48	-51	-50.4	-49	-39.8
	eNf_4 [kN]	-7	-17.1	-18.7	-30.6	-24	-12.91
	eNd_1 [mm]	-2.15	-4	-3.23	-4.9	4	-3.1
	eNd_2 [mm]	-9	-9.8	-11	-15	-11	-23.2
	eNd_3 [mm]	-20	-24	-17	-26	-19.1	-34.3
	eNd_4 [mm]	-60	-70	-54	-49	-35	-45.1
pinching	rDispP	0.55	0.5	0.65	0.5	0.72	0.6
	fForceP	0.15	0.3	0.15	0.25	0.18	0.25
	uForceP	0.03	0.05	0.02	0.05	0.02	0.05
	rDispN	0.55	0.5	0.65	0.5	0.72	0.6
	fForceN	0.15	0.3	0.15	0.25	0.18	0.25
	uForceN	0.03	0.05	0.02	0.05	0.02	0.05
Unloading stiffness degradation	gK1	0	0	0	0	0	0
	gK2	0	0	0	0	0	0
	gK3	0	0	0	0	0	0
	gK4	0	0	0	0	0	0
	gKLim	0	0	0	0	0	0
Reloading stiffness degradation	gD1	0.97	0.95	0.97	0.97	0.97	0.95
	gD2	0	0	0	0	0	0
	gD3	0	0	0	0	0	0
	gD4	0	0	0	0	0	0
	gDLim	0.05	0.1	0.08	0.1	0.03	0.1
Strength degradation	gF1	0	0	0	0	0	0
	gF2	0	0	0	0	0	0
	gF3	0	0	0	0	0	0
	gF4	0	0	0	0	0	0
	gFLim	0	0	0	0	0	0
Energy degradation	gE	1	1	1	1	1	1

Chapter 4

Parametric study on single-storey lateral behaviour of CLT-SMRFs

Bezabeh *et al*. (2014a) studied the energy dissipative capacity of a single-bay single-storey CLT infilled SMRF through Equivalent Viscous Damping (EVD). The authors performed a parametric study by varying the modeling variables of the hybrid structure. Table 3 summarizes the varied modeling variables.

Table 3: Modeling variables (Bezabeh *et al*. (2014a)

A: Bracket Spacing (m)	B: Gap (mm)	C_t: Panel Thickness (mm)	D: Panel Strength (MPa)	E: Post Yield Stiffness (%)
0.4	20	99	17.5	1
0.8	50	169	25	3
1.6	80	239	37.5	5

In their study, they performed static pushover and quasi-static cyclic loading analyses for all combinations of variables in Table 3. The aim of their static pushover analyses was to calculate the yielding and ultimate displacement of the hybrid system. As the total combination of modeling variables of Table 3 yields 243 single-bay, single-storey CLT infilled SMRFs. However, due to a shortage of space, the authors did not discuss the sensitivity of responses. Therefore the aim of this section is to focus on the response sensitivities to the modeling variables of Table 3 which aids in the model development for multi-storey hybrid structures.

4.1 Response sensitivity to bracket spacing

Figure 29 shows the variation of capacity curves with bracket spacing. The analyses were performed by keeping a constant gap of 20mm, CLT panel thickness of 90mm, and CLT crushing strength of 17.5. It is evident from Figure 29 that the initial stiffness was the same

for all models. At approximately 50mm of deflection, an increase in stiffness was observed for models with bracket spacing of 0.4m. Moreover, the ultimate strength decreased as the bracket spacing was increased.

The cyclic response sensitivity to bracket spacing is depicted in Figure 30. The comparison of cyclic response revealed that stable hysteresis loops were obtained for models with lower bracket spacing. However, a slight increase in pinching was observed for models with a bracket spacing of 0.4m. Comparatively, models with a bracket spacing of 0.8m yield a relatively stable hysteresis loops with acceptable pinching behaviour.

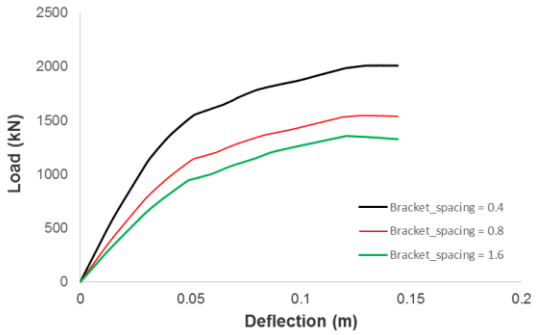

Figure 29: Variation of capacity curves with bracket spacing

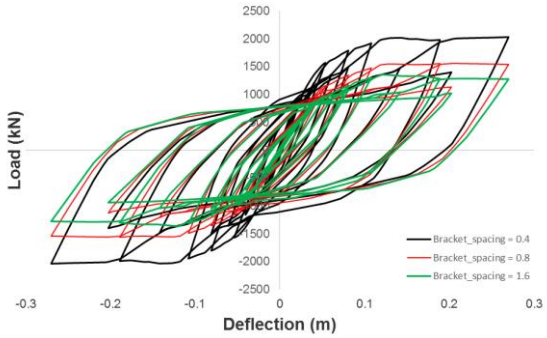

Figure 30: Cyclic response sensitivity to bracket spacing

4.2 Response sensitivity to gap

The effect of confinement gap was studied parametrically by keeping a constant panel thickness of 99 mm, CLT crushing strength of 17.5 MPa, and connection bracket spacing of 0.8m. The results of the monotonic pushover analyses are depicted in Figure 31. Initially this gap was provided to accommodate construction tolerances and allow the brackets to deform and dissipate energy. Significant variation in stiffness was observed at a deflection of 75mm (the point where the CLT starts to share the load). The post-yielding behaviour of these models is quite different as can be seen in Figure 31. Models with a gap magnitude of 80mm showed unstable response after yielding occurred. The ultimate strength of the system was

higher for models with a smaller gap. Comparatively, a model with 20 mm of gap has the desired stable capacity curve.

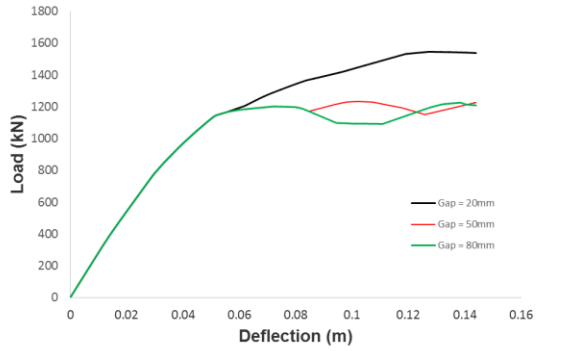

Figure 31: Variation of capacity curves with provided gap

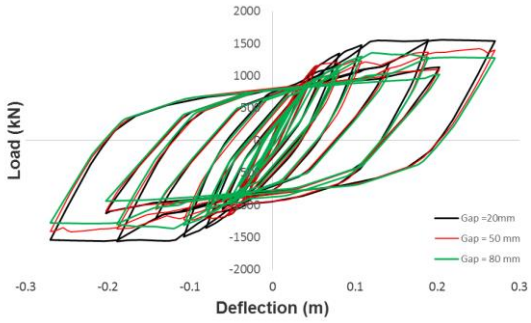

Figure 32: Cyclic response sensitivity to gap

Figure 32 shows the cyclic response sensitivity to the magnitude of provided gap. Models with a 20 and 50mm gap were characterized by a high degree of pinching. Fat hysteresis loops occurred for models with a gap of 80mm. This shows that the energy dissipation increases with the gap size. However, due to its higher loading capacity and stable hysteresis loops, a 20mm gap is suggested to model the multi-storey hybrid structure.

Chapter 5
Overview of Seismic Force Modification Factors

The Canadian national building design code (NBCC) has evolved through time learning from the devastating earthquakes in Canada and other parts of the world (Rainer and Northwood 1979; Heidebrecht 2003). The evolution of design base shear (V) in the NBCC is summarized in Table 4. Discussion and rationality of each design change provision shown in Table 4 are discussed by various researchers: Uzumeri et al. (1978) have described the developments of the 1941 to 1970 NBCC seismic loading provisions; Heidebrecht and Tso (1985) discussed changes in the 1985 NBCC; Tso (1992) discussed changes in the 1990 NBCC; Heidebrecht (2003) discussed changes in the 2005 NBCC and Mitchell *et al*. (2010) discussed the changes in 2010 NBCC. For each design code, the calculated base shear coefficient (V/W) for Vancouver is shown in Figure 33. Figure 33 shows that with the introduction of each design code, the V/W ratio has increased.

The Canadian, US and European design guideline, utilizes linear methods of analysis. However, the seismic-force-resisting systems, if detailed properly, respond in the nonlinear range. The maximum elastic base shear V_E, without consideration of nonlinearity, is obtained from response spectra (e.g. Figure 33). Subsequently, the required design loads V are obtained by modifying the V_E with seismic modification factors (denoted differently various codes: R factors in the US code; *q* factors in in European code; a product of ductility (R_d) and overstrength (R_o) factors in the Canadian code). This chapter provides an overview of these factors. In Chapter 7, the R_d and R_o factors for the hybrid building is derived.

Table 4: Evolution of Canadian design code

Year	Base shear formula	Comments
NBC 1941		NBC = National Building Code; Incorporated in an appendix and were based on concepts presented in the 1937 U.S. Uniform Building Code (UBC); C varied from 0.02 to 0.05.
NBC 1953	F = CW	Incorporated into the main text of 1953 NBC; Inclusion of Canadian seismic zoning map; and Recognition of the influence of building flexibility; F = seismic design force; W = total weight (dead load + 25% of the design snow load); C = horizontal force factor for minimum earthquake load; Zone 1: C = 0.15/(N+4.5); Zone 2: C = 0.30/(N+4.5); Zone 2: C = 0.60/(N+4.5)
NBC 1965	V = RCIFSW	R = seismic regionalizing factor (values are 0, 1, 2, and 4 for earthquake intensity zones 0, 1, 2, and 3, respectively); C = type of construction factor (=0.75 for moment resisting space frame; = 1.25 for non-ductile structures); I = importance factor (1 or 1.3); F = foundation factor;; S = structural flexibility factor = 0.25/(N+9); W = total weight (dead load + 25% of the design snow load + design live load for storage area)
NBC 1970	F = ¼R(KCIFW)	Seismic zoning map is revised; R, I, F, and W same as NBC 1965; K = type of construction factor (values range from 0.67 to 1.33 for buildings); C = structural flexibility factor = $0.05/T^{1/3} \leq 0.10$; T = fundamental period of the structure ($0.05h_n/D^{1/2}$ or 0.10N); h_n = height of the structure in feet; D = dimension of the building in direction parallel to seismic force in feet; N = number of stories
NBC 1975	V = ASKIFW	I, F, and W same as NBC 1965; A = assigned horizontal design ground acceleration; S = seismic response factor ($0.5/T^{1/3} \leq 1$); K = numerical coefficient reflecting the influence of the type of construction on the damping, ductility, and (or) energy-absorption capacity of the structures (values range from 0.7 to 2 for buildings)
NBCC 1980	V = ASKIFW	
NBCC 1985	V = *v*SKIFW	New methodology in the calculation of seismic risk; A change in the probability level at which risk is computed; Use of both the PGA and PGV as ground motion parameter to represent the intensity of shaking; An increase in the number of seismic zones in Canada; K, I, F, and W same as NBC 1980; *v* = zonal velocity ratio; S = new seismic response factor depending on the periods of the structure
NBCC 1990	$V_{90} = \frac{V_e}{R} U$	U = 0.6, calibration factor; R = force modification factor (Range from 1 to 4)
NBCC 1995	$V = \frac{V_e}{R} U$ $V_e = vSIFW$	U = 0.6, calibration factor; R = force modification factor (Range from 1 to 4); V_e = Elastic lateral seismic force; *v* = zonal velocity ratio, ; S = seismic response factor, I = importance factor (1, 1.3, 1.5); F = foundation on site factor; W = dead load
NBCC 2005	$V = \frac{S(T_a)M_v I_E W}{R_d R_o}$	I_E = importance factor (1, 1.3, 1.5); $R_d R_o$: $1 \leq R_d \leq 5$ and $1 < R_o < 1.7$
NBCC 2010	$V = \frac{S(T_a)M_v I_E W}{R_d R_o}$	I_E = importance factor (1, 1.3, 1.5); $R_d R_o$: $1 \leq R_d \leq 5$ and $1 < R_o < 1.7$

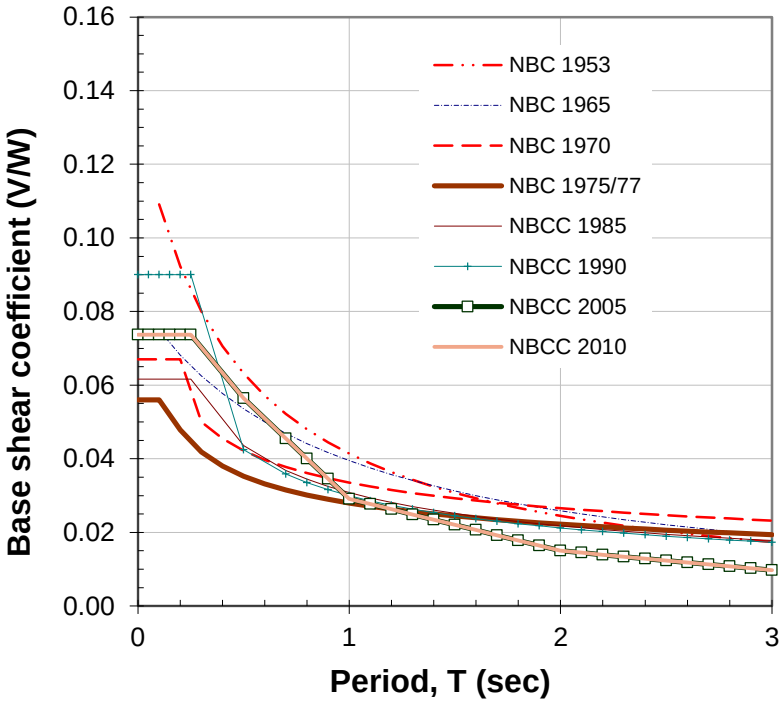

Figure 33: Evolution of base shear coefficients for the National Building Code of Canada, example for Vancouver, BC

5.1 Site Seismic Hazard

Evolution of the seismic design code also entails the changes in the seismic hazard considered. The first attempt seismic hazard quantification in Japan and North America follows the 1923 Kanto (Tokyo) earthquake and 1933 Long Beach California earthquake (Atkinson 2004; Otani 2004). Initially, the earthquake hazard quantification was introduced through the introduction of seismic coefficients. The evolution of seismic hazard provisions in the national building code (NBC) and national building code of Canada (NBCC) is summarized in Table 4. In 1945, seismic coefficients were varied between 0.02 and 0.05 and were included as an appendix. Subsequently, in the 1953 NBC, the seismic hazard zone was introduced. However, these zones were introduced on a qualitative basis (Atkinson 2004). In

late 1960s, the probabilistic quantification of hazard has gained popularity, and for the first time, seismic hazard was evaluated probabilistically. To date, the state of knowledge has improved, more advanced probabilistic methods are used for modern design codes and engineering design purpose. However, these new hazard factors calibrate the newer code to a previous version (Atkinson 2004). In the 1985, 1990, and 1995 NBCC, zonal velocity ratios were introduced, whereas in the 2005 NBCC, uniform hazard spectrum (UHS) was introduced. In this paper, the UHS is used as a basis for quantifying site seismic hazard, as used in the NBCC 2005. The derivation of the UHS for Canadian cities is beyond the scope of this report, and a thorough treatise is provided in Adams and Atkinson (2003) and Atkinson (2004). In this report, the SSH is quantified for the ground shaking only.

5.2 Evolution of ductility R_o and overstrength R_d in Canada building design code

The first edition of the NBCC was published in 1941 and included provisions for seismic design based on the Uniform Building Code (UBC, 1935). The 1965 code introduced the first seismic modification factor C (shown in Equation 5), as the construction factor in the calculation of the minimum seismic base shear (NRC, 1965).

$$V = RCIFSW \qquad [5]$$

where R = the seismic regionalization factor; C = construction factor; I = importance factor; F = foundation factor; S = flexibility factor; and W = dead load, live load and 25% of the snow load. The construction factor varied based on the predicted ductile behaviour of the system. Moment resisting frames and reinforced concrete shear walls had a construction factor of 0.75 while other buildings had a factor of 1.25.

In 1970 the seismic code was changed to include a construction factor (K) and structural flexibility factor (C) as shown in Equation 6 (NRC, 1970).

$$V = \frac{1}{4} R(KCIFW) \quad [6]$$

The structural flexibility factor was dependent on the fundamental period (T), height of the structure (h_n), dimension of the building parallel to the seismic force (D) and the number of storeys (N). The construction factors can be seen in Table 5 for various structural systems and their respective ductility.

In 1975 the NBCC introduced limit states design allowing designers to work with load factors and material resistance factors rather than the factors of safety associated with the working stress design. Designers were also allowed to use dynamic analysis in determining the seismic design forces (Mitchell *et al*., 2010). Table 6 shows the structural ductility factor μ for dynamic analysis of seismic design forces.

Table 5: Summary of K factors representing type of construction, damping, ductility and energy absorption (Mitchell *et al*., 2010)

Resisting Elements	**K (1970)**	**K (1975 to 1985)**
Ductile moment-resisting space frame resisting 100% of required force	0.67	0.7
Dual system of ductile moment-resisting space frame and ductile flexural walls (frame must be designed to resist at least 25% of total base shear)	0.8	0.7
Dual system of ductile moment-resisting space frame and shear walls or steel bracing (frame must be designed to resist at least 25% of total base shear and walls or bracing must be designed to resist 100% of base shear)		0.8
Other framing systems not defined above	1.0	
Ductile flexural walls and ductile framing systems not defined above		1.0
Systems without space frames (box systems)	1.33	
Dual system with ductile space frame with masonry infill (infilled wall system must be designed to resist 100% of base shear and frame; without infill, must be designed to resist at least 25% of total base shear)		1.3
Systems not defined above with continuous reinforced concrete, structural steel, or reinforced masonry shear walls		1.3
Other structural systems not defined above	2.0	2.0
Unreinforced masonry		2.0

Table 6: Structural ductility factor μ for dynamic analysis (Commentary K, 1975 NRCC)

Building type	μ
Ductile moment resisting space frame	4
Combined system of 25% ductile moment resisting space frame and ductile flexural walls	3
Ductile reinforced concrete flexural walls	3
Regular reinforced concrete structures, cross-braced frame structures and reinforced masonry	2
Structures having no ductility, plain masonry	1

In 1990 the NBCC replaced the construction factors with the force modification factor R. Along with this change came the introduction of the calibration factor U. Equation 7 displays these factors in the 1990 NBCC (NRC, 1990) calculation of the minimum seismic base shear.

$$V = \frac{U(vSIFW)}{R} \qquad [7]$$

The calibration factor of U = 0.6 was aimed at providing base shears similar to those calculated in previous codes to be consistent with the force modification factors previously used. The new force modification factor "reflects the capability of a structure to dissipate energy through inelastic behaviour" (NRC, 1990). Representing the ductile behaviour of structural systems the factor ranged from 1.0 to 4.0. Unreinforced masonry buildings had an R factor of 1.0; nominally ductile walls, concrete frames and braced steel frames had an R factor of 2.0; and ductile moment-resisting space frames had an R factor of 4.0.

In 1995 new force modification factors were introduced for several structural systems. Table 7 shows these factors for the relating lateral load resisting reinforced concrete systems. The table shows the design requirements for reinforced concrete structures complying with CSA standards.

Table 7: R factors for different reinforced concrete structural systems (NRC, 1995)

Cases in NBC	R	Type of Lateral Load Resisting System	Summary of Design and Detailing Requirements in CSA Standard A23.3 with Applicable Clauses in Brackets
10	4.0	ductile moment-resisting frame	(a) beams capable of significant flexural hinging (21.3 and 21.7); (b) columns properly confined and stronger than the beams (21.4 and 21.7) (c) joints properly confined and capable of transmitting shears from beam hinging (21.6)
11	4.0	ductile coupled wall	(a) at least 66% of base overturning moment resisted by wall must be carried by axial tension and compression in coupled wall resulting from shears in coupling beams; (b) wall strength to permit nominal strength of coupling beams to be achieved (21.5.8); (c) ductile coupling beams capable of developing flexural hinging or provide specially detailed diagonal reinforcement (21.5.8)
12	3.5	ductile flexural wall	(a) wall capable of significant flexural hinging without local instability and without shear failure (21.5 and 21.7)
12	3.5	ductile partially coupled wall	(a) wall strength to permit nominal strength of coupling beams to be achieved (21.5.8); (b) ductile coupling beams capable of developing flexural hinging or provide specially detailed diagonal reinforcement (21.5.8)
13	2.0	moment-resisting frame with nominal ductility	(a) beams and columns must satisfy nominal detailing requirements (21.9.2.1-2); (b) beams and columns must have minimum shear strength (21.9.2.3); (c) joints must satisfy nominal detailing requirements and must be capable of transmitting shears from beam hinging (21.9.2.4)
14	2.0	wall with nominal ductility	(a) walls must satisfy dimensional limitations and minimum detailing requirements (21.9.3.1-3); (b) walls must have minimum shear strength (21.9.3.4)
15	1.5	other lateral-force-resisting systems not defined above	(a) beams and columns (10); (b) joints (7.7.3 and 11.8); (c) walls (10 or 14)

The most significant change to seismic force modification factors came in the 2005 edition of the NBCC (NRC 2005). The code completely revised the base shear equation as:

$$V = \frac{S(T_a) M_v I_E W}{R_d R_o} \quad [8]$$

where $S(T_a)$ = design spectral response acceleration taken at the fundamental period T_a; Mv = accounts for higher mode effects on the base shear; IE = importance factor; W = weight of the structure; R_d = ductility factor; and R_o = overstregth factor. The ductility factor R_d is similar to the force modification factor R (provided in 1995 NBCC) accounting for the ability of a structure to dissipate energy through inelastic behaviour. However, the overstrength factor is new to the seismic design accounting for the reserve strength in a structure due to several factors including: the actual strength of material, confinement effects,

contribution of nonstructural elements and actual participation of some elements (Elnashai and Mwafy, 2002). A minimum base shear was also introduced in the 2005 edition of the NBCC as:

$$V \geq \frac{S(2.0)M_v I_E W}{R_d R_o} \quad [9]$$

where V less than this limiting values indicates the case where the structure required insignificant lateral restraint. Seismic force resisting structures with a ductility factor greater than 1.5 ($R_d > 1.5$) were not required to exceed the base shear provided in Equation 10 (NRC, 2005).

$$V \leq \frac{2}{3}\frac{S(0.2)I_E W}{R_d R_o} \quad [10]$$

The maximum base shear ensured that ductile structures were not over designed based on the proposed location of said structure. Ductility and overstrength factors were quantified for steel, concrete and timber structures as seen in Table 8. Included in the ductility and overstrength table is the height restrictions on each structural system.

Table 8: Force modification factors R_d and R_o for seismic force-resisting systems (NRC, 2005)

			Restrictions				
			$I_E F_a S_a(0.2)$				
Type of SFRS	**R_d**	**R_o**	**<0.20**	**≥0.20 to <0.35**	**≥0.35 to ≤0.75**	**>0.75**	**$I_E F_V S_a(1.0) > 0.30$**
Steel structures designed and detailed according to CSA standard CSA-S16-01							
Ductile moment-resisting frames	5.0	1.5	NL	NL	NL	NL	NL
Moderately ductile moment-resisting frames	3.5	1.5	NL	NL	NL	NL	NL
Limited-ductility moment-resisting frames	2.0	1.3	NL	NL	60	NP	NP
Moderately ductile concentrically braced frames							
Tension-compression bracing	3.0	1.3	NL	NL	40	40	40
Tension-only bracing	3.0	1.3	NL	NL	20	20	20
Limited-ductility concentrically braced frames							
Tension-compression bracing	2.0	1.3	NL	NL	60	60	60
Tension-only bracing	2.0	1.3	NL	NL	60	60	60
Chevron bracing	2.0	1.3	NL	NL	40	40	40
Ductile eccentrically braced frames	4.0	1.5	NL	NL	NL	NL	NL
Ductile plate walls	5.0	1.6	NL	NL	NL	NL	NL
Moderately ductile plate walls	2.0	1.5	NL	NL	60	60	60
Conventional construction	1.5	1.3	NL	NL	15	15	15
Other steel SFRS(s) not defined previously	1.0	1.0	15	15	NP	NP	NP
Concrete structures designed and detailed according to CSA standard CSA-A23.3-94 (2004 edition under preparation)							
Ductile moment-resisting frames	4.0	1.7	NL	NL	NL	NL	NL
Moderately ductile moment-resisting frames	2.5	1.4	NL	NL	60	40	40
Ductile coupled walls	4.0	1.7	NL	NL	NL	NL	NL
Ductile partially coupled walls	3.5	1.7	NL	NL	NL	NL	NL
Ductile shear walls	3.5	1.6	NL	NL	NL	NL	NL
Moderately ductile shear walls	2.0	1.4	NL	NL	NL	60	60
Conventional construction							
Moment-resisting frames	1.5	1.3	NL	NL	15	NP	NP
Shear walls	1.5	1.3	NL	NL	40	30	30
Other concrete SFRS(s) not listed previously	1.0	1.0	15	15	NP	NP	NP
Timber structures designed and detailed according to CSA standard CSA-O86-01							
Shear walls							
Nailed shear walls with wood-based panels	3.0	1.7	NL	NL	30	20	20
Shear walls with wood-based and gypsum panels in combination	2.0	1.7	NL	NL	20	20	20
Braced or moment-resisting frames with Ductile connections							
Moderately ductile frames	2.0	1.5	NL	NL	20	20	20
Limited-ductility frames	1.5	1.5	NL	NL	15	15	15
Other wood- or gypsum-based SFRS(s) not listed previously	1.0	1.0	15	15	NP	NP	NP

The 2010 National Building Code of Canada saw few changes to the force modification factors as the base shear equation remained unchanged. However, there were a few seismic force-resisting steel systems added with respect to their force modification factors. Table 9 shows the updated steel seismic modification factors.

Table 9: Seismic force modification factors for steel seismic force-resisting systems (NRC, 2010)

Type of SFRS	R_d	R_o	Restrictions				
			Cases Where $I_E F_a S_a(0.2)$				Cases Where $I_E F_V S_a(1.0)$
			<0.20	≥0.20 to <0.35	≥0.35 to ≤0.75	>0.75	>0.3
Steel Structures Designed and Detailed According to CSA S16							
Ductile moment-resisting frames	5.0	1.5	NL	NL	NL	NL	NL
Moderately ductile moment-resisting frames	3.5	1.5	NL	NL	NL	NL	NL
Limited ductility moment-resisting frames	2.0	1.3	NL	NL	60	30	30
Moderately ductile concentrically braced frames							
Tension-compression braces	3.0	1.3	NL	NL	40	40	40
Tension only braces	3.0	1.3	NL	NL	20	20	20
Limited ductility concentrically braced frames							
Tension-compression braces	2.0	1.3	NL	NL	60	60	60
Tension only braces	2.0	1.3	NL	NL	40	40	40
Ductile buckling-restrained braced frames	4.0	1.2	NL	NL	40	40	40
Ductile eccentrically braced frames	4.0	1.5	NL	NL	NL	NL	NL
Ductile plate walls	5.0	1.6	NL	NL	NL	NL	NL
Limited ductility plate walls	2.0	1.5	NL	NL	60	60	60
Conventional construction of moment-resisting frames, braced frames or plate walls							
Assembly occupancies	1.5	1.3	NL	NL	15	15	15
Other occupancies	1.5	1.3	NL	NL	60	40	40
Other steel SFRS(s) not defined above	1.0	1.0	15	15	NP	NP	NP

The current 2010 NBCC enables the designer to design the lateral force-resisting system efficiently based on the location, soil type, importance factor and type of structure. The

problem arises when a designer is tasked with designing a structure using two material types (hybrid structure). In the case of hybrid structures the designer must then conduct dynamic analyses to determine the resulting overstrength and ductility values or take the more conservative value and potentially overdesign the structure.

5.2.1 Overstrength factor (R_o)

The overstrength factor (R_o) can be calculated by taking a ratio of the ultimate shear capacity to the yield shear capacity. The ultimate shear capacity and yield shear capacity are obtained through pushover analysis or dynamic analyses (to collapse). The results of the analysis show that the structure requires greater load to reach the actual yield point of the system as shown in Figure 34.

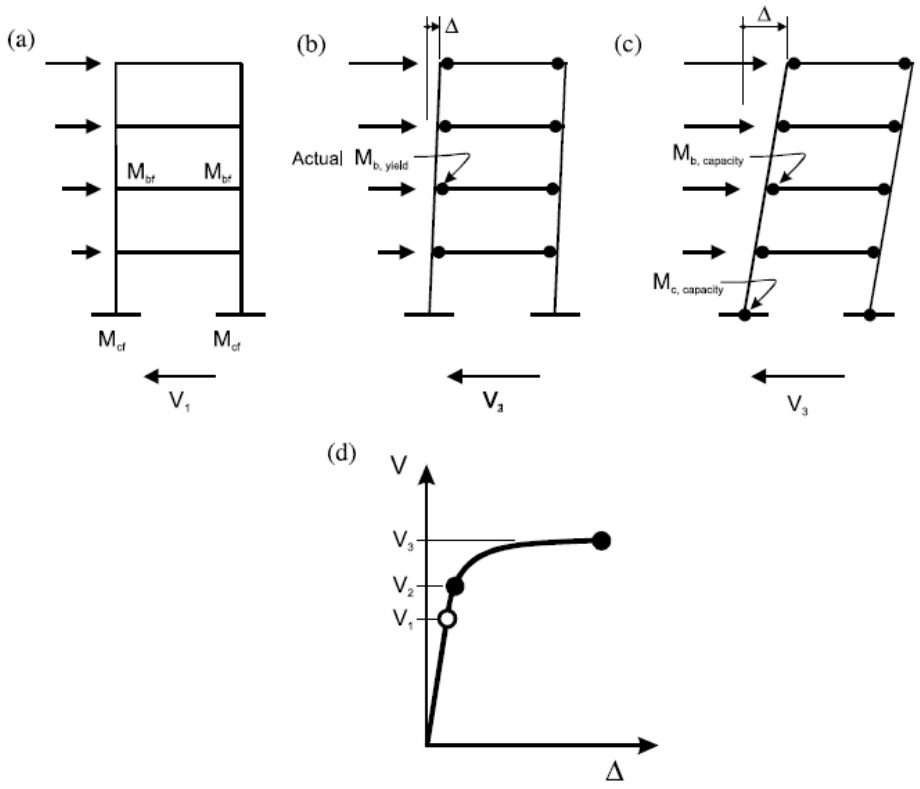

Figure 34: Stages in the response of a frame structure (Mitchell *et al*., 2003)

The greater yield is due to the overstrength in the structure as the members are typically greater than required for the design yield stress (Mitchell *et al*., 2003). Factors that contribute to a structures overstrength are summarized in Table 12.

Table 10: Sources of structure overstrength (Park, 1996)

	Factors that contribute to structural overstrength factor
•	Steel and concrete strengths greater than specified.
•	Use of strength reduction factors or material factors in design.
•	Section sizes larger than assumed.
•	Effects of member deformations at large displacements.
•	Additional reinforcement placed for construction purposes or to satisfy minimum reinforcement requirements or to satisfy available bar sizes, and unaccounted for in the design calculations.
•	More critical loading cases for the design of some sections for gravity or wind loads.
•	Moment redistribution after yielding greater than assumed in design.
•	Participation of non-structural elements.
•	Overestimation of structural stiffness leading to high design seismic forces.

Mitchell *et al*. (2003) formulated an equation for overstrength based on five factors as:

$$R_o = R_{size} R_{\phi} R_{yield} R_{sh} R_{mech} \quad [11]$$

where the R_{size} = size factor, accounts for the overstrength due to rounding and limited member sizes; R_{ϕ} = the material resistance factor, accounts for the difference between nominal and factored resistances; R_{yield} = the yield factor, accounts for the actual yield strength of the structure in comparison to the specified minimum yield strength; R_{sh} = the strain hardening factor, accounts for the overstrength due to strain hardening in a structure; and R_{mech} = the mechanical factor, accounts for the full capacity of the structure mobilizing to form a collapse mechanism (Mitchell *et al*. 2003). Table 13, Table 14, and Table 15 summarizes the derivation of the overstrength factor for steel, concrete and timber structures, respectively.

Table 11: Derivation of overstrength modification factor for steel seismic force resisting systems (Mitchell *et al*. 2003)

	Calculation of R_o						
Type of SFRS	**R_{size}**	**R_{ϕ}**	**R_{yield}**	**R_{sh}**	**R_{mech}**	**R_o**	**NBCC R_o**
Ductile moment-resisting frames	1.05	1.11	1.10	1.15	1.00	1.47	1.5
Moderately ductile moment-resisting frames	1.05	1.11	1.10	1.15	1.00	1.47	1.5
Limited-ductility moment-resisting frames	1.05	1.11	1.10	1.05	1.00	1.35	1.3
Moderately ductile concentrically braced frames	1.05	1.11	1.10	0.05	1.00	1.35	1.3
Limited-ductility concentrically braced frames	1.05	1.11	1.10	1.05	1.00	1.35	1.3
Ductile eccentrically braced frames	1.05	1.11	1.10	1.15	1.00	1.47	1.5
Ductile plate walls	1.10	1.11	1.10	1.10	1.10	1.63	1.6
Limited-ductility plate walls	1.10	1.11	1.10	1.05	1.05	1.48	1.5
Conventional construction	1.05	1.11	1.10	1.00	1.00	1.28	1.3

Table 12: Derivation of overstrength modification factor for concrete seismic force resisting systems (Mitchell *et al*. 2003)

	Calculation of R_o						
Type of SFRS	**R_{size}**	**R_{ϕ}**	**R_{yield}**	**R_{sh}**	**R_{mech}**	**R_o**	**NBCC R_o**
Ductile moment-resisting frames	1.05	1.18	1.05	1.25	1.05	1.71	1.7
Moderately ductile moment-resisting frames	1.05	1.18	1.05	1.10	1.00	1.43	1.4
Moment-resisting frames with conventional construction	1.05	1.18	1.05	1.00	1.00	1.30	1.3
Ductile coupled walls	1.05	1.18	1.05	1.25	1.05	1.71	1.7
Ductile partially coupled walls	1.05	1.18	1.05	1.25	1.05	1.71	1.7
Ductile shear walls	1.05	1.18	1.05	1.25	1.00	1.63	1.6
Moderately ductile shear walls	1.05	1.18	1.05	1.10	1.00	1.43	1.4
Shear walls with conventional construction	1.05	1.18	1.05	1.00	1.00	1.30	1.3

Table 13: Derivation of overstrength modification factor for timber seismic force resisting systems (Mitchell *et al*. 2003)

	Calculation of R_o						
Type of SFRS	**R_{size}**	**R_{ϕ}**	**R_{yield}**	**R_{sh}**	**R_{mech}**	**R_o**	**NBCC R_o**
Nailed shear walls with wood-based panel	1.15	1.43	1.00	1.05	1.00	1.73	1.7
Shear walls with wood-based and gypsum panels in combination	1.15	1.43	1.00	1.05	1.00	1.73	1.7
Moderately ductile braced or moment-resisting frames	1.05	1.43	1.00	1.00	1.00	1.50	1.5
Limited-ductility braced or moment-resisting frames	1.05	1.43	1.00	1.00	1.00	1.50	1.5

5.3 European Code

The European code (Eurocode) has a different approach to seismic force modification factors. Within Eurocode 8 there are behaviour factors outlined for concrete, steel, concrete-steel composite and timber structures. Detailing of each structure is to be completed through the procedures outlined in the code with the pertaining behaviour factor. The design base shear is formulated based on many factors and varies with period

$$F_b = \frac{2.5 \cdot a_g \cdot S \cdot T_c}{q \cdot T} m \cdot \lambda \quad [12]$$

where F_b = the base shear; a_g = design ground acceleration; S = soil factor; T_c = upper limit of period; q = behaviour factor; T = vibration period of linear single degree of freedom system; m = mass of the structure; and λ = factor based on the period and height of a structure.

For steel moment resisting frames the Eurocode defines the behaviour factor as seen in

$$F_b = \frac{2.5 \cdot a_g \cdot S \cdot T_c}{q \cdot T} m \cdot \lambda \quad [13]$$

The first term in the formulation of *q* represents the ratio in a pushover analysis of the multiplier of the seismic forces at ultimate capacity to the multiplier at first yield (Sanchez-Ricart 2010). This ratio is known as the plastic redistribution parameter and is given a value of 1.25 if no plastic analysis is performed by the designer. If a plastic analysis is performed the maximum value is limited to 1.6. The second term in the equation represents the behaviour factor for the lateral force resisting system. In this equation that value is 5 for moment resisting steel frames. The other lateral force resisting systems behaviour factors for steel structures is summarized in Table 15.

Table 14: Behaviour factors for steel systems regular in elevation (CEN, 2003)

Structural Type	Ductility Class	
	DCM	DCH
a) Moment resisting frames	4	$5\alpha_u/\alpha_1$
b) Frame with concentric bracings		
Diagonal bracings	4	4
V-bracings	2	2,5
c) Frame with eccentric bracings	4	$5\alpha_u/\alpha_1$
d) Inverted pendulum	2	$2\alpha_u/\alpha_1$
e) Structures with concrete cores or concrete walls	See section **5**	
f) Moment resisting frame with concentric bracing	4	$4\alpha_u/\alpha_1$
g) Moment resisting frames with infills		
Unconnected concrete or masonry infills, in contact with the frame	2	2
Connected reinforced concrete infills	See section **7**	
Infills isolated from moment frame (see moment frames)	4	$5\alpha_u/\alpha_1$

Unlike the NBCC, there is only one behaviour factor in the Eurocode. There is no specific overstrength or ductility factor contributing to the minimum base shear. However, the behaviour factor includes provisions for both ductility as well as overstrength. Sanchez-Ricart and Plumier (2008) show that the reduction factor of 6 for highly ductile MRSF cannot be justified without the consideration of structural overstrength. Therefore, it can be observed that the behaviour factors from the Eurocode are quite similar to the values obtained in the NBCC from product of the overstrength (R_o) and ductility (R_d) factors.

5.4 Seismic modification factors in the United States

The United States does not have one seismic code pertaining to the entire country as in Canada or Europe. Rather, each municipality, or the state in some cases, utilizes one or more of the following guidelines: the Uniform Building Code (UBC), National Building Code (NEHRP), and the Applied Technology Council (ATC). The seismic force modification factors are examined in ATC 19 and ATC 34 where it was observed that there have been no

changes to the factors since the 1950s' (ATC 19, 1995). Therefore, the modification factors have no mathematical basis in current American seismic codes and therefore cannot be justified (Sanchez-Ricart, 2010). The development of the modification factor R is currently based on the engineering judgments made on observations from past earthquakes. Using the UBC 1997 code the base shear can computed as:

$$V = \frac{C_v \cdot I}{R \cdot T} W \qquad [14]$$

where V = design base shear; C_v = seismic coefficient; I = importance factor; R = modification factor accounting for inherent overstrength and global ductility capacity (Table 15); T = elastic fundamental period; and W = total seismic dead load acting on the structure. Similar to the Eurocode, the UBC has only one seismic modification factor that accounts for both overstrength and ductility. Values in Table 15 for R may seem high however; when considering other factors in the base shear equation the results are similar to the NBCC and Eurocode values.

Table 15: 1997 Uniform Building Code ductility and overstrength factors (UBC, 1997)

BASIC STRUCTURAL SYSTEM	LATERAL-FORCE-RESISTING SYSTEM DESCRIPTION	R	Ω_o	HEIGHT LIMIT FOR SEISMIC ZONES 3 AND 4 (feet) x 304.8 for mm
1. Bearing wall system	1. Light-framed walls with shear panels			
	a. Wood structural panel walls for structures three stories or less	5.5	2.8	65
	b. All other light-framed walls	4.5	2.8	65
	2. Shear walls			
	a. Concrete	4.5	2.8	160
	b. Masonry	4.5	2.8	160
	3. Light steel-framed bearing walls with tension-only bracing	2.8	2.2	65
	4. Braced frames where bracing carries gravity load			
	a. Steel	4.4	2.2	160
	b. Concrete	2.8	2.2	-
	c. Heavy timber	2.8	2.2	65
2. Building frame system	1. Steel eccentrically braced frame (EBF)	7.0	2.8	240
	2. Light-framed walls with shear panels			
	a. Wood structural panel walls for structures three stories or less	6.5	2.8	65
	b. All other light-framed walls	5.0	2.8	65
	3. Shear walls			

	a. Concrete	5.5	2.8	240
	b. Masonry	5.5	2.8	160
	4. Ordinary braced frames			
	a. Steel	5.6	2.2	160
	b. Concrete	5.6	2.2	-
	c. Heavy timber	5.6	2.2	65
	5. Special concentrically braced frames			
	a. Steel	6.4	2.2	240
3. Moment-resisting frame system	1. Special moment-resisting frame (SMRF)			
	a. Steel	8.5	2.8	N.L.
	b. Concrete	8.5	2.8	N.L.
	2. Masonry moment-resisting wall frame (MMRWF)	6.5	2.8	160
	3. Concrete intermediate moment-resisting frame (IMRF)	5.5	2.8	-
	4. Ordinary moment-resisting frame (OMRF)			
	a. Steel	4.5	2.8	160
	b. Concrete	3.5	2.8	-
	5. Special truss moment frames of steel (STMF)	6.5	2.8	240
4. Dual systems	1. Shear walls			
	a. Concrete with SMRF	8.5	2.8	N.L.
	b. Concrete with steel OMRF	4.2	2.8	160
	c. Concrete with concrete IMRF	6.5	2.8	160
	d. Masonry with SMRF	5.5	2.8	160
	e. Masonry with steel OMRF	4.2	2.8	160
	f. Masonry with concrete IMRF	4.2	2.8	-
	g. Masonry with masonry MMRWF	6.0	2.8	160
	2. Steel EBF			
	a. With steel SMRF	8.5	2.8	N.L.
	b. With steel OMRF	4.2	2.8	160
	3. Ordinary braced frames			
	a. Steel with steel SMRF	6.5	2.8	N.L.
	b. Steel with steel OMRF	4.2	2.8	160
	c. Concrete with concrete SMRF	6.5	2.8	-
	d. Concrete with concrete IMRF	4.2	2.8	-
	4. Special concentrically braced frames			
	a. Steel with steel SMRF	7.5	2.8	N.L.
	b. Steel with steel OMRF	4.2	2.8	160
5. Cantilevered column building systems	1. Cantilevered column elements	2.2	2.0	35
6. Shear wall-frame interaction systems	1. Concrete	5.5	2.8	160
7. Undefined systems	See Sections 1629.6.7 and 1629.9.2	-	-	-

The FEMA P695 is one of the most rational and comprehensive means of generating the design parameters. The R factor given Equation 14 is equivalent in principle to the product of the R_d and R_o factor in NBCC. A recent evaluation of the FEMA P695 by NIST (2012),

Tentative Framework for Development of Advanced Seismic Design Criteria for New Buildings (NIST GCR 12-917-20), have indeed started moving forward from the single R values and similar R_d and R_o factors as in NBCC. Furthermore, in NIST (2012), have shown that these factors are sensitivities to the period of the structure, and period dependent factors are suggested.

Chapter 6
Multi-Storey Steel-Timber Archetype Buildings

The archetype buildings are selected based on the building type considered by the co-applicants and FEMA's P695 guidelines (Quantification of Building Seismic Performance Factors FEMA P695 / June 2009). As such, these archetype buildings are not intended to simulate a specific complex building to be used; rather this study is to develop the required engineering design parameters needed for design. Once the overstrength factor, ductility factor and fundamental period of the hybrid building is developed in congruence with national building code, designers will use this factors to select the appropriate seismic load (for example) and proportion the loads on each floor following the standard design guideline.

Details of the archetypical buildings steel moment resisting frame buildings with CLT infill considerations are outlined below. The different variation, e.g., building height, fundamental period of the structure, seismic design consideration of the steel moment resisting frame will be used to develop different bins for the archetypical buildings (this forms performance group of each building).

- **Building Height**. In this study, a total of seven building heights, 1, 3, 6, 9, 12, 15, and 20-storey, steel moment resisting frame buildings will be considered (Figure 35) without irregularity in plan (Figure 36).
- **CLT Infill Configuration**. For the seven building heights and 3-bay frame, two infill configuration (one interior day and two exterior bays) will be considered. Initial preliminary analysis was carried out, and showed the infill in all three bays shows no appreciable difference than the two exterior bays infill. The bay widths considered are: 9 m for the exterior bay, and 6 m for the interior bay (Figure 35).
- **CLT-Steel Connections**. Important component of the hybrid CLT-Steel structures are at the CLT-Steel connection details. In this proposal, appropriate connection models (strength, ductility, hysteretic models, etc.) that are required in analytical models is developed (Chapter 3). The connection model developed for example, can be used SAP2000 finite element commercial software. With this connection

model, designers can use and integrate this model in their routine analysis and design. Two bracket spacing, 0.8 and 1.6 m, will be considered.

- **Steel Moment Resisting Frame Design and Connections**. Seismic Design Category dictates special design and detailing requirements, and subsequently influences component inelastic deformation capacity. As a result, two different design category (ductile and limited ductility), and where appropriate, different moment connection details (e.g., welded, bolted, or reduced-beam section) will be considered. Preliminary analysis showed that, the limited ductility, beyond 9 storey, showed brittle failure. As a result, the design considerations are: ductile structure (for 1, 3, 6, 9, 12, 15, and 20-storey) and limited ductility (for 1, 3, 6, and 9-storey).
- **Design and Modelling**. The 1, 3, 6, 9, 12, 15, and 20-storey archetypical buildings steel moment resisting frame buildings with CLT infill will be designed for seismicity and loading conditions of Vancouver, BC. The static pushover analysis will be used to derive the over strength and ductility factors, and validated through non-linear incremental dynamic analysis.

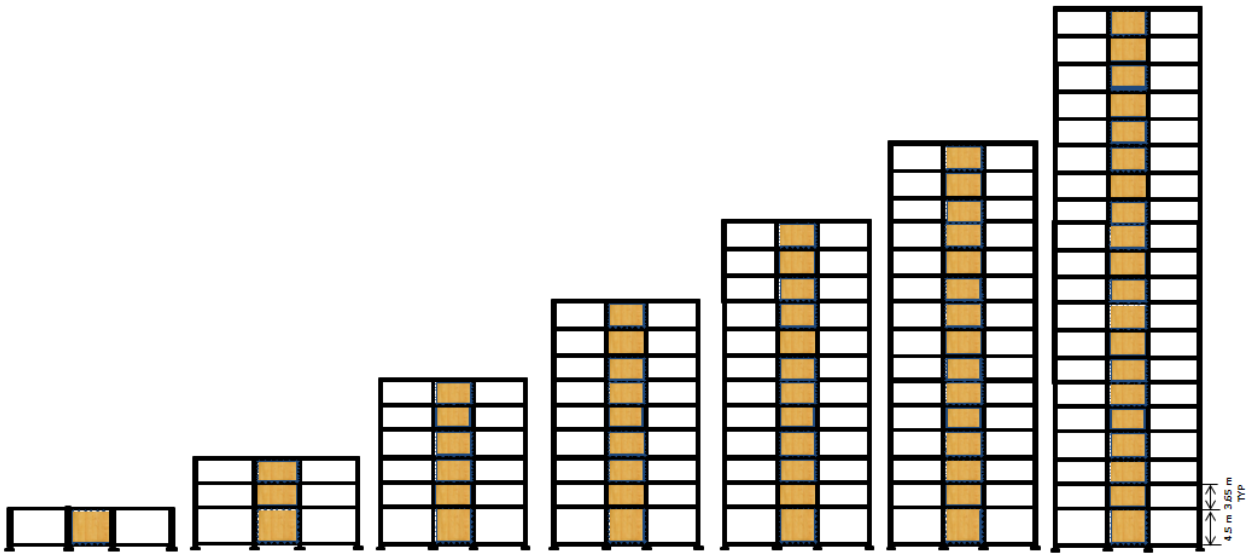

Figure 35: Seven building heights: 1, 3, 6, 9, 12, 15 and 20 storeys

The first storey height is 4.5 m and the height of all other storeys above is 3.65 m. The three bay frames considered have bay widths of 9 m for the exterior bay and 6 m for the interior bay. A simplified floor plan is shown in Figure 36.

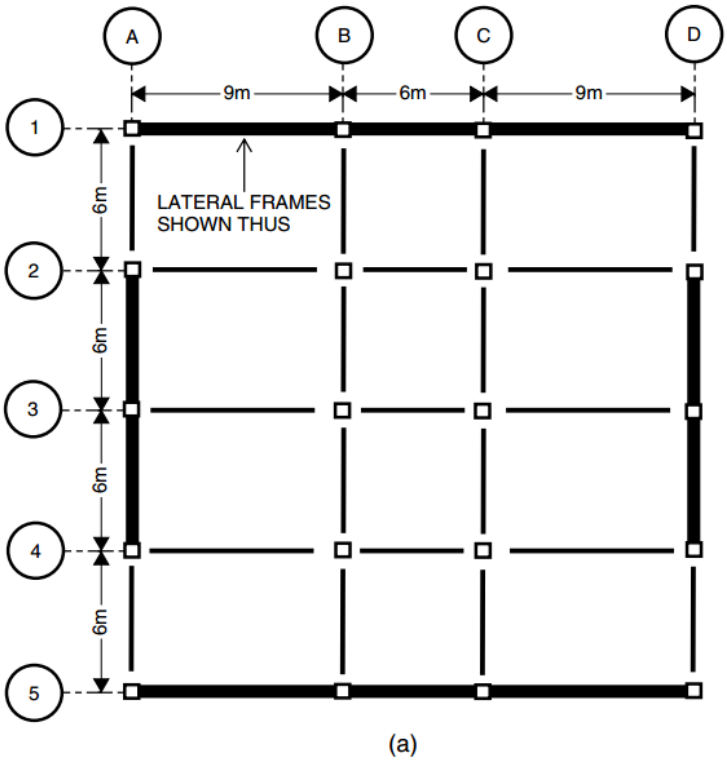

Figure 36: Hybrid structure floor plan

The infill walls consist of cross laminated timber (CLT) members as seen in Figure 37. Important components of the hybrid CLT-Steel structures are at the CLT-Steel connection details. The connection will be varied based on the connection type and corresponding spacing.

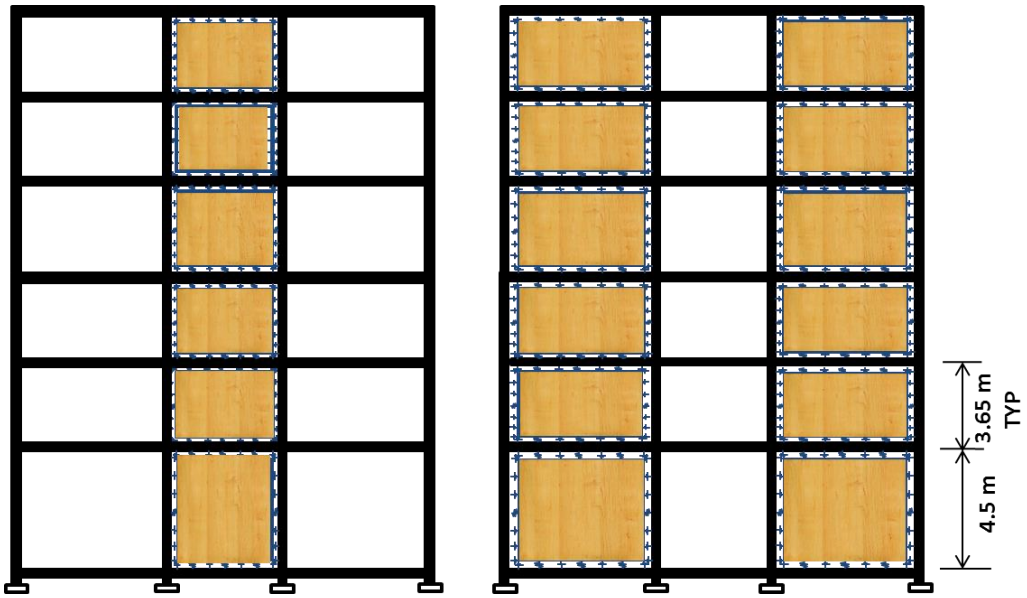

Figure 37: Three infill configurations: one interior bay, two exterior bays and all bays.

Chapter 7
Overstrength and Ductility Factors using Static Pushover Analysis

In this chapter, the overstrength and ductility factors of the index archetype buildings of Chapter 6 are developed following the guidelines of FEMA P695. FEMA P695 prescribes an iterative approach for the derivation of seismic force modification factors of new buildings. This process accounts for the potential uncertainties in ground motions, component design parameters, structural configurations, and behavior characteristics of structural elements based on available laboratory test data. The remainder of this chapter consisted of the following main tasks:

- Discussion of calculations related to ductility R_d and overstrength R_o factors, following FEMA P695 and NBCC approaches;
- Design hybrid buildings using assumed response modification factors;
- Develop nonlinear hybrid building models in OpenSees;
- Quantify and assess the developed nonlinear structural models using static pushover analyses.

7.1 Seismic performance factors of FEMA P695 and NBCC 2005

The National Earthquake Hazards Reduction Program (NEHRP) (FEMA 2004) and NBCC 2005 define seismic performance factors that reduce the elastic design loads of structures to ensure the ability of structures to go under inelastic deformation during seismic event. Consistent with ASCE/SEI 7-05 and NEHRP recommended provisions, FEMA P695 developed a methodology to quantify response modification factors for new buildings. For new structure, in FEMA P695 (2009) a new guideline is provided in the Quantification of

Building Seismic Performance Factors, i.e. overstrength factors (denoted as Ω) and ductility factors (denoted as R). These factors are depicted in Figure 38.

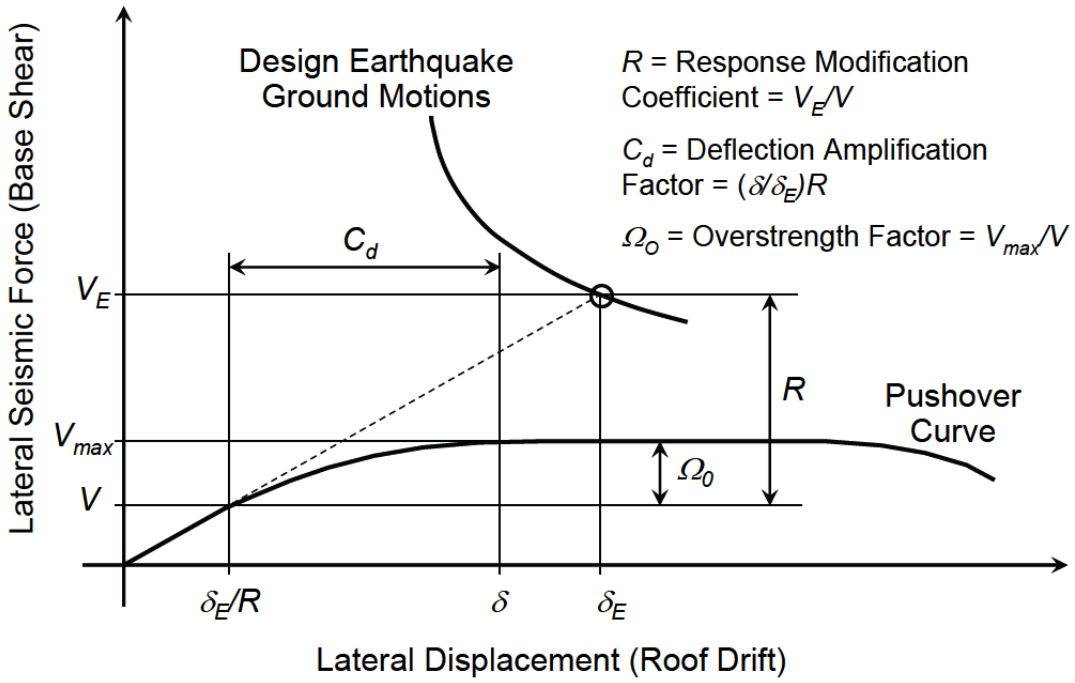

Figure 38: Illustration of seismic performance factors (R, Ω_O, and C_d) (reproduced from FEMA P695)

Figure 38 shows a plot of the lateral seismic force vs. lateral displacement curve obtained through the from a static pushover analysis. In Figure 38, V_E = the force level that would be developed in the seismic-force-resisting system, if the system remained entirely linearly elastic for design earthquake ground motions, V_{max} = represents the actual, maximum strength of the fully-yielded system, and V = seismic base shear required for design. Using Figure 38, the corresponding equations used to derive Ω and R, are:

$$\Omega = \frac{V_{max}}{V} \quad [15]$$

$$R = \frac{V_E}{V} \quad [16]$$

The deflection amplification factor (C_d) is given as shown

$$C_d = \frac{\delta}{\delta_E} R \quad [17]$$

where δ_E /R is the drift at the design shear force and δ is drift value when the system is exposed to design based earthquake ground motion. Moreover, FEMA P695 defines the period based ductility μ_T as the ratio of collapse roof displacement δ_u and yielding displacement ($\delta_{y,eff}$) as:

$$\mu_T = \frac{\delta_u}{\delta_{y,eff}} \quad [18]$$

from the Elastic Perfectly Plastic (EPP) approximation of idealized pushover curve as shown in Figure 39.

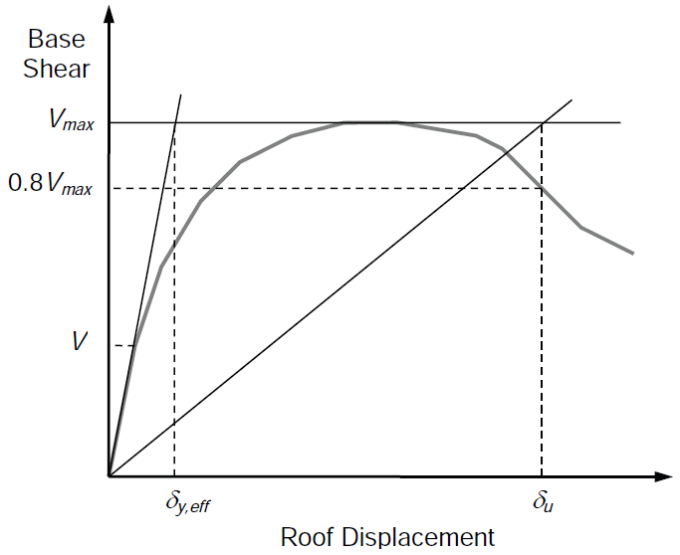

Figure 39: Idealized nonlinear static pushover curve (FEMA, 2009)

Newmark and Hall (1982) developed relationship between the period based ductility (μ_T) and ductility related force reduction factor (R_μ) as

$R_\mu = 1$ when T < 0.03 sec

$R_\mu = \sqrt{2\mu - 1}$ when 0.12 < T < 0.5 sec [19]

$R_\mu = \mu$ when T > 1 s

NBCC 2005 splits the R factors of NEHRP recommendation provisions (NEHRP 1997) in to R_d (ductility related force reduction factor) and R_o (Overstrength related force reduction factor). Figure 40, from Mitchell et al. (2003), defines these force reduction factors using idealized pushover curve.

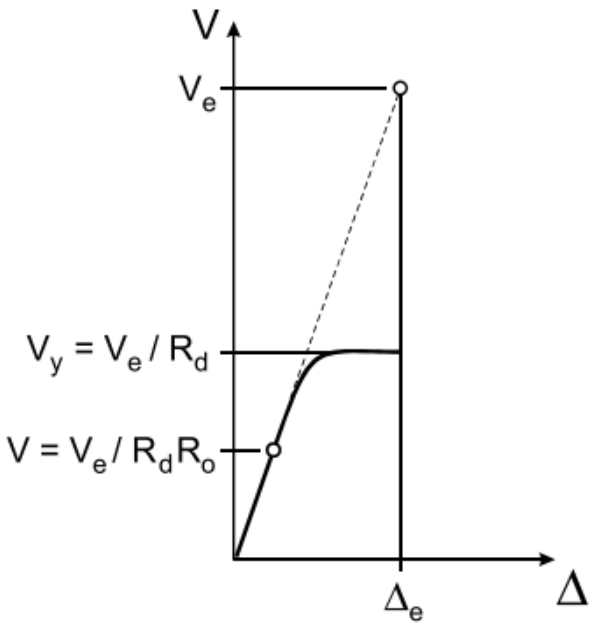

Figure 40: Ductility and force reduction factors of NBCC 2005 (Mitchell et al. (2003))

7.2 Hybrid buildings considered for analysis

Following the defined index archetype buildings of Chapter 6, for the current study, different performance groups are developed by varying modeling parameters of the hybrid buildings. The varied parameters for the current study are: building height (1, 3, 6, 9, 12, 15 and 20 storeys), CLT infill configuration (one-bay infilled and two-bays infilled), and ductility class of steel members: Ductile (D) and Limited Ductile (LD) (up to 9 storey)). The total combination of the varied parameters constitutes the 22 different buildings of the current study. The Seismic Design Category dictates special design and detailing requirements, and subsequently influences component inelastic deformation capacity. As a result, two different design categories (ductile (D) and limited ductility (LD)) are considered with appropriate detailing requirement of CSA S16-09. Details of the hybrid buildings are summarized in Tables 16 to 18.

Table 16: CLT-steel buildings (low rise)

Building No.	Storey height	Bracket spacing (m)	Ductility class	Infilled bays
1	1	0.8	D	1
2				2
4			LD	1
3				2
4	3	0.8	D	1
5				2
6			LD	1
7				2

Table 17: CLT-steel buildings (mid rise)

Building No.	Storey height	Bracket spacing (m)	Ductility class	Infilled bays
8	6	0.8	D	1
9				2
10			LD	1
11				2
12	9	0.8	D	1
13				2
15			LD	1
16				2

Table 18: CLT-steel buildings (high rise)

Building No.	Storey height	Bracket spacing (m)	Ductility class	Infilled bays
17	12	0.8	D	1
18				2
19	15	0.8	D	1
20				2
21	20	0.8	D	1
22				2

Each building designed using Equivalent Static Procedure of NBCC 2010 by considering a live load of 4.8 kPa for typical office floors and a load of 2.4 kPa elsewhere. Dead loads were considered for floors and roofs as 4.05 kPa and 3.4 kPa, respectively (NRC, 2010). The buildings studied are assumed to be located in Vancouver, BC, Canada assuming a site class C soil condition (dense soil and soft rock). The steel members designed are assumed to have yield strength F_y of 350 MPa and a modulus of elasticity E_s of 200 GPa. Following Dickof et al. (2014), the design base shear was calculated for ductility and overstrength factors of $R_d = 2.0$ and $R_o = 1.5$, respectively. Equivalent static load calculation method of NBCC 2010 has been adopted to distribute the design base shear along the height of the building. The steel frames were then sized to meet the additional criteria for a ductile (type D) moment frame and a limited ductility (type LD), as specified in the CSA S16 code (CISC, 2010).

Tables 19 to 22 have summarized the details of the designed beam and column sections for each structure including both ductile and limited ductile designs.

Table 19: Designed beam dimensions for ductile type

Building storey	Storey no	External	Internal
1	1	W310×158	W310×158
3	1,2	W310×129	W310×129
	3	W310×67	W310×67
6	1,2	W310x129	W310×143
	3,4,5	W310×129	W310×129
	6	W310×129	W310×129
9	1,2,3	W310×158	W310×158
	4,5,6	W310×129	W310×129
	9	W310×74	W310×74
12	1,2,3	W310×202	W310×202
	4,5	W310×202	W310×202
	6-12	W310×179	W310×179
15	1-5	W310×253	W310×253
	6-9	W310×253	W310×253
	10-15	W310×179	W310×179
20	1-5	W310×375	W310×375
	6-10	W310×375	W310×375
	10-20	W310×375	W310×375

Table 20: Designed beam dimensions for limited ductility type

Building storey	Storey no	External	Internal
1	1	W310×143	W310×143
3	1,2	W310×107	W310×107
	3	W310×67	W310×67
6	1,2	W310×118	W310×143
	3,4,5	W310×118	W310×129
	6	W310×67	W310×67
9	1,2,3	W310×158	W310×158
	4,5,6	W310×129	W310×129
	9	W310×67	W310×67

Table 21: Designed column dimensions for ductile type

Building storey	Storey no	Left External	Right External	Internal
1	1	W310×179	W310×179	W310×179
3	1,2	W310×143	W310×143	W310×143
	3	W310×86	W310×86	W310×143
6	1	W310×202	W310×202	W310×202
	2	W310×202	W310×202	W310×202
	3	W310×179	W310×179	W310×179
	4,5,6	W310×129	W310×129	W310×129
9	1,2,3	W310×179	W310×179	W310×226
	4,5,6	W310×143	W310×1143	W310×179
	7,8	W310×107	W310×107	W310×107
	9	W310×107	W310×107	W310×107
12	1,2,3	W360×287	W360×287	W360×382
	4,5	W360×287	W360×287	W360×382
	6-9	W360×196	W360×196	W360×237
	10,12	W360×196	W360×196	W360×237
15	1-5	W360×347	W360×347	W360×421
	5-10	W360×347	W360×347	W360×421
	11-15	W360×314	W360×314	W360×347
20	1-5	W360×509	W360×509	W360×509
	5-10	W360×509	W360×509	W360×509
	11-15	W360×509	W360×509	W360×509
	15-20	W360×509	W360×509	W360×509

Table 22: Designed column dimensions for limited ductility type

Building storey	Storey no	Right External	Left External	Internal
1	1	W310×158	W310×158	W310×158
3	1,2	W310×143	W310×86	W310×143
	3	W310×86	W310×86	W310×143
6	1	W310×143	W310×143	W310×202
	2	W310×86	W310×86	W310×143
	3	W310×86	W310×86	W310×129
	4,5,6	W310×86	W310×86	W310×129
9	1,2,3	W310×158	W310×158	W310×226
	4,5,6	W310×129	W310×129	W310×129
	7,8	W310×86	W310×86	W310×86
	9	W310×86	W310×67	W310×67

7.3 Pushover analysis results

Model instability and 10% drift value are used as a convergence criterion for the analysis. Static lateral loads with inverted triangular shape are used to push the structure until either model instability or formation of enough plastic hinges to create a sway mode of collapse. The applied static loads with the assumed distribution are increased monotonically until the point where the structure is considered to be collapsed. The results of the monotonic pushover analysis are depicted in Figures 41 and 42 for appropriate connection spacing. The pushover analyses results indicates that bracket yielding does not influence the initial stiffness of the hybrid system. For models with one infilled bay, significant change in stiffness is observed when the steel beams are yielding. However, when the number of infilled bays is increasing the change in the initial stiffness comes from either column yielding or panel crushing. Moreover, the panel crushing in multi-degree-of-freedom systems of the hybrid structures occurs arbitrary. These reasons prompted the use of a bilinear approximation of the pushover curves to obtain the force and displacement of the hybrid structure at yielding point.

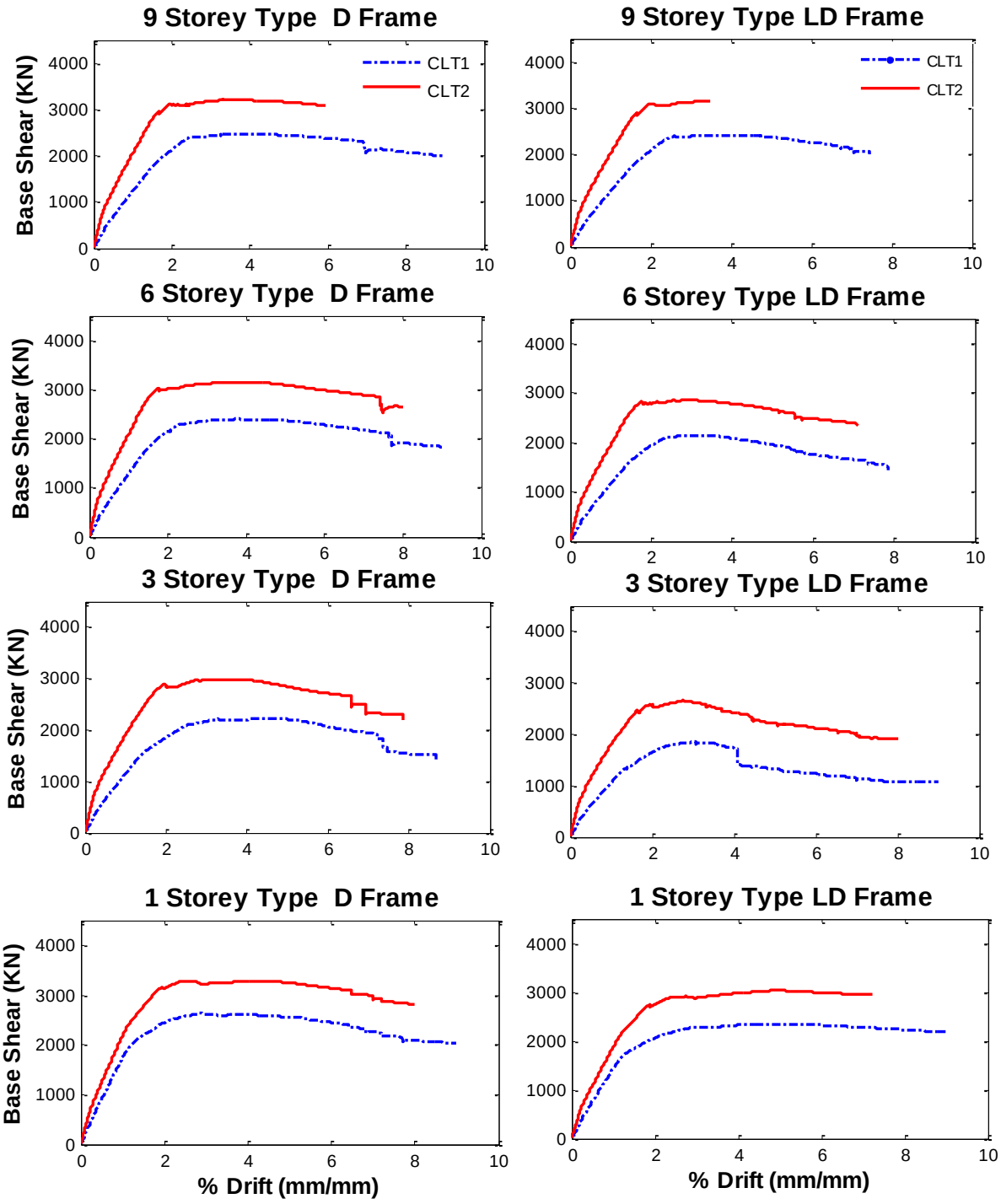

Figure 41: Results of nonlinear monotonic pushover analysis for low- and mid-rise models with bracket spacing of 0.8m

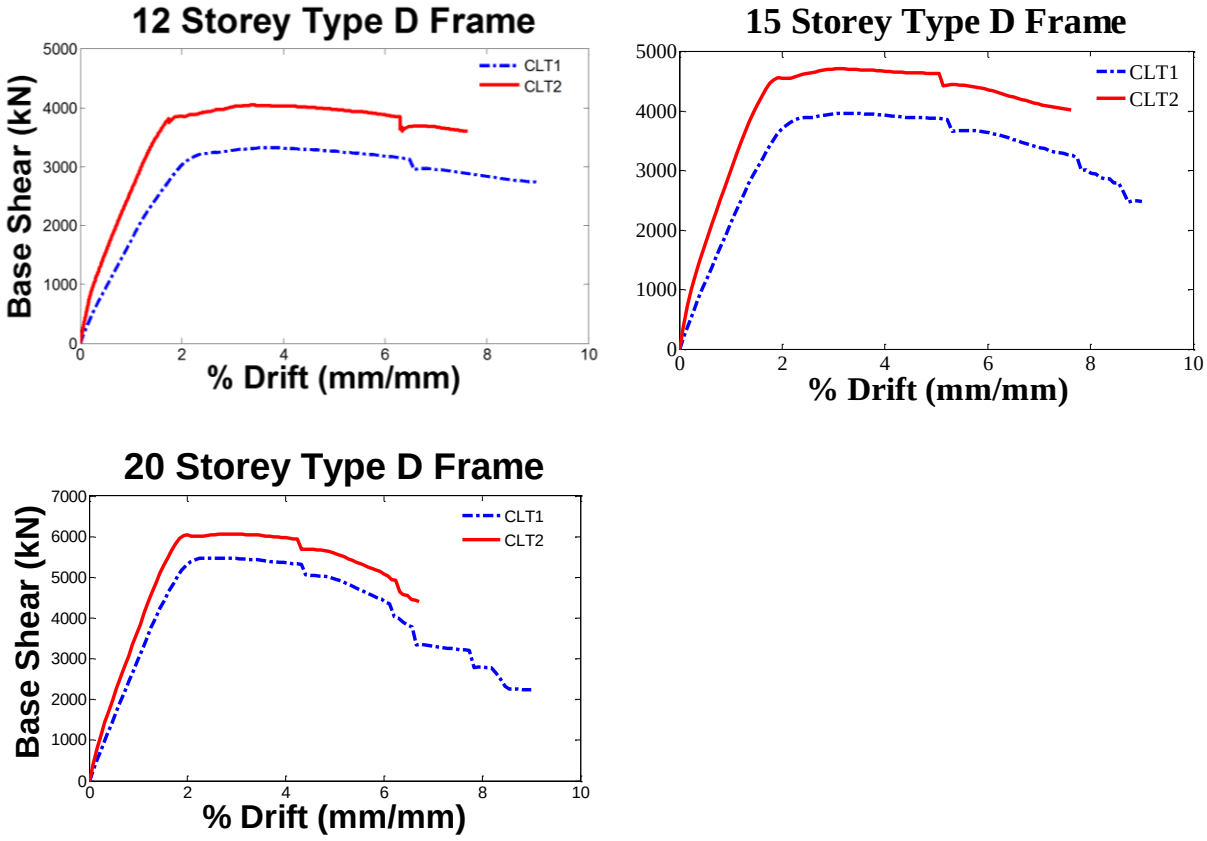

Figure 42: Results of nonlinear monotonic pushover analysis for high-rise models with bracket spacing of 0.8m

7.4 Equivalent Energy Elastic-Plastic Approximation

An equivalent energy elastic-plastic (EEEP) curve is used to calculate the system yielding point under monotonic static pushover analysis. The EEEP idealizes the elastic-plastic curve under consideration by equating areas enclosed by the envelope and approximate curve. Figure 43 shows the EEEP curve which equates the area below the average data curve from zero with the area above this same curve until the ultimate displacement.

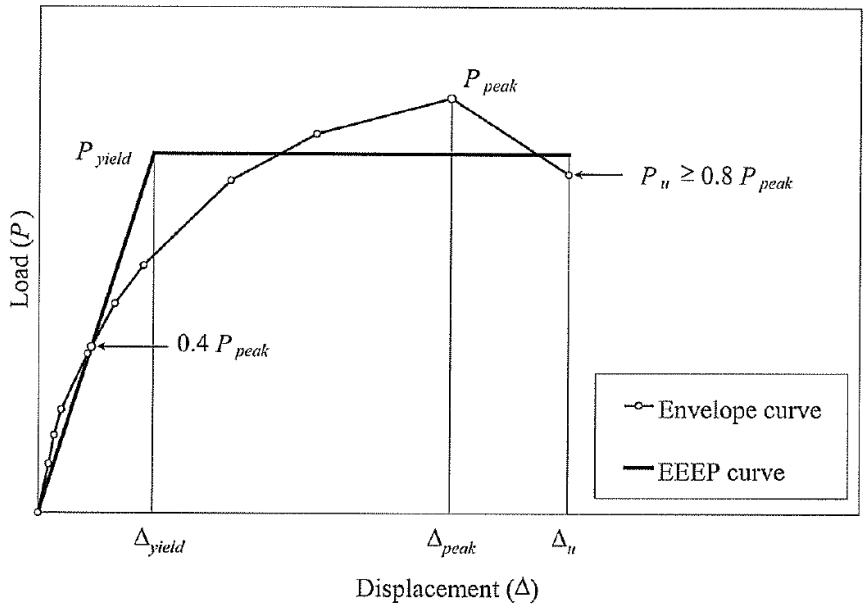

Figure 43: EEEP curve (ASTM 2126-09, 2009)

The ultimate displacement of the system is defined as $0.8P_{peak}$. Once the area, force, and displacement values are known the yield force for the system can be defined as:

$$P_{yield} = \left(\Delta_u - \sqrt{\Delta_u^2 - \frac{2A}{K_e}} \right) K_e \qquad [20]$$

where A is the area under the envelope curve from zero to the final displacement of the structure (Δ_u) and K_e is determined:

$$K_e = \frac{0.4P_{peak}}{\Delta_e} \qquad [21]$$

where P_{peak} is the maximum absolute load that the specimen can resist in the envelope, and finally Δ_e is the displacement of the specimen at $0.4P_{Peak}$.

7.5 Quantification of R_d and R_o factors

The overstrength (R_o) and ductility (R_d) factors based on NBCC (NRC 2005) and Newmark and Hall (1988) are summarized in Table 21 and Table 22 for type ductile and limited ductile frames. Dickof *et al*. (2014) compares the overstrength values that are obtained based on design base shear of frames (V_d) and base shear corresponding to the first yield of the system ($V_{y,sys}$). In this research project, consistent with FEMA P695, the overstrength factors are calculated based on the design bases shear.

Table 23: Overstrength and ductility factors for models with ductile (D) steel moment frames

Building No.	Storey height	Infilled bays	Ductility factor (R_d)	Overstrength factor (R_o)
1	3	1	2.77	2.41
2	3	2	3.35	3.25
3	6	1	4.60	2.64
4	6	2	7.29	3.46
5	9	1	5.04	2.25
6	9	2	5.12	2.91
7	12	1	5.33	2.43
8	12	2	5.99	3.09
9	15	1	4.51	2.4
10	15	2	5.12	3.11
11	20	1	3.56	2.23
12	20	2	3.88	2.8

Table 24: Overstrength and ductility factors for models with limited-ductile (LD) steel moment frames

Building No.	Storey height	Infilled bays	Ductility factor (R_d)	Overstrength factor (R_o) based V_d
1	3	1	2.40	1.93
2	3	2	3.41	2.76
3	6	1	3.87	2.16
4	6	2	6.82	2.84
5	9	1	4.03	2.07
6	9	2	3.00	2.60

The calculated R_d and R_o factors, respectively, are compared with the provisions of NBCC 2005values for bare steel moment frames on Figure 44 and Figure 45. NBCC 2005 recommends R_d factors of 5 and 2 for ductile and limited ductile SMRFs, respectively.

In Figure 44, for buildings up to 9 storey, limited ductile frames show less ductility than ductile frames. For 3 and 6 storey frames, increasing the infilled bays from one to two increases the ductility factor. However, for nine storey building, the addition of infilled bays doesn't affect the system ductility factor for ductile frames. Moreover, limited ductile nine storey frames losses its ductility with addition of infilled bay. For all considered limited ductile frames, the obtained ductility factors are greater than the NBCC 2010 requirements. However, single storey and 20 storey buildings have shown less ductility factors than the NBCC 2010 requirement. In general the analyses gave a minimum ductility factor of 2.77.

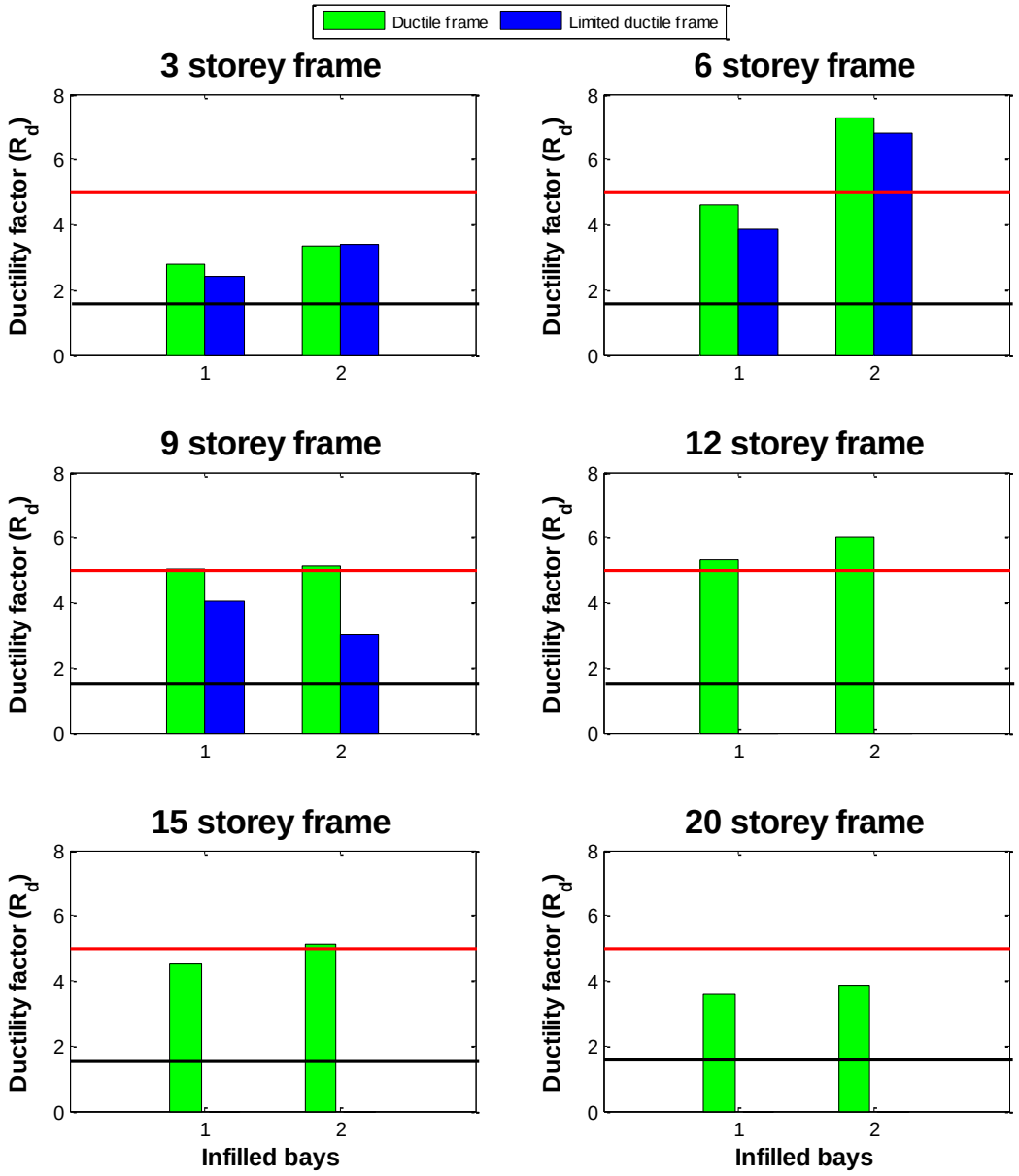

Figure 44: Ductility factors R_d

Figure 45 summarizes the R_o factors of the hybrid buildings. In general, as expected, the inclusion of CLT infill panels in SMRFs increases the R_o of the systems significantly. Irrespective of the height of the buildings, hybrid structures with two infilled bays have larger R_o. Moreover, for all considered combinations, limited ductile frames have less R_o than the ductile frames. Ductile and limited ductile frames in general have R_o greater than NBCC 2005 recommended values.

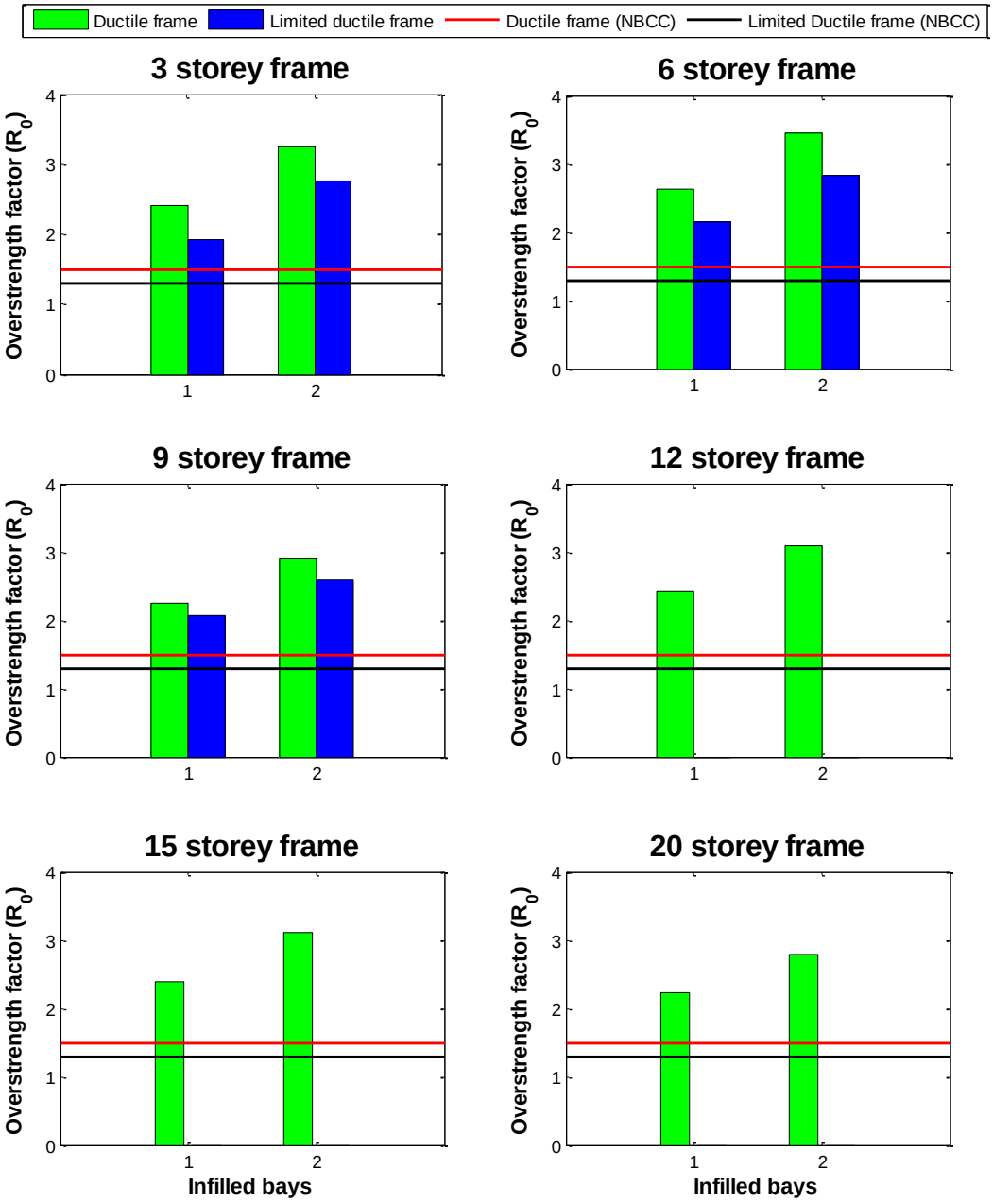

Figure 45: Overstrength factor R_o

Chapter 8
Fundamental Period

The fundamental period, T_a, is defined by the National Building Code of Canada (NBCC) as the fundamental lateral period of vibration of the structure (NRC, 2010). The NBCC gives lower bound estimates of the fundamental period based on regression analysis on past earthquakes measured periods (Saatcioglu and Humar 2003; Goel and Chopra 1997). An example of the data obtained to produce these empirical formulas can be seen in Tables A1 and A2. Kwon (2011) summarized the approximate fundamental period formula for different codes developed over the last forty years (Table 20). The table shows the development from just two empirical formulas for moment resisting frames (MRF) and other structural systems to five empirical formulas for reinforced concrete MRF, steel MRF, eccentrically braced frames, reinforced concrete/masonry shear walls, and other structural systems.

Table 25: Approximate fundamental period formulas (Kwon 2011)

	RC MRF	Steel MRF	EBF	RC/Masonry Shear Wall	Other
UBC-70, 82 BOCA-75	$T_a = 0.10N$		$T_a = 0.05h_n / D^{1/2}$		
ATC 3-06 (1978)	$T_a = C_t h_n^{3/4}$		$T_a = 0.05h_n / D^{1/2}$		
	$C_t = 0.025$	$C_t = 0.035$			
BOCA 87	$T_a = C_t h_n^{3/4}$		$T_a = 0.05h_n / D^{1/2}$		-
	$C_t = 0.030$	$C_t = 0.035$			
UBC-88, 94, 97 Eurocode 8 (2004)	$T_a = C_t h_n^{3/4}$				
	$C_t = 0.030$	$C_t = 0.035$	$C_t = 0.030$	$C_t = 0.02$ or, $C_t = 0.1 / A_c^{1/2}$	$C_t = 0.020$
ASCE 7-97 BOCA A-96 NEHRP 94, 97	$T_a = C_t h_n^{3/4}$				
	$C_t = 0.030$	$C_t = 0.035$	$C_t = 0.030$	$C_t = 0.020$	$C_t = 0.020$
	or, $T_a = 0.10N$		-	-	-
NEHRP 00, 03 ASCE 7-02,05	$T_a = C_r h_n^x$				
	$C_r = 0.016$ $x = 0.9$	$C_r = 0.028$ $x = 0.8$	$C_r = 0.030$ $x = 0.75$	$C_r = 0.020$ $x = 0.75$	$C_r = 0.020$ $x = 0.75$
	or, $T_a = 0.10N$		-	or, $T_a = 0.0019h_n / C_w^{1/2}$	-

These empirical formulas depend on the type of structural system, structural materials and the dimensions of the structure. The Eurocode (CEN 2002) and ASCE (ASCE 2010) standards have empirical formulas similar to that of the NBCC. The fundamental period can be different for each orthogonal direction.

8.1 NBCC fundamental period empirical formulas

The 2010 NBCC determines the fundamental period by the structural system as a function of the height of the structure. Table 21 shows the fundamental period empirical formulas for steel moment frames, concrete moment frames, other moment frames, braced frames, and shear wall and other structural systems.

Table 26: NBCC empirical formulas for fundamental period (NRC 2010)

$T_a = 0.085(h_n)^{3/4}$	Steel moment frames
$T_a = 0.075(h_n)^{3/4}$	Concrete moment frames
$T_a = 0.1N$	Other moment frames
$T_a = 0.025h_n$	Braced frames
$T_a = 0.05(h_n)^{3/4}$	Shear wall and other structures

In Table 21, h_n = height of the building in meters and N = total number of storeys above exterior grade. Often, the static and dynamic analyses give larger values of fundamental period than the empirical formula; therefore, the NBCC specifies that the period cannot exceed 1.5 times the empirical based period value for moment frames and 2 times for braced frames and shear walls. The limit was imposed because of the overestimation that structural models often have on the flexibility of a structural system. These structural models often neglect the non-structural stiffening elements which results in larger estimated natural periods. Moreover, the NBCC specifies a 2.0 s fundamental period maximum for moment resisting frames, braced frames, and other systems. Furthermore, for walls, coupled walls and wall-frame systems the fundamental period may not exceed 4.0 s.

8.2 FEMA P695

The Applied Technology Council (ATC) prepared a report for the Federal Emergency Management Agency (FEMA) in 2009 called the "Quantification of Building Seismic Performance Factors" better known as the FEMA P695 report (FEMA, 2009). In this report, the fundamental period is computed as:

$$T = C_u T_a \quad [22]$$

where T = fundamental period of the building, C_u = factors provided by the ASCE/SEI 7-05 shown in Table 22, and T_a = the approximate fundamental period. The approximate fundamental period equation is (NRC, 2010):

$$T_a = C_t h_n^{\ x} \quad [23]$$

where C_t and *x* values are summarized in Table 27 and h_n = the height of the building.

Table 27: Coefficient for upper limit on calculated period (ASCE 2010)

Design Spectral Response Acceleration Parameter at 1 *s*, S_{D1}		**Coefficient C_u**
≥	0.4	1.4
	0.3	1.4
	0.2	1.5
	0.15	1.6
≤	0.1	1.7

Table 28: Values of approximate period parameters C_t and x (ASCE-SEI 2010)

Structure Type	C_t	*x*
Moment-resisting frame systems in which the frames resist 100% of the required seismic force and are not enclosed or adjoined by components that are more rigid and will prevent the frames from deflecting where subjected to seismic forces:		
Steel moment-resisting frames	0.028 (0.0724)[a]	0.8
Concrete moment-resisting frames	0.016 (0.0466)[a]	0.9
Steel eccentrically braced frames in accordance with Table 12.2-1 lines B1 or D1	0.03 (0.0731)[a]	0.75
Steel buckling-restrained braced frames	0.03 (0.0731)[a]	0.75
All other structural systems	0.02 (0.0488)[a]	0.75

[a]Metric equivalents are shown in parentheses

The periods of the hybrid buildings were determined through eigenvalue analysis. Each structures first and second natural period were computed through the modal analysis of OpenSees finite element software. Table 24 shows the fundamental natural periods of the steel-timber hybrid structures studied.

Table 29: Fundamental period results

Building No.	Storey height	Ductility class	Infilled bays	Period (s)
1	1	D	1	0.30
2	1	D	2	0.24
3	1	LD	1	0.33
4	1	LD	2	0.26
5	3	D	1	0.91
6	3	D	2	0.62
7	3	LD	1	0.96
8	3	LD	2	0.68
9	6	D	1	1.66
10	6	D	2	1.15
11	6	LD	1	1.75
12	6	LD	2	1.2
13	9	D	1	2.48
14	9	D	2	1.71
15	9	LD	1	2.52
16	9	LD	2	1.74
17	12	D	1	2.80
18	12	D	2	2.08
19	15	D	1	3.18
20	15	D	2	2.44
21	20	D	1	3.50
22	20	D	2	2.96

Results show an increase in period with an increase building height as the structure gets taller due to the ductile response. Furthermore, as the number of infilled bays increase the period decreases quite significantly since the structure becomes stiffer with additional infilled CLT walls. Finally, ductility class and bracket spacing changes had the least significant

effect on the period with ductile structures having slightly lower periods than limited ductile members and a bigger bracket spacing resulted in slightly larger period values.

The periods of the bare moment resisting frames resemble pure moment resisting frames which can then be compared to the empirical code values in the NBCC. Table 25 shows the ductile moment resisting frame periods from OpenSees compared with these code values.

8.2.1 Proposed empirical factor considering building height only

The proposed empirical formula considering only building height can be seen in Equation 26. The numerical results and analytical equation are plotted in Figure 46, and the analytical results are on the lower bound of the numerical result. This is a conservative result and in agreement with the code formulation.

$$T_a = 0.137(h_n)^{3/4} \qquad R^2 = 0.91 \qquad [24]$$

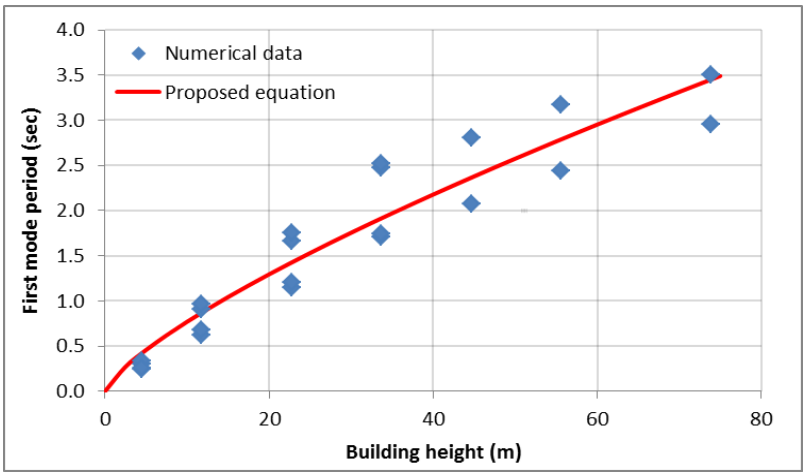

Figure 46: Proposed empirical formula considering only building height

8.2.2 Proposed empirical factor considering infill length and building height

When considering both infill length and height of structure the proposed equation was formulated through MATLAB using least square regression and is shown in Equation 27 (MATLAB, 2000). The infill length has a large impact on the period of a structure and

therefore, should be in the empirical formula. The effect of infill length and storey height on period is displayed in the plot seen in Figure 47.

$$T_a = \frac{0.155 \cdot h_n}{\sqrt{D}} \qquad R^2 = 0.85 \qquad [25]$$

where D = the infill length in meters, and h_n = the height of the structure above grade in meters.

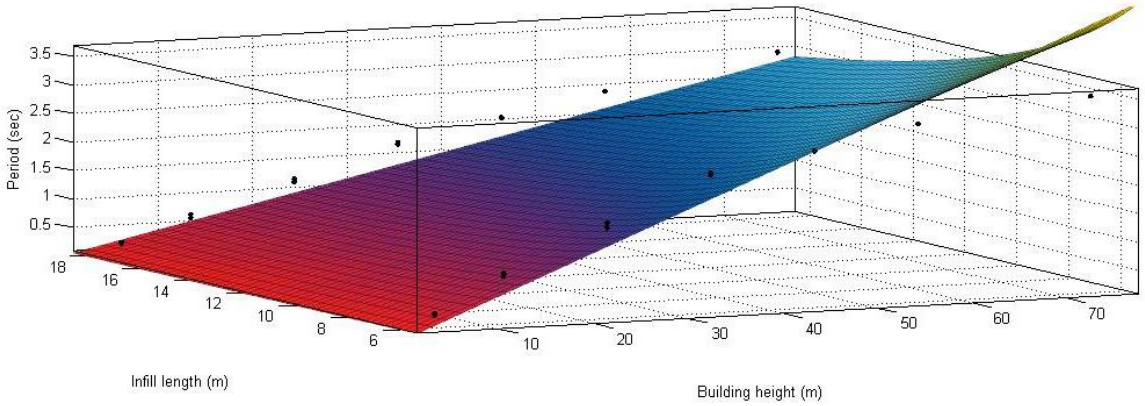

Figure 47: Fundamental period as a function of infill length and building height

Chapter 9

Seismic Hazard for Vancouver and Ground Motion Selection

9.1 Seismic Hazard in Vancouver

Greater Vancouver is vital to the healthy economic growth and normal functionality of socioeconomic activities in south-western BC. It is situated in one of the most active seismic zones in Canada. Since 1900, several destructive earthquakes occurred (Figure 48), e.g. the 1918 and 1946 earthquakes in Vancouver Island and the 1949, 1965, and 2001 (Nisqually) deep earthquakes in Washington, USA.

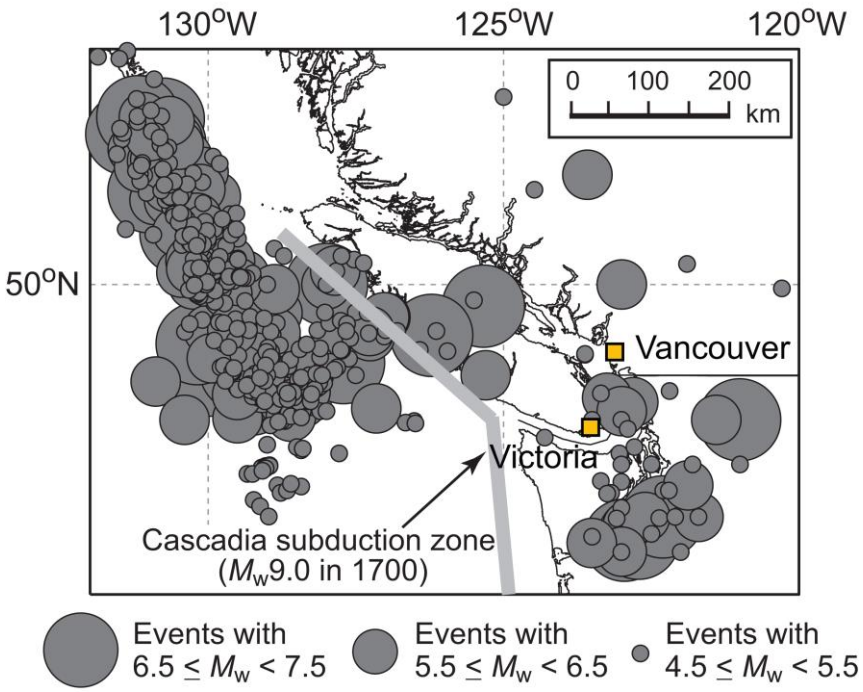

Figure 48: Regional seismicity in south-western BC, Canada

There are mainly three potential sources of damaging earthquakes: shallow crustal earthquakes, off-shore mega-thrust interface earthquakes from the Cascadia subduction zone, and deep inslab earthquakes (Hyndman and Rogers 2010). The Cascadia subduction earthquakes occur at the interface between the Juan de Fuca plate and the North American plate, where plate motions are locked and large amount of strain is accumulated over many years (rate of convergence is about 40 mm/year). The expected moment magnitude of such events is in the range of 8 to 9, and the last event occurred in 1700 (Satake *et al*. 2003). The mean recurrence period of the Cascadia subduction event ranges from 500 to 600 years (typically around 530 years) with large variability (Mazzotti and Adams 2004; Goldfinger *et al*. 2008, 2012). In comparison with crustal and inslab earthquakes, large interface ground motions, originated from the Cascadia subduction zone, have rich spectral content in the long vibration period range (because the earthquake magnitude of the Cascadia subduction events is about M_w8-9, while those of the crustal and inslab events are in the range of M_w6 to M_w7.5). Moreover, duration of the interface events will be much longer than that of the crustal and inslab events. The long duration ground motions due to a mega-thrust subduction earthquake and their influence on tall buildings at remote locations (several hundreds of kilometers from the epicenter) have been highlighted for the 2011 Tohoku, Japan, earthquake (Tatewaki *et al*. 2011).

A recent regional seismic hazard model by Atkinson and Goda (2011) has incorporated key features of seismic hazard in south-western BC, and has updated seismic hazard estimates for southwestern BC with respect to those in the NBCC 2005-2010 (Adams and Atkinson 2003). The updated assessment takes into account:

1) use of a longer earthquake catalogue based on a uniform moment magnitude scale in developing revised magnitude-recurrence relationships for seismic source zones in south-western BC;
2) use of newer ground motion prediction equations (GMPEs) with proper distance measure conversion by accounting for finite fault plane size;
3) logic-tree representation of alternative GMPEs to account for epistemic uncertainty in ground motion prediction; and
4) probabilistic scenarios for the potential mega-thrust Cascadia earthquakes.
5) seismic hazard is estimated as 'mean', rather than 'median', which is consistent with modern interpretation of probability and related assessments of seismic risk (McGuire *et al*. 2005).

In this study, the updated seismic hazard model is adopted to characterize seismic hazard in Vancouver. The site condition for PSHA is set to site class C, which is the reference site condition for national seismic hazard mapping and NBCC and can be represented by a site parameter V_{S30} (average shear-wave velocity in the uppermost 30 m) of 360 to 760 m/s. This site condition is prevalent in downtown Vancouver (Cassidy and Rogers 2004).

The first three fundamental periods for all building heights and infill patterns are summarized in Table 27. T_1 is the representative (anchor) fundamental vibration period for a given building storey class (with different infill patterns). This period is used for the record selection and scaling for seismic performance assessment. In addition, the limiting vibration period T_{min} and T_{max} are defined for each storey class such that the first three vibration periods fall within the specified range. This range is used when response spectrum matching of candidate records with the target response spectrum is carried out (see Section 9.2).

Table 30: First three fundamental periods of all building storeys and infill patterns

Building storey	Infill pattern	Period (s) Mode-1	Mode-2	Mode-3	T_1	$[T_{min}, T_{max}]$
1	0-1-0	0.30	0.05	0.03	0.30	[0.05, 1.0]
	1-0-1	0.24	0.05	0.03		
3	0-1-0	0.92	0.29	0.14	0.80	[0.10, 2.0]
	1-0-1	0.62	0.21	0.12		
6	0-1-0	1.67	0.54	0.30	1.50	[0.2, 2.5]
	1-0-1	1.15	0.38	0.22		
9	0-1-0	2.49	0.85	0.48	2.00	[0.3, 3.0]
	1-0-1	1.72	0.58	0.34		
12	0-1-0	2.80	0.92	0.51	2.50	[0.4, 3.0]
	1-0-1	2.08	0.69	0.40		
15	0-1-0	3.18	1.07	0.60	3.00	[0.4, 3.0]
	1-0-1	2.44	0.81	0.47		
20	0-1-0	3.50	1.14	0.64	3.00	[0.4, 3.0]
	1-0-1	2.96	0.97	0.55		

Figure 49a shows UHS at the return period (T_R) of 2500 years for Vancouver (V_{S30} = 550 m/s). The UHS is expressed as mean estimate, which includes the effects of epistemic uncertainty in the seismic hazard model. It is important to recognize that the UHS ordinates are computed based on numerous earthquake scenarios that may occur in south-western BC, and dominant scenarios at different spectral periods are not identical, as source, path, and site characteristics affect frequency content of ground motions differently. For instance, a large magnitude event has richer long-period content in source spectrum, while short-period content of ground motion attenuates more rapidly over distance than low-frequency content. To investigate dominant earthquake scenarios contributing to overall seismic hazard in Vancouver, seismic deaggregation analysis is conducted, and the results are shown in Figure 49b, Figure 50b, and Figure 51b by considering the spectral periods of 0.3 s, 1.5 s, and 3.0 s, respectively (note: these three periods are selected for illustration). The selected vibration periods of 0.3 s, 1.5 s, and 3.0 s corresponds to the representative fundamental vibration periods (T_1) of the 3-storey, 6-storey, and 15/20-storey steel-timber hybrid structures (Table

27). The dominant scenarios are represented in terms of magnitude, distance, and earthquake type (crustal/interface/inslab). Different earthquake types are associated with distinct event features in terms of magnitude and distance. For instance, the magnitude and distance of the Cascadia subduction events range between 8 and 9 and between 100 and 150 km, respectively; these are constrained by physical characteristics of the Cascadia scenarios. At the return period of 2500 years, 13% of the dominant scenarios are originated from the Cascadia subduction zone for T_1 = 0.3 s (Figure 49b), whereas this percentages gradually increases as T_1 becomes longer; for T_1 = 3.0 s, the relative contribution of the Cascadia subduction events reaches 47% (Figure 51b). This is an important consideration in conducting record selection for seismic performance evaluation of (relatively flexible) structures in south-western BC.

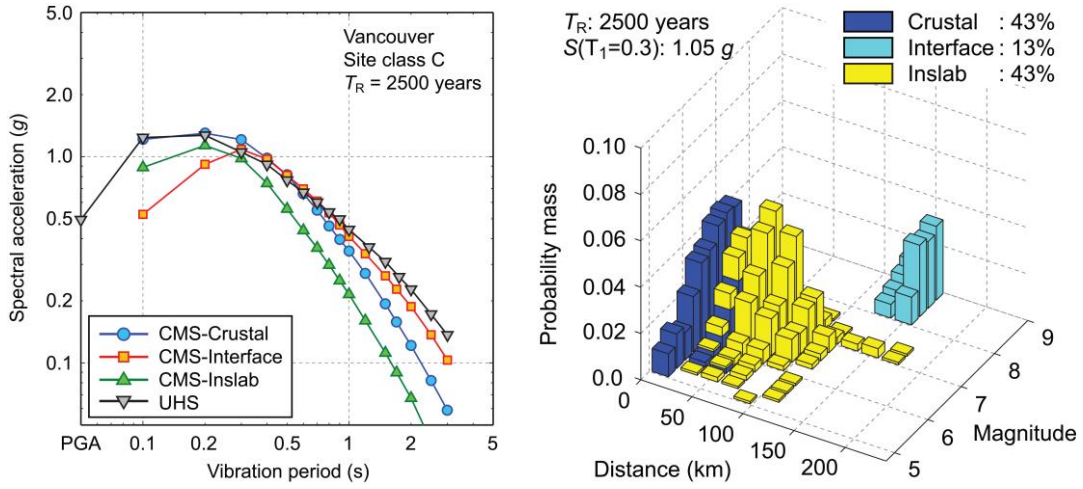

Figure 49: (a) Uniform hazard spectrum and conditional mean spectra for crustal interface, and inslab events in Vancouver, and (b) seismic deaggregation for spectral acceleration at 0.3 s in Vancouver.

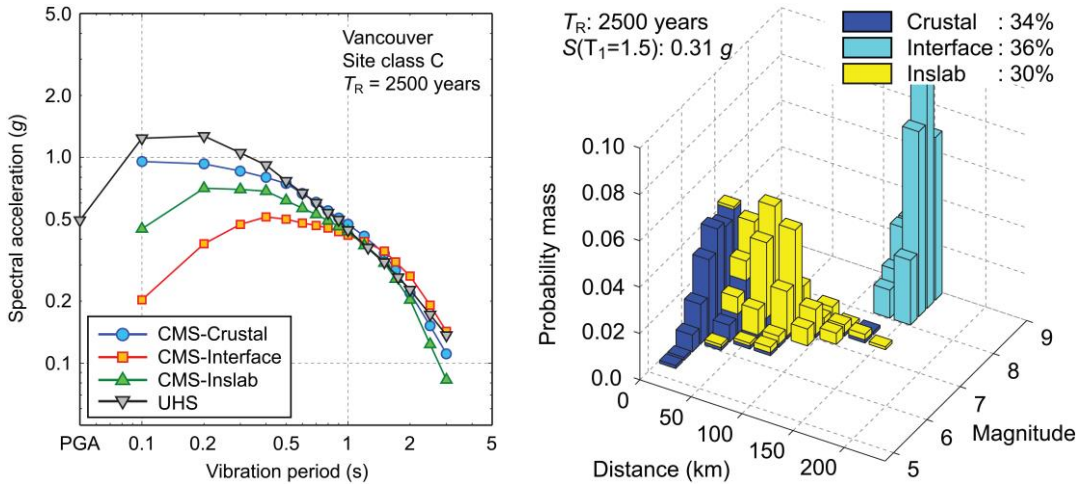

Figure 50: (a) Uniform hazard spectrum and conditional mean spectra for crustal interface, and inslab events in Vancouver, and (b) seismic deaggregation for spectral acceleration at 1.5 s in Vancouver.

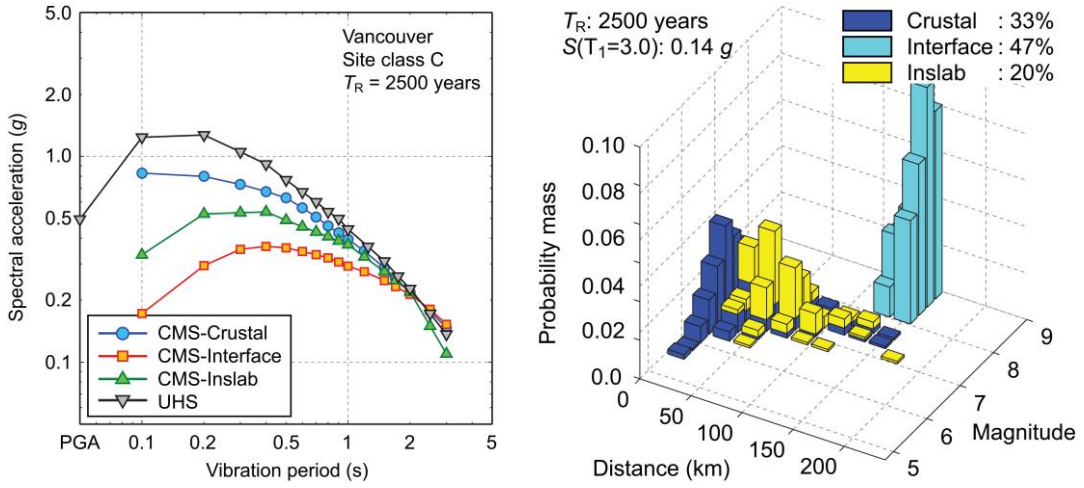

Figure 51: (a) Uniform hazard spectrum and conditional mean spectra for crustal interface, and inslab events in Vancouver, and (b) seismic deaggregation for spectral acceleration at 3.0 s in Vancouver.

9.2 Ground Motion Selection for Vancouver

The record selection is conducted based on a multiple-conditional-mean-spectra (CMS) method (Baker 2011; Goda and Atkinson 2011). The method takes into account multiple target spectra (with inter-period correlation of spectral ordinates), representing distinct response spectral features of different earthquake types (i.e. crustal versus interface versus inslab) and their relative contributions to overall seismic hazard. It utilizes seismic hazard information in terms of spectral acceleration that is available from PSHA. The method has been successfully implemented for both conventional wood-frame houses (Goda and Atkinson 2011) and RC buildings with/without masonry infills (Tesfamariam *et al*. 2014; Tesfamariam and Goda 2015). The target CMS that are developed for crustal, interface, and inslab earthquakes are shown in Figure 49a, Figure 50a, and Figure 51a by considering different anchor periods of 0.3 s, 1.5 s, and 3.0 s, respectively (i.e. T_1 for 3-storey, 6-storey, and 15/20-storey hybrid structures; see Table 27). The similarity of the target CMS for three earthquake types depend on the anchor period.

The record database is an extended dataset of real mainshock-aftershock sequences (see Tesfamariam and Goda 2015); it has been developed by combing the PEER-NGA (Pacific Earthquake Engineering Research–Next Generation Attenuation) database (Goda and Taylor 2012) with the updated version of the KKiKSK (K-NET, KiK-net, and SK-net in Japan) database (Goda 2012). The number of available mainshock-aftershock sequences is 606; among them, there are 197 crustal earthquakes, 340 interface earthquakes, and 69 inslab earthquakes. The interface events are from the 2003 Tokachi-oki earthquake or the 2011 Tohoku earthquake (which have similar event characteristics as the expected Cascadia subduction earthquake). In this study, mainshock records of the developed database are considered.

Using the target CMS, a set of ground motion records is selected by comparing response spectra of candidate mainshock records with the target spectra. The total number of selected records is set to 30 (note: each record has two horizontal components). For the 3-storey, hybrid structure, 13, 4, and 13 records are selected for the crustal, interface, and inslab

earthquakes, respectively (Figure 49b); for the 6-storey, hybrid structure, 10, 11, and 9 records are selected for the crustal, interface, and inslab earthquakes, respectively (Figure 50b); and for the 15/20-storey, hybrid structure, 10, 14, and 6 records are selected for the crustal, interface, and inslab earthquakes, respectively (Figure 51b). Figure 52 compares the magnitude-distance distributions of the selected records for the anchor vibration periods of 0.3, s, 1.5 s, and 3.0 s. Because the relative contributions of the Cascadia subduction events increase with T_1 (Figures 49 to 51), larger-magnitude records are selected more frequently for the longer-period structures. More specifically, when T_1 = 0.3 s, no records from the 2011 Tohoku earthquake was chosen (i.e. all records have moment magnitudes less than 8.5), whereas when T_1 = 1.5 s and 3.0 s, the majority of the selected interface records are from the 2011 Tohoku earthquake (i.e. records with moment magnitude of 9.0).

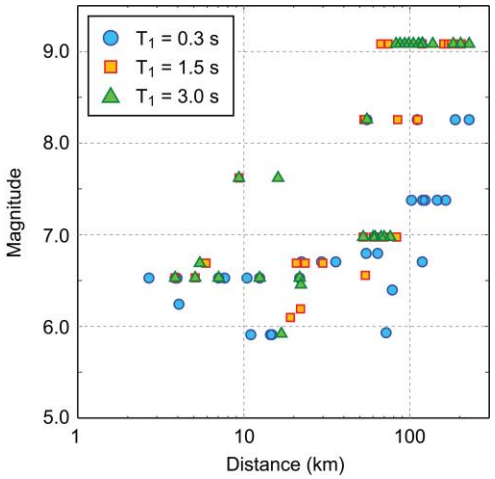

Figure 52: Magnitude-distance plot of the selected records for T_1 = 0.3 s, 1.0 s, and 3.0 s.

The detailed results for the multiple-CMS-based record selection are presented in Figure 53, Figure 54, and Figure 55 for the anchor vibration periods of 0.3, s, 1.5 s, and 3.0 s, respectively. In the CMS-based method, response spectral matching is conducted in a least

squares sense by considering the geometric mean of the response spectra of two horizontal components. The vibration period ranges for spectral matching (i.e. T_{min} and T_{max} in Table 27) are set to: from 0.1 s to 1.0 s, from 0.2 s to 2.5 s, and from 0.4 s to 3.0 s for T_1 = 0.3 s, 1.5 s, and 3.0 s, respectively (shaded segments in Figures 47 to 49). In these figures, the statistics of the response spectra of the selected ground motion records (i.e. median as well as 16th/84th percentile curves) for three earthquake types are compared with the target CMS as well as the CMS plus/minus one conditional standard deviation (Jayaram *et al*. 2011). Generally, the percentile curves of the selected records are consistent with the CMS and CMS plus/minus one conditional standard deviation. The matching performance is poor in the vibration period range outside of [T_{min}, T_{max}]; this can be improved when the number of records is increased.

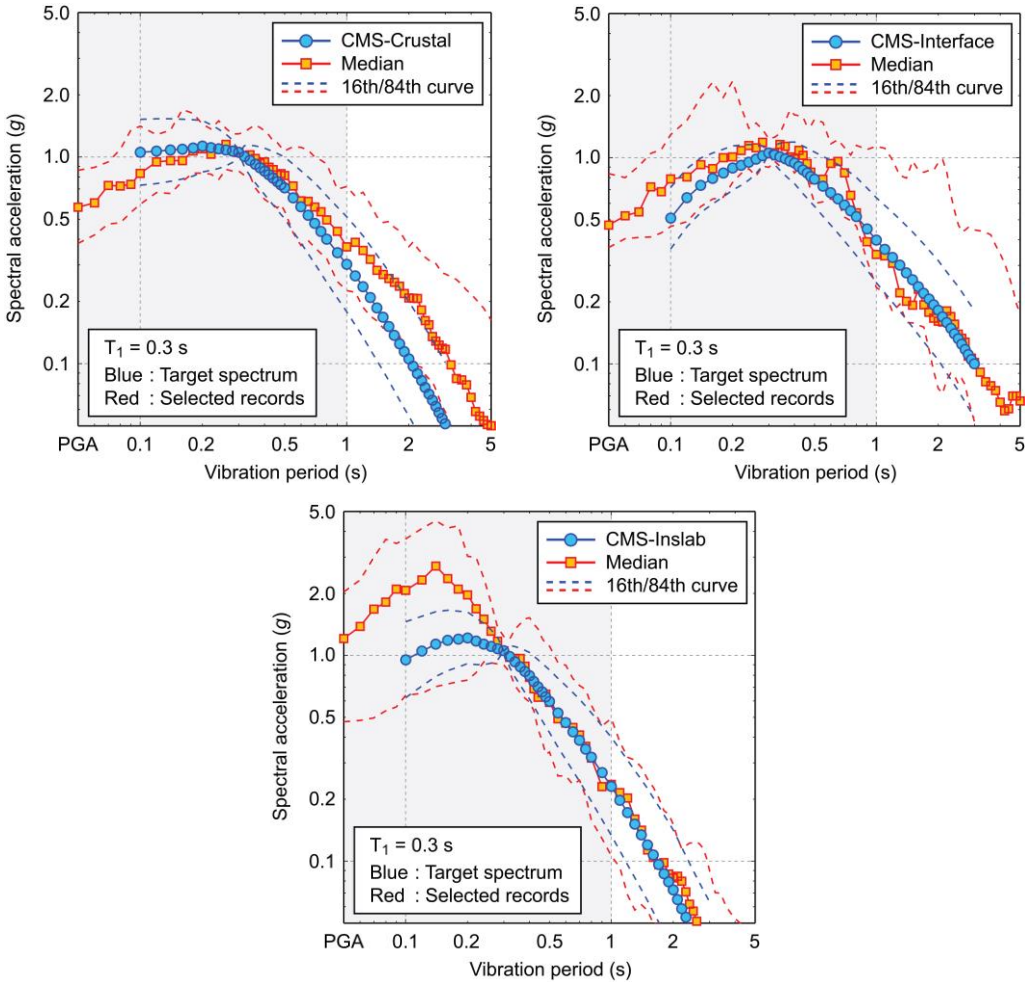

Figure 53: Comparison of response spectra of the selected ground motion records ($50^{th}/16^{th}/84^{th}$ curve) and conditional mean spectra (mean and mean plus/minus one standard deviation) for the crustal, inslab, and interface earthquakes for $T_1 = 0.3$ s.

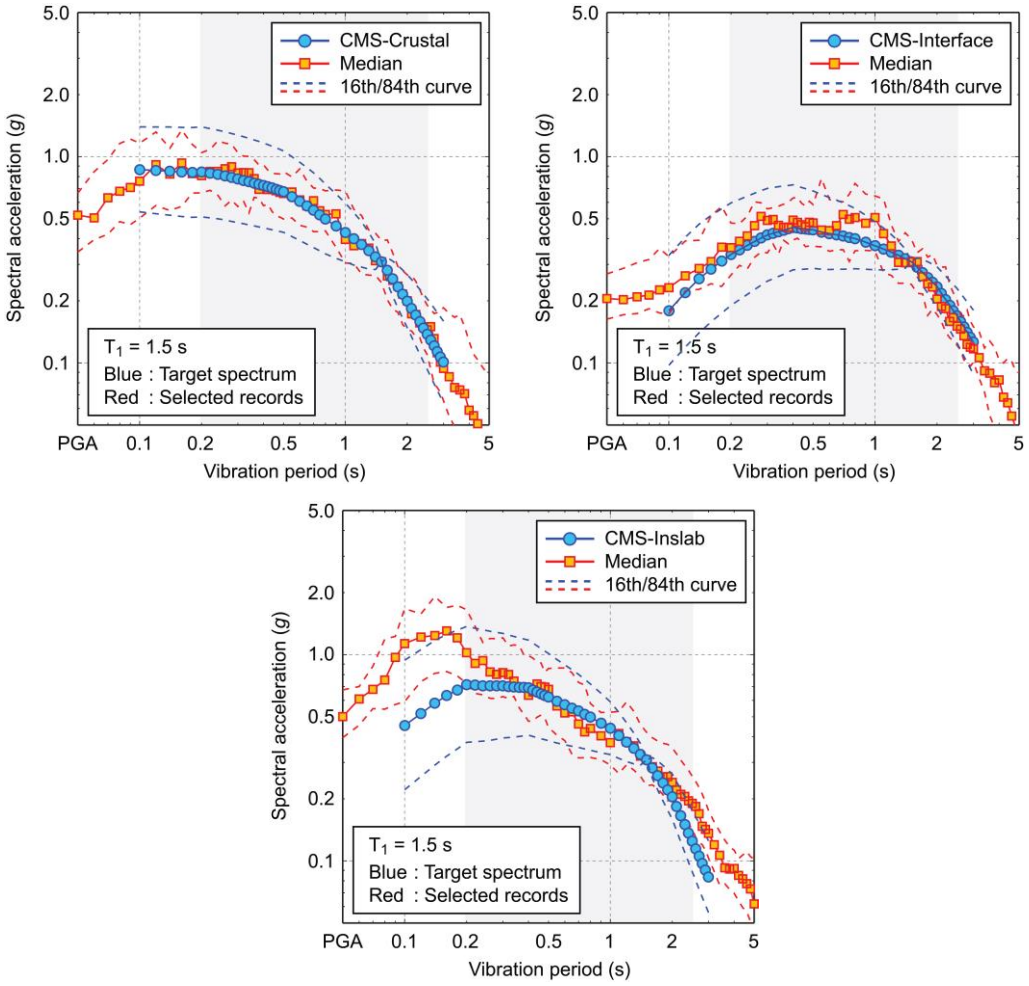

Figure 54: Comparison of response spectra of the selected ground motion records ($50^{th}/16^{th}/84^{th}$ curve) and conditional mean spectra (mean and mean plus/minus one standard deviation) for the crustal, inslab, and interface earthquakes for T_1 = 1.5 s.

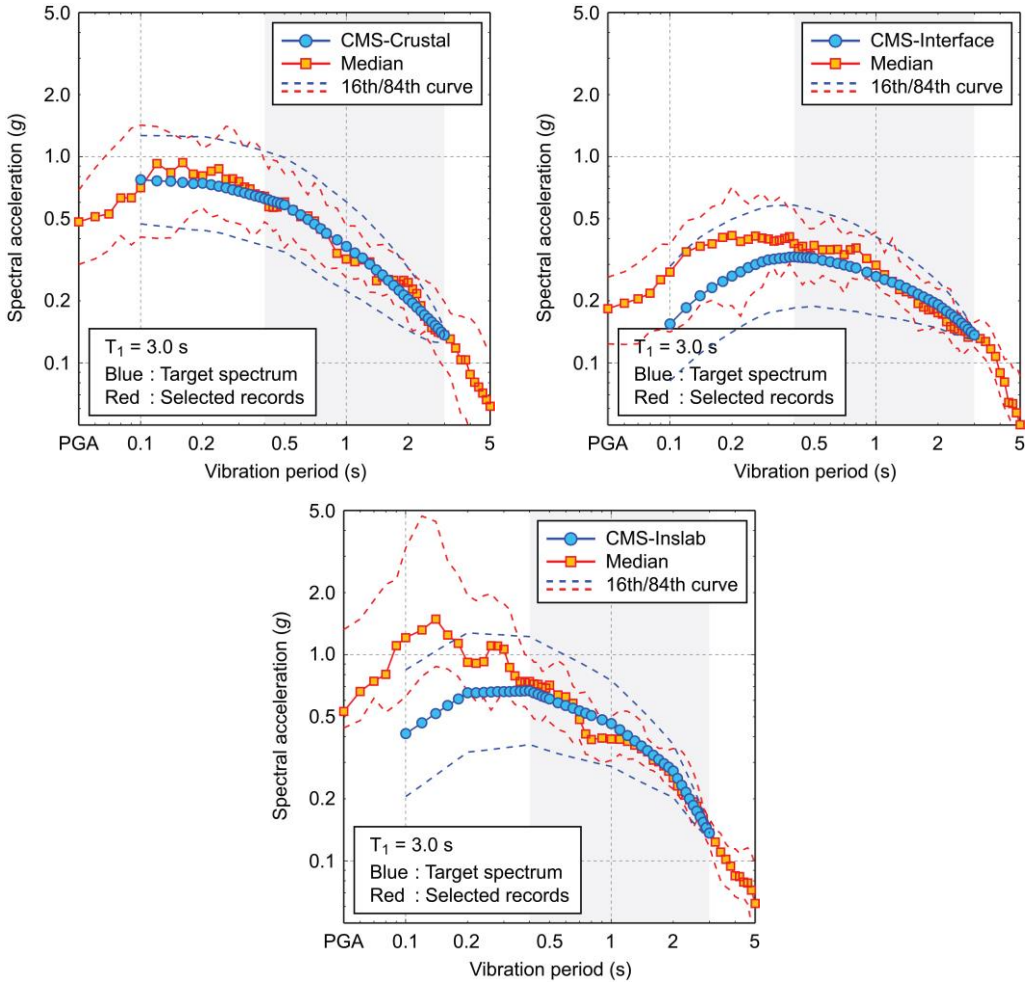

Figure 55: Comparison of response spectra of the selected ground motion records ($50^{th}/16^{th}/84^{th}$ curve) and conditional mean spectra (mean and mean plus/minus one standard deviation) for the crustal, inslab, and interface earthquakes for T_1 = 3.0 s.

9.3 FEMA P695 Ground Motions

The FEMA P695 guideline for selecting the ground motions is briefly outlined below. Several sets of specific ground motions are already selected for seismic performance assessment in the U.S.:

- **Code (ASCE/SEI 7-05) Consistent** – The records should be consistent (to the extent possible) with the ground motion requirements of Section 16.1.3.2 of ASCE/SEI 7-05 Minimum Design Loads for Buildings and Other Structures (ASCE, 2006a) for three-dimensional analysis of structures. In particular, "ground motions shall consist of pairs of appropriate horizontal ground motion acceleration components that shall be selected and scaled from individual recorded events."
- **Very Strong Ground Motions** – The records should represent very strong ground motions corresponding to the MCE motion. In high seismic regions where buildings are at greatest risk, few recorded ground motions are intense enough, and significant upward scaling of the records is often required.
- **Large Number of Records** – The number of records in the set should be "statistically" sufficient such that the results of collapse evaluations adequately describe both the median value and record-to-record (RTR) variability of collapse capacity.
- **Structure Type Independent** – Records should be broadly applicable to collapse evaluation of a variety of structural systems, such as systems that have different dynamic response properties or performance characteristics. Accordingly, records should not depend on period, or other building-specific properties of the structure.
- **Site Hazard Independent** – The records should be broadly applicable to collapse evaluation of structures located at different sites, such as sites with different ground motion hazard functions, site and source conditions. Accordingly, records should not depend on hazard deaggregation, or other site- or hazard-dependent properties.

The ground motion records selected for the FEMA 695P guideline may not be applicable to south-western BC directly for several reasons. The regional seismicity in south-western BC is contributed by not only shallow crustal earthquakes, but also mega-thrust Cascadia events and deep inslab events. The dominant frequency content and duration for these earthquakes are significantly different from those for moderate crustal earthquakes (which are adopted by the FEMA 695P guideline). To examine the differences of the response spectral characteristics of the FEMA-695P-based records and the multiple-CMS-based records (Section 9.2), the statistics of the response spectra for these record sets are compared in Figure 49 for the anchor vibration periods of 0.3, s, 1.5 s, and 3.0 s. Note that the records for the FEMA 695P guideline are the so-called far-field record set containing 22 records (i.e.

44 horizontal components) from worldwide shallow crustal earthquakes; typical magnitude ranges for these records are between M_w6.5 and M_w7.5. Note that the effects of 'epsilon' are not taken into account in Figure 56 for the FEMA-695P-based records. The comparisons shown in Figure 56 are carried out by considering the record scaling (target spectral ordinates are the UHS for Vancouver). Figure 56 indicates that the similarity and dissimilarity depend significantly on the anchor vibration period. When T_1 = 0.3 s, noticeable differences are observed in the moderate-to-long vibration period range, whereas when T_1 = 1.5 s and 3.0 s, significant differences are present in the short vibration period range. Therefore, careful record selection for Vancouver is warranted.

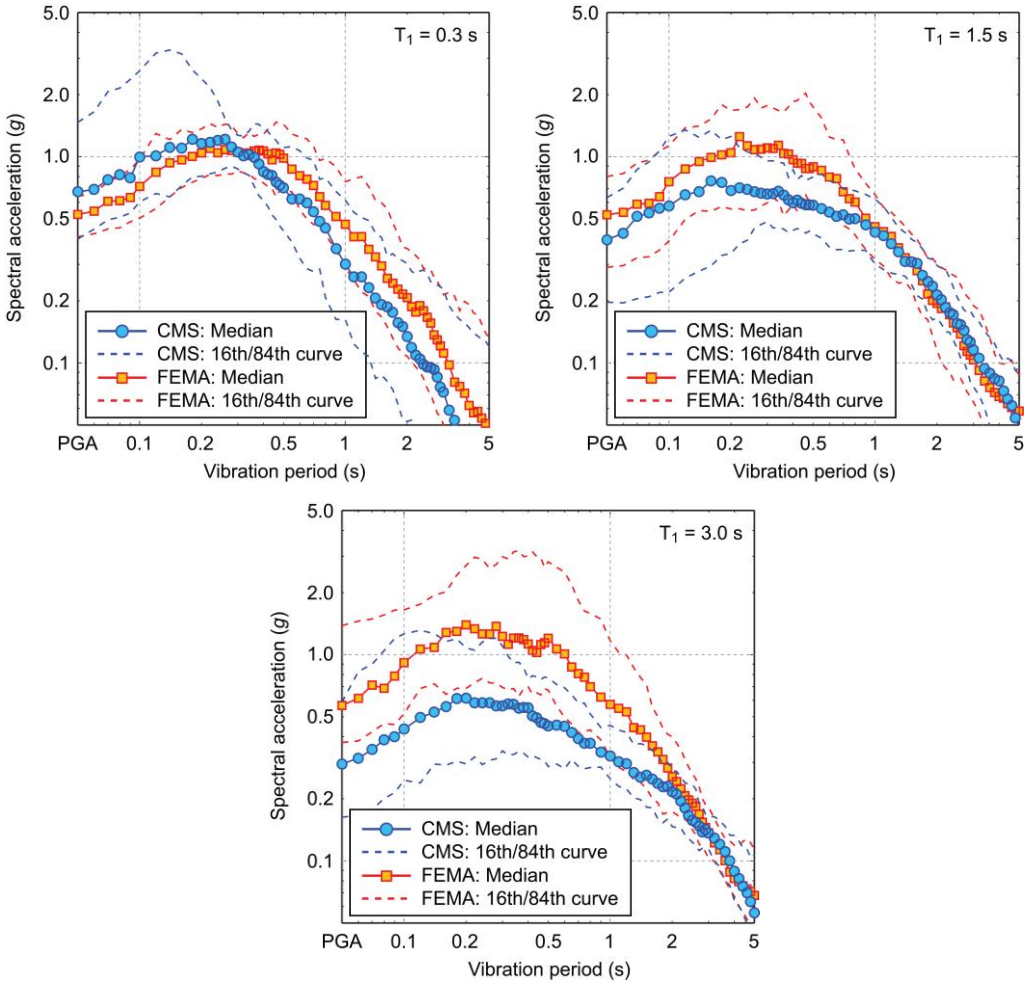

Figure 56: Comparison of the statistics of the response spectra ($50^{th}/16^{th}/84^{th}$ curve) for the records selected based on conditional mean spectra and for the 'far-field' records adopted in the FEMA 695P guideline by considering the anchor vibration periods of 0.3 s, 1.5 s, and 3.0 s.

Chapter 10
Validation of Proposed R_oR_d Factors

This chapter presents the performance evaluation procedure and results of the initially assumed ductility (R_d) and overstrength (R_o) factors. This evaluation process includes nonlinear time history analysis using 60 ground motion records (i.e., 30 records, 2 components each with 2 % probability of exceedance in 50 years) and Incremental Dynamic Analysis (IDA) (Vamvastikos and Cornell 2002). The chapter is organized as follows. First, the general adopted performance evaluation methodology is discussed in detail. Subsequently, results of performance check for collapse prevention limit state according to NBCC 2010 are presented. Finally, the obtained results and discussions are presented for performance evaluation through IDA.

10.1 Performance evaluation methodology

The assumed R_d and R_o of factors of Chapter 7 are evaluated through dynamic time history analyses. For this purpose, NLTHA and IDA have been conducted using 60 ground motion records (i.e., 30 records, 2 components each) with 2 % probability of exceedance in 50 years. The former analysis was carried out to check against collapse prevention limit state of NBCC 2010, while the latter analysis is to check the collapse margin ratio according the FEMA P695 methodology.

The assessment of overall seismic performance of the hybrid buildings (designed in Chapter 7) using NLTHA is evaluated through the maximum interstorey drift (MISD) demand of the buildings. NBCC 2010 poses a 2.5% MISD limit to represent extensive damage on the buildings. In this approach, the overall objective is to make sure that the

average MISD in the building (irrespective of the storey height it is calculated) is less than 2.5%.

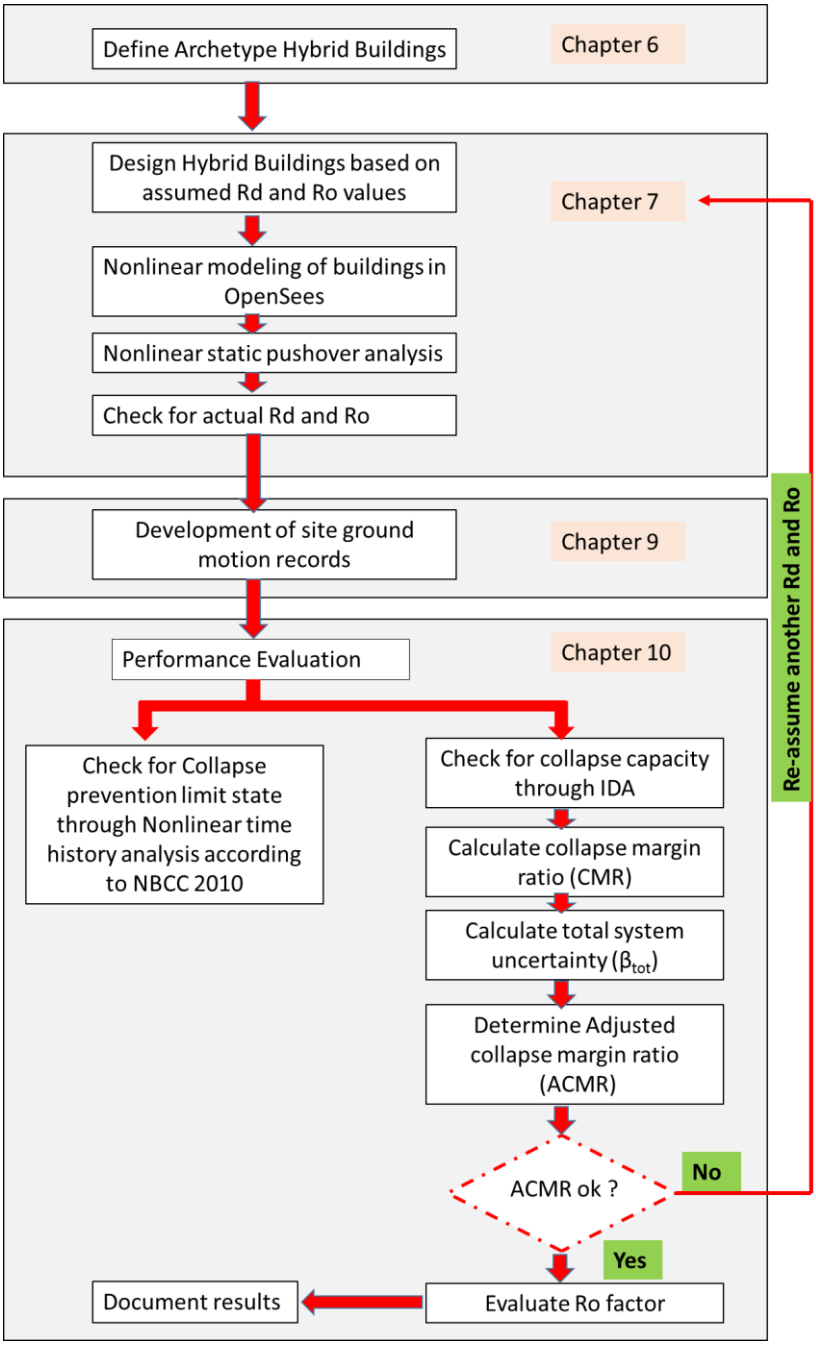

Figure 57: Performance evaluation methodology

To verify the acceptability of the assumed R_d and R_o factors, FEMA P695 suggests the use of IDA to calculate the probability of collapse. As a rule of thumb, FEMA P695 limits the probability of collapse for each performance group to be 10% under earthquakes with 2% in 50 years hazard. According to this approach, the acceptability of assumed force reduction factors is judged based on their collapse margin ratio from IDA. The considered collapse margin ratio is adjusted for total system uncertainty and spectral shapes. The general framework for the adopted methodology is depicted in Figure 57.

As the first step in the performance evaluation process, according to FEMA P695, it is required to obtain the collapse data from IDA. In IDA, the considered ground motion records are scaled up until collapse is achieved. The collapse data is used to calculate the collapse margin ratio (CMR) and to draw the interim collapse fragility curves. This fragility curves show the probability of collapse with respect to ground motion intensity under consideration. In this research, each fragility curve of a given hybrid building is assumed to be a lognormal curve, which is defined by median collapse intensity ($\hat{S}_{CT}$) and standard deviation of natural logarithm (β_{RTR}). The median collapse capacity can be calculated from IDA or other simple approximation methods. Moreover, FEMA P695 defined β_{RTR} to be dispersion of IDA results due to variability within ground motion records. Due its insignificance on the final CMR, FEMA P695 suggest a constant value of $\beta_{RTR} = 0.4$ for structures with period based ductility ($\mu>3$).

Once the median collapse intensity is evaluated from IDA, the next step is to calculate the collapse margin ratio *CMR* as:

$$CMR = \frac{\hat{S}_{MT}}{S_{MT}} \qquad [26]$$

where S_{MT} is spectral acceleration value at the fundamental period of the archetype structure under consideration.

Once CMR of each archetype is calculated, FEMA P695 adjust this value to Adjusted Collapse Margin Ratio (ACMR) to account for Spectral Shape Factor (SSF) as:

$$ACMR_i = SSF_i * CMR_i \quad [27]$$

However, in this research, ground motions were selected and scaled for each archetype models based on their spectral acceleration values at the fundamental period of the considered archetype building. Therefore, SSF will be 1, and for each archetype building $ACMR_i = CMR_i$.

In order to accurately calculate the safety against collapse, FEMA P695 considers more sources of uncertainties other than β_{RTR} during the performance evaluation process. The following set of bullets describe the considered system uncertainties.

- **Design requirement uncertainty (DR):** According to FEMA P695, this type of uncertainty is related to the robustness and completeness of design requirements of archetypes. Table 31 summarizes quantitative values of this uncertainty based on the rating of quality of the proposed design requirements as lognormal standard deviation parameter (β_{DR}). More information can be obtained from FEMA P695.

Table 31: Quality Rating of Design Requirements (FEMA P695)

	Confidence in Basis of Design Requirements		
Completeness and Robustness	**High**	**Medium**	**Low**
High. High. Extensive safeguards against unanticipated failure modes. All important design and quality assurance issues are addressed.	(A) Superior $\beta_{DR} = 0.1$	(B) Good $\beta_{DR} = 0.2$	(C) Fair $\beta_{DR} = 0.35$
Medium. Reasonable safeguards against unanticipated failure modes. Most of the important design and quality assurance issues are addressed.	(B) Good $\beta_{DR} = 0.2$	(C) Fair $\beta_{DR} = 0.35$	(D) Poor $\beta_{DR} = 0.5$
Low. Questionable safeguards against unanticipated failure modes. Many important design and quality assurance issues are not addressed.	(C) Fair $\beta_{DR} = 0.35$	(B) Poor $\beta_{DR} = 0.5$	–

- **Test data uncertainty (TD):** is uncertainty related to the quality of test data to calibrate and model the archetype buildings. Table 32 summarizes quantitative values of this uncertainty based on the rating of quality of the test data as lognormal standard deviation parameter (β_{TD}). More information can be obtained from FEMA P695.

Table 32: Quality Rating of Test Data from an Experimental Investigation Program (FEMA P695)

	Confidence in Test Results		
Completeness and Robustness	**High**	**Medium**	**Low**
High. Material, component, connection, assembly, and system behavior well understood and accounted for. All, or nearly all, important testing issues addressed	(A) Superior $\beta_{TD} = 0.1$	(B) Good $\beta_{TD} = 0.2$	(C) Fair $\beta_{TD} = 0.35$
Medium. Material, component, connection, assembly, and system behavior generally understood and accounted for. Most important testing issues addressed.	(B) Good $\beta_{TD} = 0.2$	(C) Fair $\beta_{TD} = 0.35$	(D) Poor $\beta_{TD} = 0.5$
Low. Material, component, connection, assembly, and system behavior fairly understood and accounted for. Several important testing issues not addressed.	(C) Fair $\beta_{TD} = 0.35$	(D) Poor $\beta_{TD} = 0.5$	–

- **Modeling uncertainty (MDL):** is uncertainty related to the accuracy, robustness and quality of the numerical models to capture seismic response and simulate the collapse mechanism of archetype buildings. Table 33 summarizes quantitative values of this uncertainty based on the rating of quality of the proposed numerical models as lognormal standard deviation parameter (β_{MDL}). More information can be obtained from FEMA P695.

Table 33: Quality Rating of Index Archetype Models

	Confidence in Basis of Design Requirements		
Completeness and Robustness	**High**	**Medium**	**Low**
High. Index models capture the full range of the archetype design space and structural behavioral effects that contribute to collapse.	(A) Superior $\beta_{MDL} = 0.1$	(B) Good $\beta_{MDL} = 0.2$	(C) Fair $\beta_{MDL} = 0.35$
Medium. Index models are generally comprehensive and representative of the design space and behavioral effects that contribute to collapse.	(B) Good $\beta_{MDL} = 0.2$	(C) Fair $\beta_{MDL} = 0.35$	(D) Poor $\beta_{MDL} = 0.5$
Low. Significant aspects of the design space and/or collapse behavior are not captured in the index models.	(C) Fair $\beta_{MDL} = 0.35$	(D) Poor $\beta_{MDL} = 0.5$	–

Based on the above sources of uncertainty, the total uncertainty for the performance evaluation process is obtained by combining RTR, DR, TD, and MDL. This total uncertainty is used to modify the interim fragility curves of each archetype buildings. The new collapse fragility curve is defined by a random variable (S_{CT}) as:

$$S_{CT} = \hat{S}_{CT}\lambda_{TOT} \quad [28]$$

where $\hat{S}_{CT}$ is median collapse intensity from IDA and λ_{TOT} is lognormally distributed random variable with a unit median and standard deviation of β_{TOT}. The formal definition of λ_{TOT} according to FEMA P695 is given as:

$$\lambda_{TOT} = \lambda_{RTR}\lambda_{DR}\lambda_{TD}\lambda_{MDL} \quad [29]$$

where $\lambda_{RTR}, \lambda_{DR}, \lambda_{TD}, \lambda_{MDL}$ are independent lognormally distributed random variables with median of unity and standard deviation of $\beta_{RTR}, \beta_{DR}, \beta_{TD}, \beta_{MDL}$ respectively. At this point it is to be noted that the above four random variables are statically independent (their joint probability distribution is the product of their marginal distribution), and the total collapse uncertainty parameter (β_{TOT}) can be calculated as:

$$\beta_{TOT} = \sqrt{\beta_{RTR}^2 + \beta_{DR}^2 + \beta_{TD}^2 + \beta_{MDL}^2} \quad [30]$$

For record-to-record uncertainty (β_{RTR}) of 0.4, Table 34 through Table 37 summarizes the values of β_{TOT}.

Table 34: Total System Collapse Uncertainty (β_{tot}) for Model Quality (A) Superior and Period-Based Ductility, $\mu_T \geq 3$ (FEMA, 2009)

Quality of Test Data	Quality of Design Requirements			
	(A) Superior	(B) Good	(C) Fair	(D) Poor
(A) Superior	0.425	0.475	0.550	0.650
(B) Good	0.475	0.500	0.575	0.675
(C) Fair	0.550	0.575	0.650	0.725
(D) Poor	0.650	0.675	0.725	0.825

Table 35: Total System Collapse Uncertainty (β_{tot}) for Model Quality (B) Good and Period-Based Ductility, $\mu_T \geq 3$ (FEMA, 2009)

Quality of Test Data	Quality of Design Requirements			
	(A) Superior	(B) Good	(C) Fair	(D) Poor
(A) Superior	0.475	0.500	0.575	0.675
(B) Good	0.500	0.525	0.600	0.700
(C) Fair	0.575	0.600	0.675	0.750
(D) Poor	0.675	0.700	0.750	0.825

Table 36: Total System Collapse Uncertainty (β_{tot}) for Model Quality (C) Fair and Period-Based Ductility, $\mu_T \geq 3$ (FEMA, 2009)

Quality of Test Data	Quality of Design Requirements			
	(A) Superior	(B) Good	(C) Fair	(D) Poor
(A) Superior	0.550	0.575	0.650	0.725
(B) Good	0.575	0.600	0.675	0.750
(C) Fair	0.650	0.675	0.725	0.800
(D) Poor	0.725	0.750	0.800	0.875

Table 37: Total System Collapse Uncertainty (β_{tot}) for Model Quality (D) Poor and Period-Based Ductility, $\mu_T \geq 3$ (FEMA, 2009)

Quality of Test Data	Quality of Design Requirements			
	(A) Superior	(B) Good	(C) Fair	(D) Poor
(A) Superior	0.650	0.675	0.725	0.825
(B) Good	0.675	0.700	0.750	0.825
(C) Fair	0.725	0.750	0.800	0.875
(D) Poor	0.825	0.825	0.875	0.950

Acceptable values of adjusted collapse margin ratio of each archetype buildings can be calculated based on the assumption that the collapse value of spectral intensity is lognormally distributed random variable. This distribution has median of S_{CT} and lognormal standard deviation of β_{TOT}. By considering β_{TOT} and acceptable collapse probability as 10% and 20%, Table 38 summarizes the $ACMR_{10\%}$ and $ACMR_{20\%}$.

FEMA P695 proposed acceptability criteria to verify the adequacy of initially assumed force reduction factors based on $ACMR_{10\%}$ and $ACMR_{20\%}$. The assumed R_d factors will be accepted if the calculated ACMR ratios within the performance group and individually fulfill the following criterion:

- The calculated Average Adjusted Collapsed Margin Ratio (ACMR) within the defined performance group exceeds $ACMR_{10\%}$

$$\overline{ACMR_i} \geq ACMR_{10} \quad [31]$$

- The calculated individual Adjusted Collapsed Margin Ratio (ACMR) of each archetype building exceeds $ACMR_{20\%}$

$$ACMR_i \geq ACMR_{20} \quad [32]$$

Evaluation of the overstrength factor is carried out based on the following recommendations of FEMA P695.

- The chosen system overstrength factor should be greater than the calculated largest average value of overstrength among the considered performance groups.
- Following ASCE/SEI 7-05, limiting overstrength factor of 3 is recommended due to practical design considerations.

However, for this research project, following NBCC 2010, the limiting overstrength factor is 1.7.

Table 38: Acceptable Values of Adjusted Collapse Margin Ratio ($ACMR_{10\%}$ and $ACMR_{20\%}$) (FEMA, 2009)

Total System Collapse Uncertainty	Collapse Probability				
	5%	10% ($ACMR_{10\%}$)	15%	20% ($ACMR_{20\%}$)	25%
0.275	1.57	**1.42**	1.33	**1.26**	1.20
0.300	1.64	**1.47**	1.36	**1.29**	1.22
0.325	1.71	**1.52**	1.40	**1.31**	1.25
0.350	1.78	**1.57**	1.44	**1.34**	1.27
0.375	1.85	**1.62**	1.48	**1.37**	1.29
0.400	1.93	**1.67**	1.51	**1.40**	1.31
0.425	2.01	**1.72**	1.55	**1.43**	1.33
0.450	2.10	**1.78**	1.59	**1.46**	1.35
0.475	2.18	**1.84**	1.64	**1.49**	1.38
0.500	2.28	**1.90**	1.68	**1.52**	1.40
0.525	2.37	**1.96**	1.72	**1.56**	1.42
0.550	2.47	**2.02**	1.77	**1.59**	1.45
0.575	2.57	**2.09**	1.81	**1.62**	1.47
0.600	2.68	**2.16**	1.86	**1.66**	1.50
0.625	2.80	**2.23**	1.91	**1.69**	1.52
0.650	2.91	**2.30**	1.96	**1.73**	1.55
0.675	3.04	**2.38**	2.01	**1.76**	1.58
0.700	3.16	**2.45**	2.07	**1.80**	1.60
0.725	3.30	**2.53**	2.12	**1.84**	1.63
0.750	3.43	**2.61**	2.18	**1.88**	1.66
0.775	3.58	**2.70**	2.23	**1.92**	1.69
0.800	3.73	**2.79**	2.29	**1.96**	1.72
0.825	3.88	**2.88**	2.35	**2.00**	1.74
0.850	4.05	**2.97**	2.41	**2.04**	1.77
0.875	4.22	**3.07**	2.48	**2.09**	1.80
0.900	4.39	**3.17**	2.54	**2.13**	1.83
0.925	4.58	**3.27**	2.61	**2.18**	1.87
0.950	4.77	**3.38**	2.68	**2.22**	1.90

10.2 Check for Collapse Prevention Limit State according to NBCC 2010

In this section NLTHA is employed to assess the seismic performance of hybrid buildings. NBCC 2010 poses a 2.5% MISD to represent extensive damage on the buildings. In this approach, the overall objective is to make sure that the average MISD in the building (irrespective of the storey height that it is calculated) should less than 2.5% under design based earthquake ground motions. For this purpose, NLTHA has been conducted using 60 ground motion records (i.e., 30 records, 2 components each) with 2% probability of exceedance in 50 years. The interstorey drift demand along the height of the buildings are presented in Figure 58 and Figure 59 for low-rise and mid-rise buildings, respectively. In order to check the upper bound requirement, in the given figures, mean plus one standard deviation (SD) plots are included. In the Figures the grey lines represent the response of buildings under individual earthquake ground motion records.

It is evident from Figures 58 and 59 that the mean and mean + 1SD maximum interstorey drift demands are less than 2.5 %. It can be seen from Figure 2c and d that the MISD values of 6 ground motion records exceeded the collapse prevention limit of NBCC 2010. However, as depicted in Figure 59a and b, only 2 ground motions causes the exceedance of 2.5% limit for 6 storey buildings. In general, the results suggest that the mean MISD responses are almost 40 % less than the limit. Therefore, the assumed R_d and R_o factors are suitable and efficient from the collapse prevention limit state requirement of NBCC 2010.

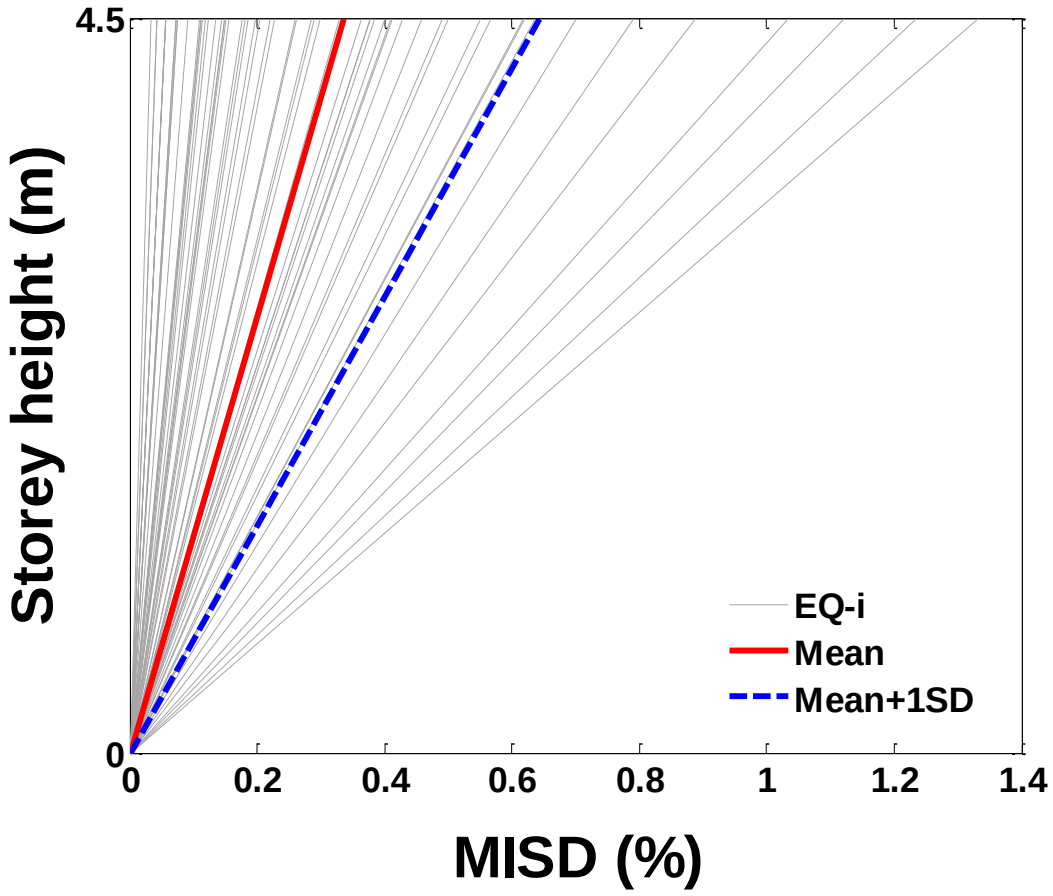

a) 1 storey ductile frame

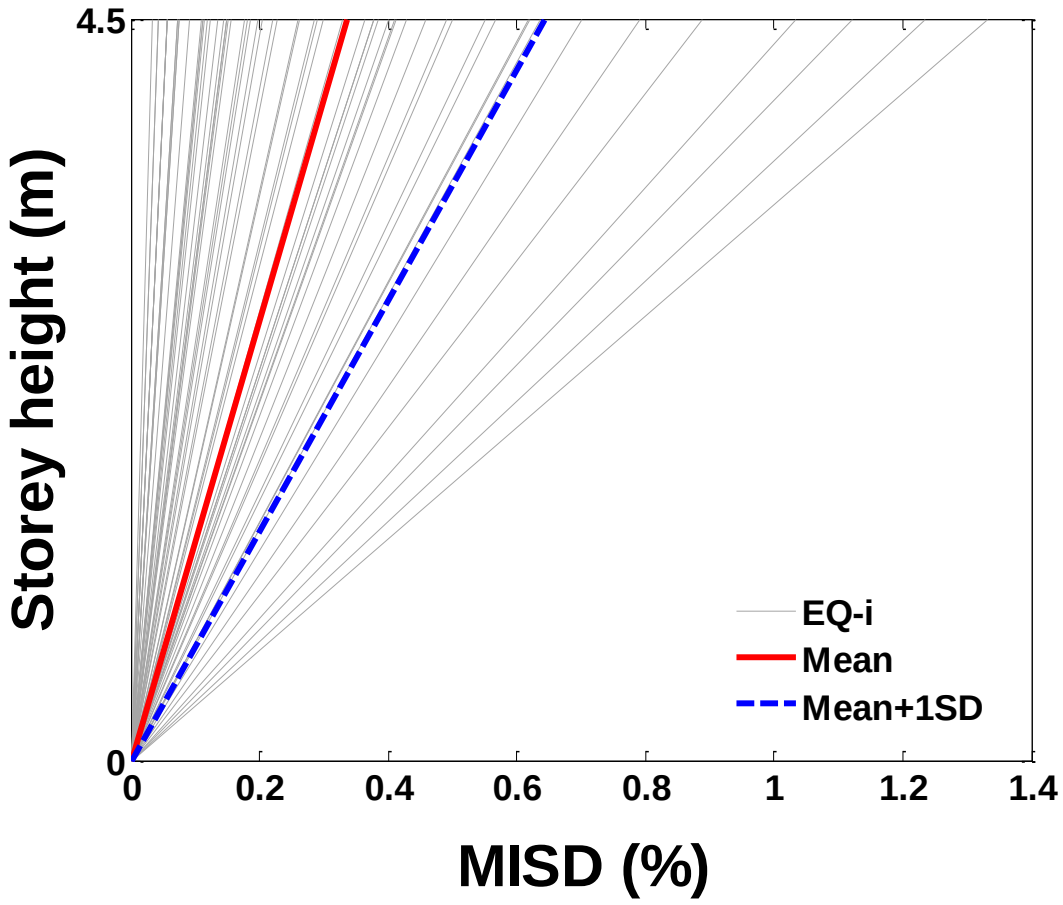

b) 1 storey limited ductile frame

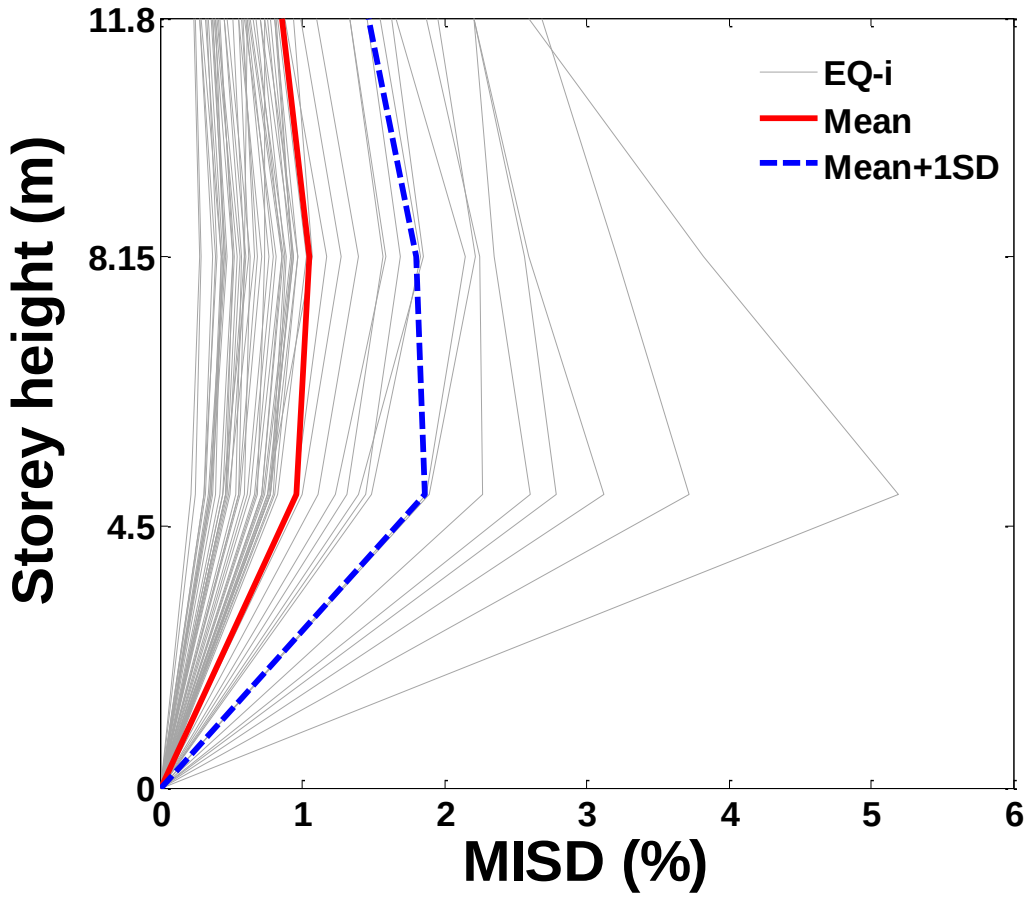

c) 3 storey ductile frame

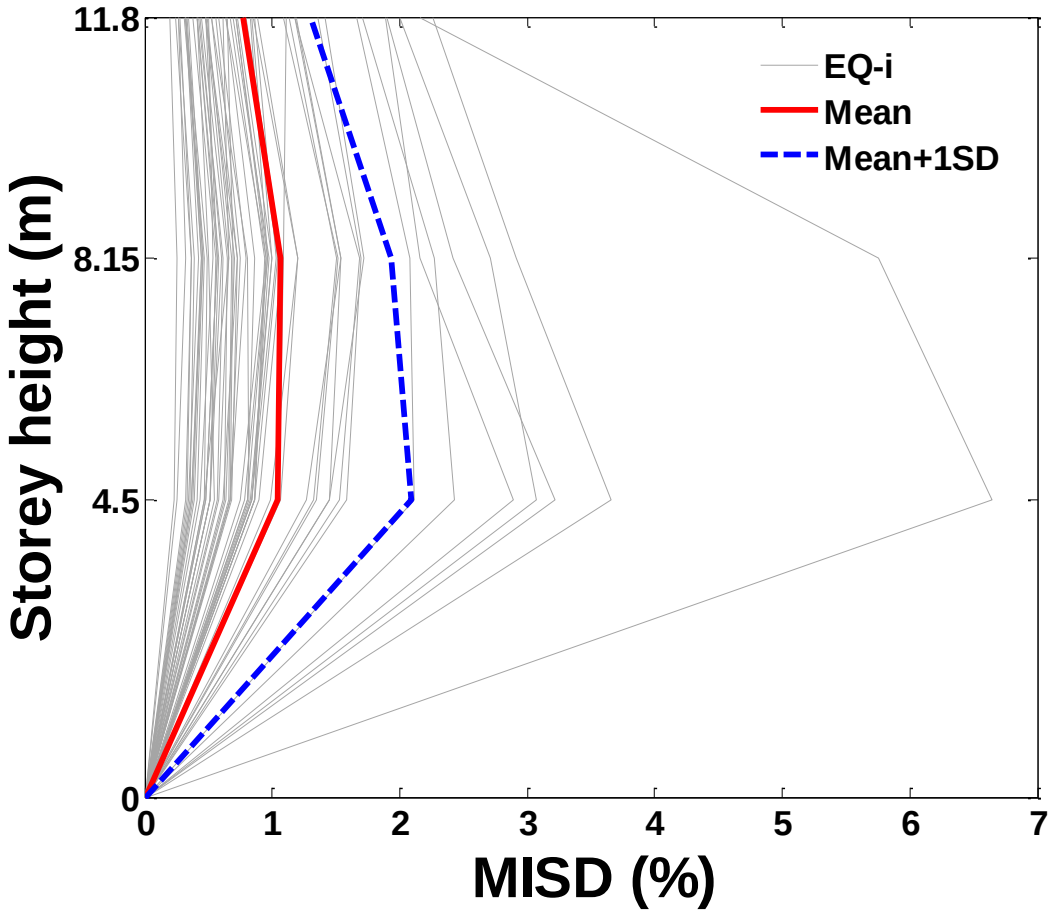

d) 3 storey limited ductile frame

Figure 58: Interstorey drift under design based earthquake ground motions for low-rise buildings

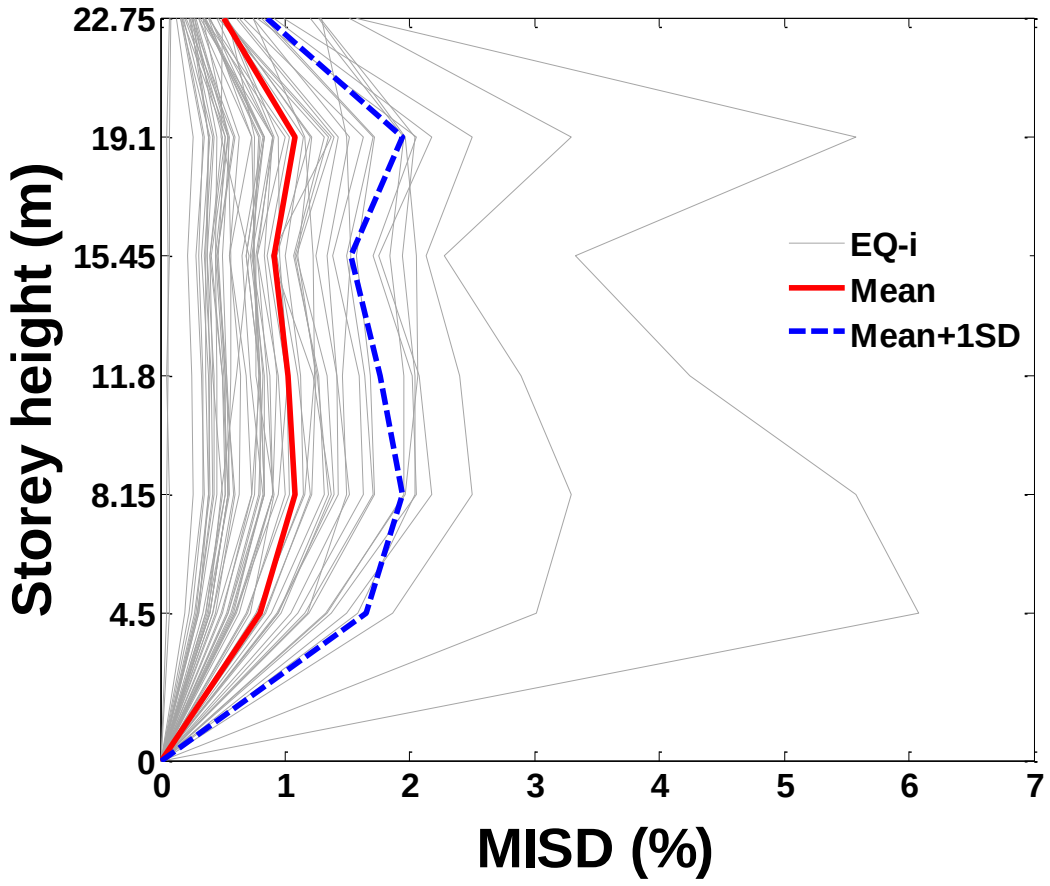

a) 6 storey ductile frame

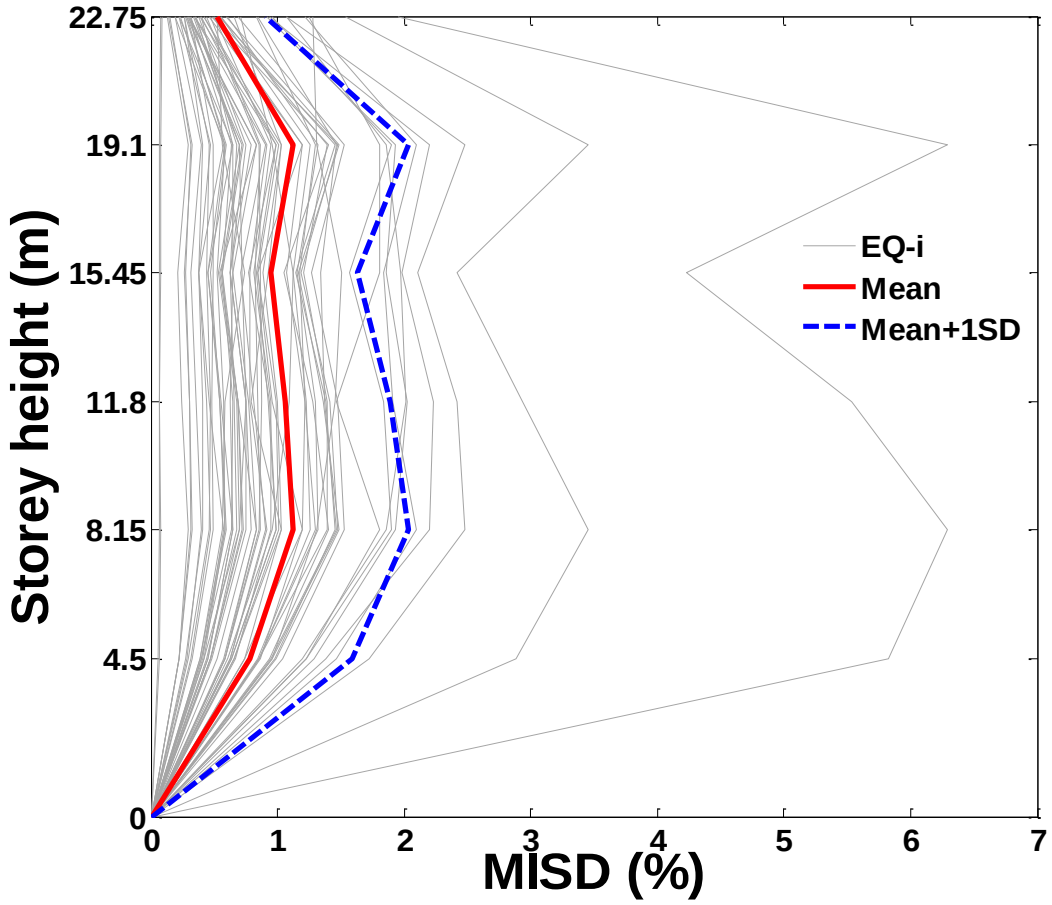

b) 6 storey limited ductile frame

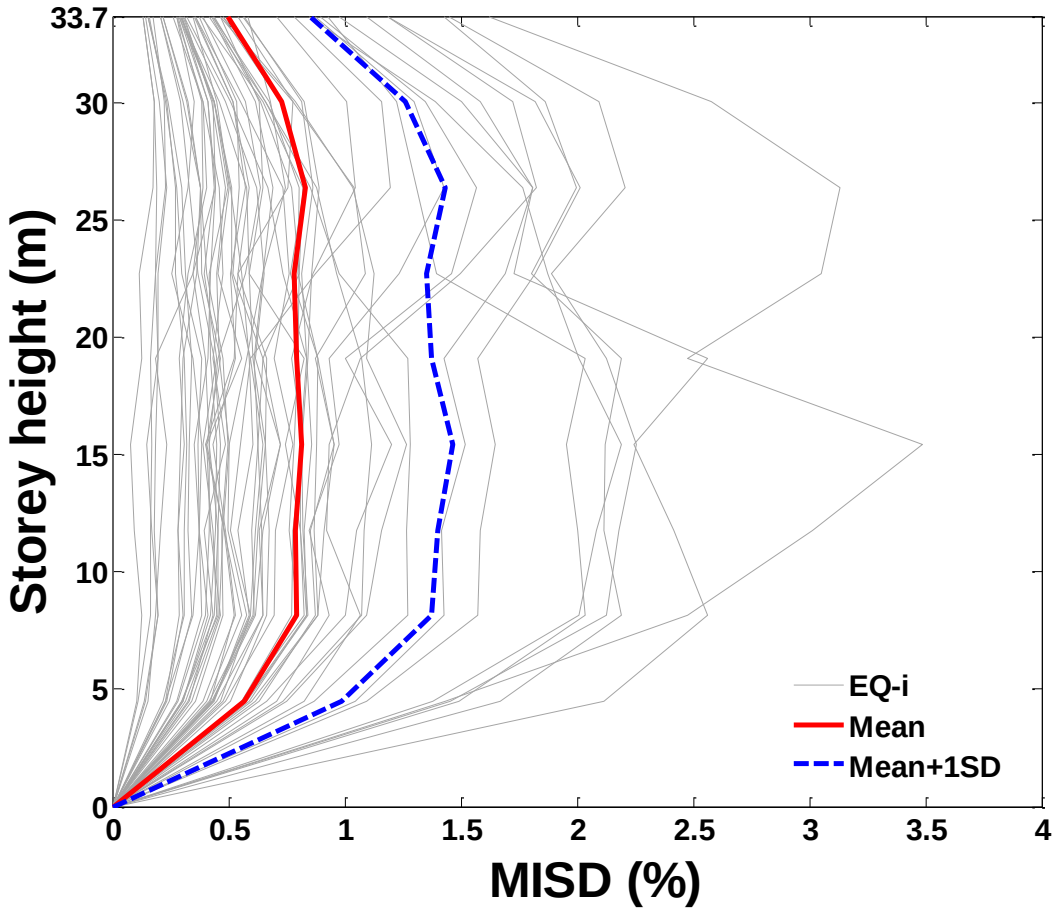

c) 9 storey ductile frame

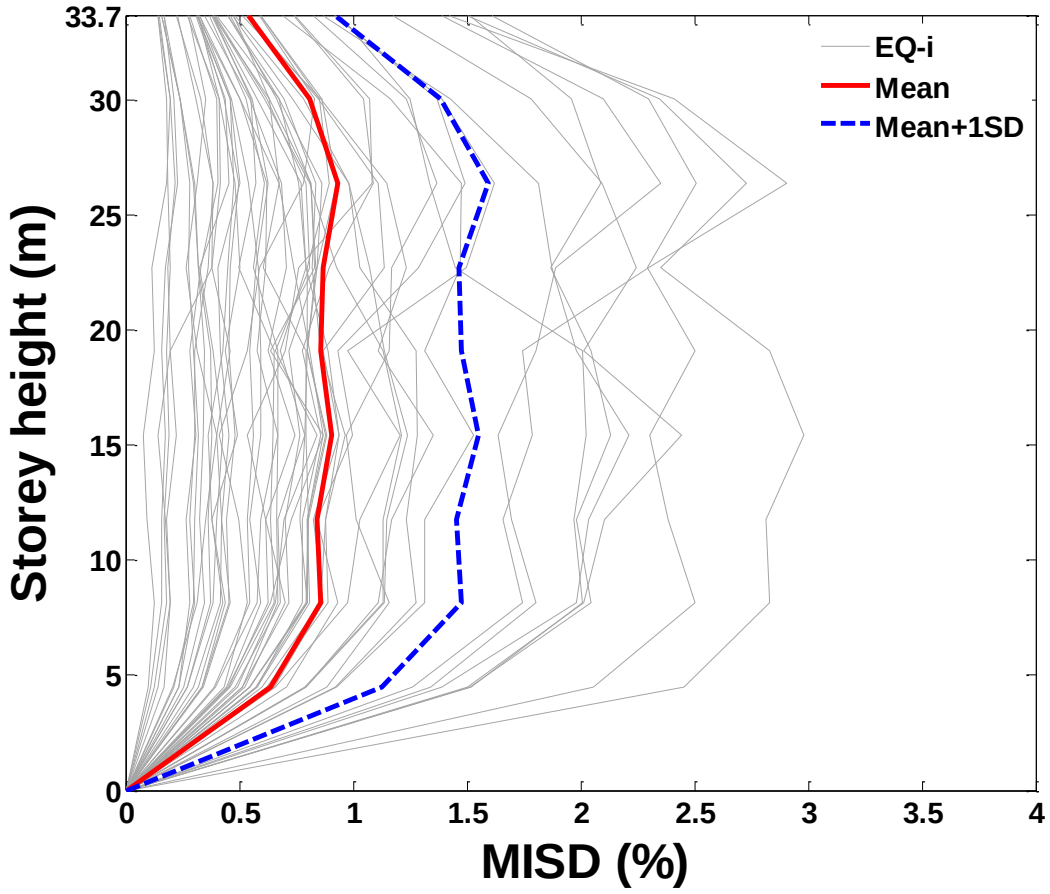

d) 9 storey limited ductile frame

Figure 59: Interstorey drift under design based earthquake ground motions for mid-rise buildings

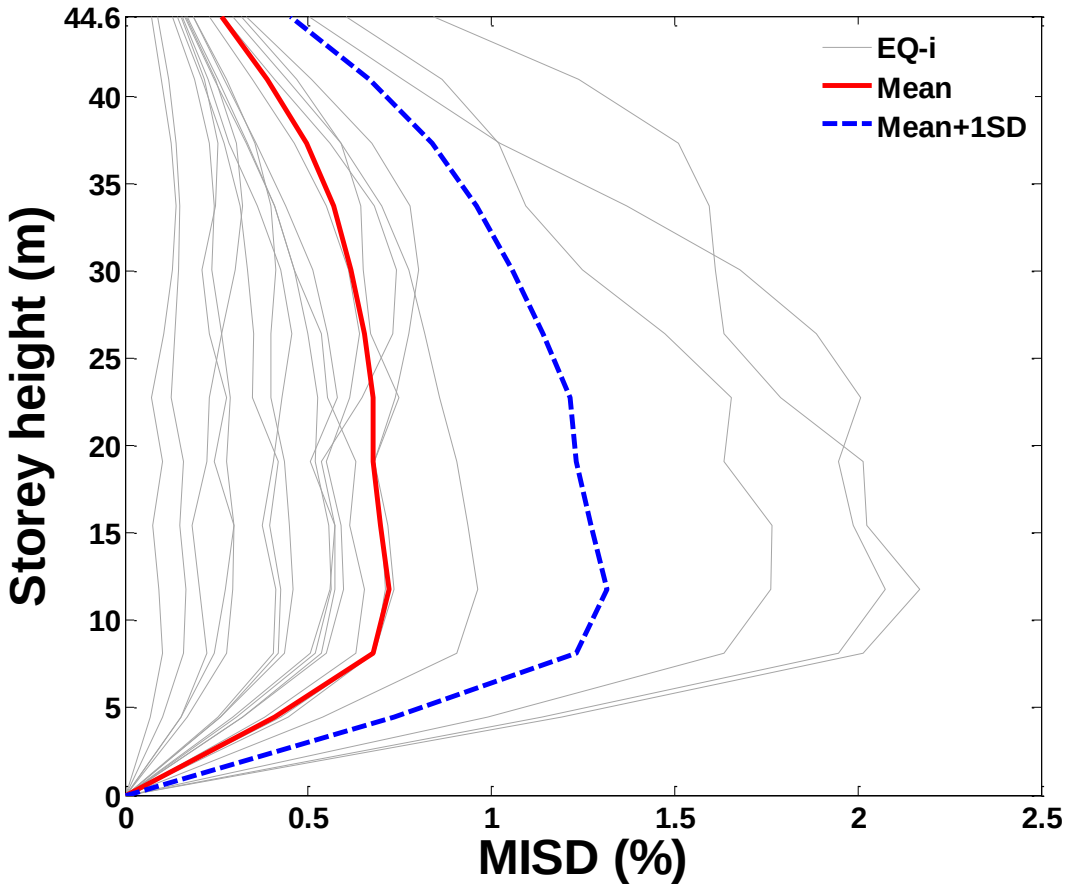

a) 12 storey ductile frame

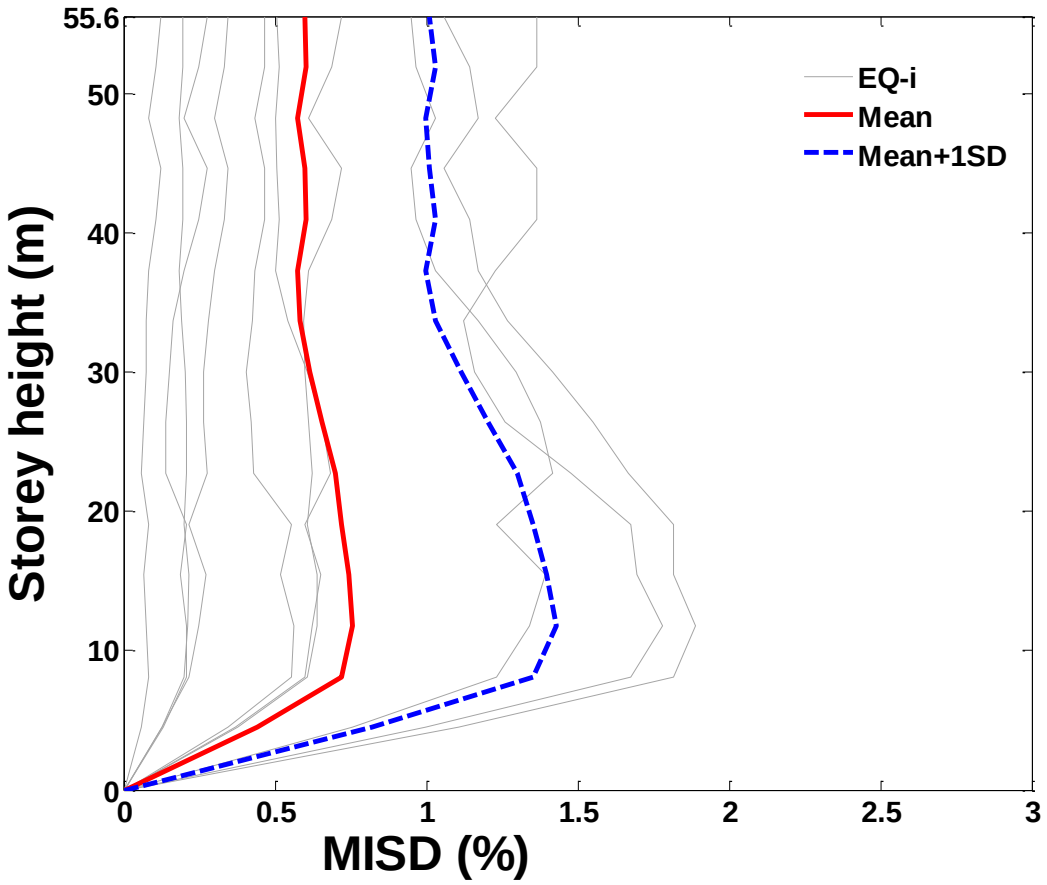

b) 15 storey ductile frame

Figure 60: Interstorey drift under design based earthquake ground motions for high-rise buildings

Chapter 11

Conclusions and Future Recommendation

Bibliography

Adams, J., and Halchuk, S. (2003). Fourth generation seismic hazard maps of Canada: values for over 650 Canadian localities intended for the 2005 National Building Code of Canada. Open-File 4459, Geological Survey of Canada, Ottawa, Ontario, Canada.

ASCE. (2006). ASCE standard ASCE/SEI 41-06: Seismic rehabilitation of existing buildings. (No. 41). Reston, Virginia: American Society of Civil Engineers.

ASCE. (2010). ASCE standard ASCE/SEI 7-10: Minimum design loads for buildings and other structures. Reston, Virginia: American Society of Civil Engineers.

ATC. (1995). ATC-19 Structural Response Modification Factors. Redwood City, California: Applied Technology Council.

Atkinson, G.M. 2004. An overview of developments in seismic hazard analysis. *13th World Conference on Earthquake Engineering*, Vancouver, B.C., Canada, August 1-6, 2004; Paper No. 5001.

Atkinson, G.M., and Goda, K. (2010). Inelastic seismic demand of real versus simulated ground-motion records for Cascadia subduction earthquakes. *Bulletin of the Seismological Society of America*, 100, 102-115.

Atkinson, G.M., and Goda, K. (2011). Effects of seismicity models and new ground motion prediction equations on seismic hazard assessment for four Canadian cities. *Bulletin of the Seismological Society of America*, 101, 176-189.

Baker, J.W. (2011). The conditional mean spectrum: a tool for ground motion selection. *Journal of Structural Engineering*, 137, 322-331.

Bezabeh, M. A., Tesfamariam, S., and Stiemer, S. F. (2014). Equivalent Viscous Damping for CLT infilled Steel Moment Frame Structures. Proceedings of the 14th World Conference on Timber Engineering, Quebec, Canada.

Bezabeh, M.A. (2014). Lateral behaviour and direct displacement based design of a novel hybrid structure: Cross laminated timber infilled steel moment resisting frames. (M.A.Sc, University of British Columbia).

Boore, D.M. (2009). Comparing stochastic point-source and finite-source ground-motion simulations: SMSIM and EXSIM. *Bulletin of the Seismological Society of America*, 99, 3202-3216.

Cassidy, J.F., and Garry C. Rogers, G.C 2004. Variation in ground shaking on the Fraser River Delta (Greater Vancouver, Canada). *In Proceedings of the 13th World Conference on Earthquake Engineering*, Vancouver, B.C., Canada, Paper 1010.

Ceccotti, A. (2008). New technologies for construction of massive buildings in seismic regions: The XLAM case. *Structural Engineering International*, 18(2), 156-165.

CEN Eurocode 8. (2002). Design of structures for earthquake resistance.

Chopra, A. K. (2005). Dynamics of Structures: Theory and Applications to Earthquake Engineering (3rd ed.). Upper Saddle River, NJ: Pearson Prentice Hall.

CISC. (2010). Handbook of Steel Construction (10th ed.). Toronto, ON: Quadratone Graphics Ltd.: Canadian Institute of Steel Construction.

Dickof, C. (2013). CLT infill in steel moment resisting frames as a hybrid seismic force resisting system. MASc thesis, The University of British Columbia.

Dickof, C., Stiemer, S. F., and Tesfamariam, S. (2012). Wood-steel hybrid seismic force resisting systems: seismic ductility. World Conference of Timber Engineering. Auckland, NZ.

Dickof, C., Stiemer, S. F., Bezabeh, M. A., and Tesfamariam, S. (2014). CLT-steel hybrid system: Ductility and overstrength values based on static pushover analysis. *Journal of Performance of Constructed Facilities*, 28(6) doi:10.1061/(ASCE)CF.1943-5509.0000614

Elnashai, A. S., and Mwafy, A. M. (2002). Overstrength and force reduction factors of multistorey reinforced-concrete buildings. *Structural Design of Tall Buildings*, 11(5), 329-351. doi:10.1002/tal.204

FEMA. (2009). P695 Quantification of Building Seismic Performance Factors. Redwood City, California: Applied Technology Council.

Fragiacomo, M., Dujic, B., and Sustersic, I. (2011). Elastic and ductile design of multi-storey massive wooden buildings under seismic actions. *Engineering Structures*, 33(11), 3043-3053.

Ghofrani, H., Atkinson, G.M., Goda, K., and Assatourians, K. (2013). Stochastic finite-fault simulations of the 11th March Tohoku, Japan, earthquake. *Bulletin of the Seismological Society of America*, 103, 1307-1320.

Goda, K. (2012). Nonlinear response potential of mainshock–aftershock sequences from Japanese earthquakes. *Bulletin of the Seismological Society of America*, 102, 2139-2156.

Goda, K., and Atkinson, G.M. (2011). Seismic performance of wood-frame houses in south-western British Columbia. *Earthquake Engineering and Structural Dynamics*, 40, 903-924.

Goda, K., and Taylor, C.A. (2012). Effects of aftershocks on peak ductility demand due to strong ground motion records from shallow crustal earthquakes. *Earthquake Engineering and Structural Dynamics*, 41, 2311-2330.

Goda, K., Kurahashi, S., Ghofrani, H., Atkinson, G.M., and Irikura, K. (2014). Nonlinear response potential of real versus simulated ground motions for the 11th March 2011 Great East Japan earthquake. *Earthquake Spectra*, (in press).

Goel, R. K. and Chopra, A. K. (1997). Period formulas for moment resisting frame buildings. *Journal of Structural Engineering*, 123(11), 1454-1461.

Hamburger, R. O., Krawinkler, H., Malley, J. O., and Adan, S. M. (2009). Seismic design of steel special moment frames: a guide for practicing engineers. National Earthquake Hazards Reduction Program.

Heidebrecht, A.C. 2003. Overview of seismic provisions of the proposed 2005 edition of the National Building Code of Canada. *Canadian Journal of Civil Engineering*, 30, 241-254.

Hyndman, R.D., and Rogers, G.C. (2010). Great earthquakes on Canada's west coast: a review. *Canadian Journal of Earth Sciences*, 47, 801-820.

Ibarra, L.F., Medina, R.A., and Krawinkler, H. (2005). Hysteretic models that incorporate strength and stiffness deterioration. *Earthquake Engineering and Structural Dynamics*, 34, 1489-1511.

ICC. (1997). Uniform Building Code. International Code Council.

Jayaram, N., Lin, T., and Baker, J.W. (2011). A computationally efficient ground-motion selection algorithm for matching a target response spectrum mean and variance. *Earthquake Spectra*, 27, 797-815.

Koduru, S.D., and Haukaas, T. (2010). Probabilistic seismic loss assessment of a Vancouver high-rise building. Journal of Structural Engineering 136, 235-245.

Kurahashi, S., and Iikura, K. (2013). Short-period source model of the 2011 M_w 9.0 off the Pacific coast of Tohoku earthquake. *Bulletin of the Seismological Society of America*, 103, 1373-1393.

Kwon, O. (2011). Evaluation of building period formulas for seismic design. (No. 2011-01). University of Toronto: Centre for the Resilience of Critical Infrastructure.

Lignos, D., and Krawinkler, H. (2011). Deterioration modeling of steel components in support of collapse prediction of steel moment frames under earthquake loading. *Journal of Structural Engineering*, 137(11), 1291-1302.

MATLAB. (2000). Matlab 6.1. Natick, MA: The MathWorks Inc.

Mazzoni, S., McKenna, F., Scott, M. H., and Fenves, G. L. (2007). OpenSees command language manual. Pacific Earthquake Engineering Research (PEER) Center.

Mazzoni, S., McKenna, F., Scott, M., Fenves, G., and Jeremic, B., 2006. Open system for earth-quake engineering simulation (OpenSees), Berkeley, California.

Mehanny, S.S., and Deierlein, G.G. (2000). Modeling of assessment of seismic performance of composite frames with reinforced concrete columns and steel beams. Report No 135, The John A. Blume Earthquake Engineering Center, Stanford University, CA.

Mitchell, D., Paultre, P., Tinawi, R., Saatcioglu, M., Tremblay, R., Elwood, K., and DeVall, R. (2010). Evolution of seismic design provisions in the National building code of Canada. Canadian Journal of Civil Engineering, 37(9), 1157-1170.

Mitchell, D., Tremblay, R., Karacabeyli, E., Paultre, P., Saatcioglu, M., and Anderson, D.L. (2003). Seismic force modification factors for the proposed 2005 edition of the National Building Code of Canada. *Canadian Journal of Civil Engineering*, 30(2), 308-327.

Motazedian, D., and Atkinson, G.M. (2005). Stochastic finite-fault modeling based on a dynamic corner frequency. *Bulletin of the Seismological Society of America*, 95, 995-1010.

National Research Council (NRC). (1965). National building code of Canada 1965. National Research Council of Canada, Ottawa.

National Research Council (NRC). (1970). National building code of Canada 1970. National Research Council of Canada, Ottawa.

National Research Council (NRC). (1990). National building code of Canada 1990. National Research Council of Canada, Ottawa.

National Research Council (NRC). (1995). National building code of Canada 1995. National Research Council of Canada, Ottawa.

National Research Council (NRC). (2005). National building code of Canada 2005. National Research Council of Canada, Ottawa.

National Research Council (NRC). (2010). National building code of Canada 2010. National Research Council of Canada, Ottawa.

NIST (2012). *Tentative Framework for Development of Advanced Seismic Design Criteria for New Buildings (NIST GCR 12-917-20)*. National Institute of Standards and Technology, NEHRP Consultants Joint Venture.

Opensees. (2010). Open System for Earthquake Engineering Simulation (Opensees) framework-Version 2.5. Pacific Earthquake Engineering Reseach Center, University of California, Berkley, http://opensees.berkley.edu/.

Otani, S. 2004. Earthquake resistant design of reinforced concrete buildings past and future. *Journal of Advanced Concrete Technology*, 2(1): 3-24.

Pacific Earthquake Engineering Research Center (PEER) Strong Motion Database. (2005). NGA Database. University of California at Berkley: http://peer.berkeley.edu/nga/.

Park, R. (1996). Explicit incorporation of element and structure overstrength in the design process. Eleventh World Conference on Earthquake Engineering.

Popovski, M., and Karacabeyli, E. (2012). Seismic Behaviour of Cross-Laminated Timber Structures. Proceedings of the 12th World Conference on Timber Engineering, Auckland, New Zealand, 2012.

Rainer, J.H. and Northwood, T.D. 1979. *CBD-208 Earthquakes and Buildings in Canada*. Canadian Building Digest. National Research Council.

Reid, S., and Peng, C. (1997). Dynamic uniaxial crushing of wood. *Int. J. Impact Eng.*, 19(97), 531-570.

Sanchez-Ricart, L. (2010). Reduction factors in seismic codes: on the components to be taken into account for design purposes. *Georisk*, 4(4), 208-229.

Sanchez-Ricart, L., and Plumier, A. (2008). Parametric study of ductile moment resiting frames. First step for Eurocode 9 calibration. *Earthquake Engineering & Structural Dynamics*, 37(7):1135 - 1155.

Schneider, J. (2009). Connections in cross-laminated-timber shear walls considering the behaviour under monotonic and cyclic lateral loading. M.A.Sc. thesis, Univ. of Stutgart, Stutgart, Germany.

Schneider, J., Karacabeyli, E., Popovski, M., Stiemer, S. F., and Tesfamariam, S. (2014). Damage assessment of connections used in cross-laminated timber subject to cyclic loads. *Journal of Performance of Constructed Facilities*, 28(6) doi:10.1061/(ASCE)CF.1943-5509.0000528

Shen, Y., Schneider, J., Tesfamariam, S., Stiemer, S., and Mu, Z. (2013). Hysteresis behaviour of bracket connection in cross-laminated-timber shear walls. *Construction and Building Materials*, 48, 980-991.

Takewaki, I., Murakami, S., Fujita, K., Yoshitomi, S., and Tsuji, M. (2011). The 2011 off the Pacific coast of Tohoku earthquake and response of high-rise buildings under long-period ground motions. *Soil Dynamics and Earthquake Engineering*, 31, 1511-1528.

Takewaki, I., Murakami, S., Fujita, K., Yoshitomi, S., and Tsuji, M. 2011. The 2011 off the Pacific coast of Tohoku earthquake and response of high-rise buildings under long-period ground motions. *Soil Dynamics and Earthquake Engineering* 31, 1511-1528.

Tesfamariam, S., and Goda, K. (2015). Loss estimation for non-ductile reinforced concrete building in Victoria, British Columbia, Canada: effects of mega-thrust M_w9-class subduction earthquakes and aftershocks. *Earthquake Engineering and Structural Dynamics* (in review).

Tesfamariam, S., Goda, K., and Mondal, G. (2014). Seismic vulnerability of RC frame with unreinforced masonry infill due to mainshock-aftershock earthquake sequences. *Earthquake Spectra* (in press).

Tesfamariam, S., Stiemer, S., Dickof, C., and Bezabeh, M. (2014). Seismic Vulnerability Assessment of Hybrid Steel-Timber Structure: Steel Moment-Resisting Frames with CLT Infill. *Journal of Earthquake Engineering*, 18:6, 929-944.

Topkaya, C., and Kurban, C. O. (2009). Natural periods of steel plate shear wall systems. *Journal of Constructional Steel Research*, 65(3), 542-551.

Tso, W.K. 1992. Overview of seismic provision changes in National Building Code of Canada 1990. *Canadian Journal of Civil Engineering*, 19(3), 383-388.

Uniform Building Code (UBC). (1935). Uniform Building Code 1935. Longbeach, California: International Conference of Building Officials (ICBO).

Uzumeri, S.M. Otani, S. and Collins, M.P. 1978. An overview of Canadian code requirements for earthquake resistant concrete buildings. *Canadian Journal of Civil Engineering*, 5, 427-441.

Vamvatsikos, D. and Cornell, C. A. (2002), Incremental dynamic analysis. Earthquake Engng. Struct. Dyn., 31: 491–514. doi: 10.1002/eqe.141.

Appendix A

Table A1: Period data for reinforced concrete moment resisting frames (Goel and Chopra, 1997)

No. (1)	Location (2)	ID number (3)	No. of stories (4)	Height (ft) (5)	Earthquake (6)	Period T (s)	
						Longitudinal (7)	Transverse (8)
1	Emeryville	NA	30	300	Loma Prieta	2.80	2.80
2	Los Angeles	NA	9	120	San Fernando	1.40	1.30
3	Los Angeles	NA	14	160	San Fernando	1.80	1.60
4	Los Angeles	NA	13	166	San Fernando	1.90	2.40
5	Los Angeles	ATC-12	10	137.5	San Fernando	1.40	1.60
6	Los Angeles	ATC-14	7	61	San Fernando	0.90	1.20
7	Los Angeles	ATC-2	7	68	San Fernando	1.00	1.00
8	Los Angeles	ATC-3	12	159	San Fernando	SW	1.33
9	Los Angeles	ATC-5	19	196.8	San Fernando	2.15	2.22
10	Los Angeles	ATC-6	11	124	San Fernando	1.43	1.60
11	Los Angeles	ATC-7	22	204.3	San Fernando	1.90	2.20
12	Los Angeles	ATC-9	16	152	San Fernando	1.10	1.80
13*	Los Angeles	C24236	14	148.8	San Fernando	NA	2.28
14*	Los Angeles	C24463	5	119	Northridge	1.46	1.61
15*	Los Angeles	C24463	5	119	Northridge	1.40	1.30
16*	Los Angeles	C24569	15	274	San Fernando	3.11	3.19
17*	Los Angeles	C24579	9	141	San Fernando	1.39	1.28
18*	Los Angeles	N220-2	20	196.8	San Fernando	2.27	2.09
19*	Los Angeles	N220-2	20	196.8	San Fernando	2.27	2.13
20*	Los Angeles	N220-2	20	196.8	San Fernando	2.24	1.98
21*	Los Angeles	N446-8	22	204.3	San Fernando	1.94	2.14
22*	Los Angeles	N446-8	22	204.3	San Fernando	1.84	2.17
23*	North Hollywood	C24464	20	169	Northridge	2.60	2.62
24	North Hollywood	C24464	20	169	Whittier	2.15	2.21
25	Pomona	C23511	2	30	Upland	0.28	0.30
26	Pomona	C23511	2	30	Whittier	0.27	0.29
27	San Bruno	C58490	6	78	Loma Prieta	0.85	1.10
28	San Bruno	C58490	6	78	Lomat Prieta	0.85	1.02
29	San Jose	NA	5	65	Morgan Hill	0.83	0.83
30	San Jose	C57355	10	124	Loma Prieta	1.01	SW
31	San Jose	C57355	10	124	Morgan Hill	0.91	SW
32	San Jose	C57355	10	124	Mount Lewis	0.91	SW
33*	Sherman Oaks	ATC-4	13	124	San Fernando	1.20	1.40
34*	Sherman Oaks	C24322	13	184.5	Whittier	1.90	2.30
35*	Sherman Oaks	C24322	13	184.5	Whittier	NA	2.44
36	Van Nuys	ATC-1	7	65.7	San Fernando	0.79	0.88
37*	Van Nuys	C24386	7	65.7	Whittier	1.40	1.20

Note *Denotes buildings with ago $\geq$ 0.15g; NA indicates data not available; SW implies shear walls form the lateral-load resisting system; number followed by "C" or "N" indicates the station number and by "ATC" indicates the building number in ATC3-06 report.

Table A2: Steel moment resisting frame fundamental period (Kwon, 2011)

Type	No.	Location	ID number	No. storeys	Height (m)	Earthquake	Period Lo.	Period Tr.
SMRF	1	Long Beach	C14323	7	27.74	Whittier	1.19	1.50
SMRF	2	Los Angeles	N157-9	39	139.90	San Fernando	4.65	N/A
SMRF	1	La Jolla	C03233	2	16.25	Anza	0.39	0.42
SMRF	3	Palm Springs	C12299	4	15.70	Hector Mine	0.69	0.63
SMRF	5	Moreno Valley	C13213	3	13.72	Big Bear City	0.40	0.39
SMRF	7	Newport Beach	C13291	7	41.15	Chino Hills	1.17	1.22
SMRF	10	Long Beach	C14323	7	27.74	Whittier	1.11	1.37
SMRF	11	Long Beach	C14533	15	87.78	Whittier	3.72	3.62
SMRF	12	Los Angeles	C14766	4	13.72	Anza	0.76	0.78
SMRF	13	Redlands	C23481	7	24.38	Landers	1.46	1.55
SMRF	15	San Bernardino	C23515	9	35.84	Landers	2.16	1.92
CBF	16	San Bernardino	C23516	3	12.59	Landers	0.55	0.53
SMRF	17	San Bernardino	C23634	5	21.03	Big Bear	0.49	0.49
SMRF	19	Simi Valley	C24104	2	8.69	San Simeon	0.36	0.37
SMRF	20	Cahtsworth	C24198	2	10.36	San Simeon	0.59	N/A
SMRF	21	Los Angeles	C24288	32	102.72	Chino Hills	2.93	3.28
SMRF	22	Burbank	C24370	6	25.15	Northridge	1.35	1.36
SMRF	23	Pasadena	C24546	12	54.50	Northridge	1.85	2.10
SMRF	24	Pasadena	C24566	12	51.21	Anza	2.06	2.07
SMRF	25	Los Angeles	C24569	15	71.93	Landers	3.09	3.23
SMRF	27	Lancaster	C24609	5	23.93	Big Bear City	0.66	0.66
SMRF	28	Los Angeles	C24629	54	218.08	Northridge	5.37	5.85
CBF	29	Los Angeles	C24643	19	86.26	Northridge	4.00	3.52
SMRF	36	San Jose	C57357	13	52.76	Loma Prieta	2.10	2.04
SMRF	37	San Jose	C57562	3	15.09	Loma Prieta	0.69	0.73
SMRF	40	Fremont	C57783	3	13.72	Gilroy	0.42	0.36
SMRF	42	Walnut Creek	C58199	3	13.72	Berkeley	0.14	0.32
SMRF	43	San Francisco	C58261	4	16.00	Loma Prieta	0.66	0.61
SMRF	44	San Francisco	C58480	18	69.89	Loma Prieta	2.20	3.15
SMRF	46	Richmond	C58506	3	14.08	Loma Prieta	0.60	0.72
SMRF	47	San Francisco	C58532	47	171.91	Loma Prieta	6.07	5.49
SMRF	49	Redwood City	C58615	16	67.79	Glen Ellen	1.85	1.74
SMRF	50	Castro Valley	C58661	2	8.84	Gilroy	0.29	0.34
SMRF	52	San Francisco	C58776	14	55.38	Gilroy	0.53	1.61
SMRF	53	Santa Rosa	C68669	4	17.50	Santa Rosa	0.56	0.54
SMRF	55	Los Angeles	ATC.ST01	19	63.55	San Fernando	3.00	3.21
SMRF	56	Pasadena	ATC.ST02	9	39.17	San Fernando	1.29	1.44
SMRF	57	Los Angeles	ATC.ST03	-	36.58	San Fernando	2.41	2.23
SMRF	58	Los Angeles	ATC.ST04	27	112.32	San Fernando	4.38	4.18
SMRF	59	Los Angeles	ATC.ST05	19	81.38	San Fernando	3.97	3.50
SMRF	60	Los Angeles	ATC.ST06	17	63.09	San Fernando	3.00	2.28
SMRF	61	Los Angeles	ATC.ST07	-	76.20	San Fernando	3.88	3.88
SMRF	62	Los Angeles	ATC.ST08	32	130.61	San Fernando	5.00	5.40
SMRF	63	Los Angeles	ATC.ST09	-	63.55	Northridge	3.20	3.20
SMRF	64	Los Angeles	ATC.ST10	39	150.57	San Fernando	5.00	4.76

SMRF	65	Los Angeles	ATC.ST11	15	61.57	San Fernando	2.91	2.79
SMRF	66	Los Angeles	ATC.ST12	31	102.57	San Fernando	3.26	3.00
SMRF	67	Los Angeles	ATC.ST13	-	31.09	San Fernando	1.71	1.62
SMRF	68	Los Angeles	ATC.ST14	-	48.31	San Fernando	2.76	2.38
SMRF	69	Los Angeles	ATC.ST15	41	182.58	San Fernando	6.00	5.50
SMRF	70	Los Angeles	ATC.ST17	-	24.84	San Fernando	1.85	1.71
SMRF	71	Los Angeles	N151-3	15	61.57	San Fernando	2.84	2.77
SMRF	72	Los Angeles	N163-5	41	182.58	San Fernando	6.06	5.40
SMRF	73	Los Angeles	N172-4	31	102.57	San Fernando	3.38	2.90
SMRF	74	Los Angeles	N184-6	27	121.31	San Fernando	4.27	4.26
SMRF	75	Los Angeles	N187-9	19	82.30	San Fernando	3.43	3.41
SMRF	76	Pasadena	N267-8	9	39.62	Lytle Creek	1.02	1.13
SMRF	77	Los Angeles	N428-30	32	135.18	San Fernando	4.86	5.50
SMRF	78	Los Angeles	N440-2	17	63.09	San Fernando	2.85	3.43
SMRF	79	Los Angeles	N461-3	19	70.62	San Fernando	3.27	3.34
SMRF	80	San Francisco	NA01_STMRF	60	257.01	Loma Prieta	3.57	3.57
SMRF	81	Alhambra	U482	13	60.35	Northridge	2.15	2.20
SMRF	82	Los Angeles	U5208	6	31.70	Northridge	0.94	0.96
SMRF	83	Los Angeles	U5233	32	131.06	Northridge	3.43	3.36
SMRF	84	Norwalk	U5239	7	29.26	Whittier	1.30	1.22